ANALYTIC MODELING OF ROCK-STRUCTURE INTERACTION

Semiannual Technical Report
August 1972

U.S. BUREAU OF MINES
Contract Number H0220035

Sponsored By
ADVANCED RESEARCH PROJECTS AGENCY
ARPA Order No. 1579, Amend. No. 3
Program Code 2F10

JEREMY ISENBERG
Principal Investigator

AGBABIAN ASSOCIATES
Engineering and Applied Sciences Division
Los Angeles, California

122

DISCLAIMER NOTICE

THIS DOCUMENT IS THE BEST QUALITY AVAILABLE.

COPY FURNISHED CONTAINED A SIGNIFICANT NUMBER OF PAGES WHICH DO NOT REPRODUCE LEGIBLY.

DOCUMENT CONTROL DATA - R&D

(Security classification of title, body of abstract and indexing annotation must be entered when the overall report is classified)

1. ORIGINATING ACTIVITY (Corporate author) Agbabian Associates 8939 So. Sepulveda Blvd. Los Angeles, Calif. 90095	2a. REPORT SECURITY CLASSIFICATION UNCLASSIFIED 2b. GROUP --

3. REPORT TITLE

Analytic Modeling of Rock-Structure Interaction

4. DESCRIPTIVE NOTES (Type of report and inclusive dates)

Semiannual Technical Report

5. AUTHOR(S) (Last name, first name, initial)

Isenberg, Jeremy

6. REPORT DATE	7a. TOTAL NO. OF PAGES	7b. NO. OF REFS
1 September 1972	159	49

8a. CONTRACT OR GRANT NO.	9a. ORIGINATOR'S REPORT NUMBER(S)
H0220035 b. PROJECT NO. c. d.	9b. OTHER REPORT NO(S) (Any other numbers that may be assigned this report) R-7215-2299

10. AVAILABILITY/LIMITATION NOTICES

11. SUPPLEMENTARY NOTES	12. SPONSORING MILITARY ACTIVITY
	Advanced Research Projects Agency of the Department of Defense

13. ABSTRACT

A number of recent advances in finite element theory and computer technology are combined into a computer program for analyzing structures and cavities in rock. The program applies to general three-dimensional structures, considers nonlinear material properties, including joints, anisotropic and time-dependent material properties, gravity loading and sequence of construction or excavation. Example problems, demonstrating the ability of the program to reproduce idealized situations having closed-form, analytic solutions are solved.

DD FORM 1 JAN 64 1473

14. KEY WORDS	LINK A		LINK B		LINK C	
	ROLE	WT	ROLE	WT	ROLE	WT
finite element						
rock/structure interaction						
joints						
anisotropy						
viscous properties						
plasticity						
automatic mesh generation						
bandwidth reduction						

INSTRUCTIONS

1. ORIGINATING ACTIVITY: Enter the name and address of the contractor, subcontractor, grantee, Department of Defenae activity or other organization *(corporate author)* issuing the report.

2a. REPORT SECURITY CLASSIFICATION: Enter the overall security classification of the report. Indicate whether "Restricted Data" is included. Marking is to be in accordance with appropriate security regulations.

2b. GROUP: Automatic downgrading is specified in DoD Directive 5200.10 and Armed Forces Industrial Manual. Enter the group number. Also, when applicable, show that optional markings have been used for Group 3 and Group 4 as authorized.

3. REPORT TITLE: Enter the complete report title in all capital letters. Titles in all cases should be unclassified. If a meaningful title cannot be selected without classification, show title classification in all capitals in parenthesis immediately following the title.

4. DESCRIPTIVE NOTES: If appropriate, enter the type of report, e.g., interim, progress, summary, annual, or final. Give the inclusive dates when a specific reporting period is covered.

5. AUTHOR(S): Enter the name(s) of author(s) as shown on or in the report. Enter last name, first name, middle initial. If military, show rank and branch of service. The name of the principal author is an absolute minimum requirement.

6. REPORT DATE: Enter the date of the report as day, month, year; or month, year. If more than one date appears on the report, use date of publication.

7a. TOTAL NUMBER OF PAGES: The total page count should follow normal pagination procedures, i.e., enter the number of pages containing information.

7b. NUMBER OF REFERENCES: Enter the total number of references cited in the report.

8a. CONTRACT OR GRANT NUMBER: If appropriate, enter the applicable number of the contract or grant under which the report was written.

8b, 8c, & 8d. PROJECT NUMBER: Enter the appropriate military department identification, such as project number, subproject number, system numbers, task number, etc.

9a. ORIGINATOR'S REPORT NUMBER(S): Enter the official report number by which the document will be identified and controlled by the originating activity. This number must be unique to this report.

9b. OTHER REPORT NUMBER(S): If the report has been assigned any other report numbers *(either by the originator or by the sponsor)*, also enter this number(s).

10. AVAILABILITY/LIMITATION NOTICES: Enter any limitations on further dissemination of the report, other than those imposed by security classification, using standard statements such as:

(1) "Qualified requesters may obtain copies of this report from DDC."

(2) "Foreign announcement and dissemination of this report by DDC is not authorized."

(3) "U. S. Government agencies may obtain copies of this report directly from DDC. Other qualified DDC users shall request through

_____."

(4) "U. S. military agencies may obtain copies of this report directly from DDC. Other qualified users shall request through

_____."

(5) "All distribution of this report is controlled. Qualified DDC users shall request through

_____."

If the report has been furnished to the Office of Technical Services, Department of Commerce, for sale to the public, indicate this fact and enter the price, if known.

11. SUPPLEMENTARY NOTES: Use for additional explanatory notes.

12. SPONSORING MILITARY ACTIVITY: Enter the name of the departmental project office or laboratory sponsoring *(paying for)* the research and development. Include address.

13. ABSTRACT: Enter an abstract giving a brief and factual summary of the document indicative of the report, even though it may also appear elsewhere in the body of the technical report. If additional space is required, a continuation sheet shall be attached.

It is highly desirable that the abstract of classified reports be unclassified. Each paragraph of the abstract shall end with an indication of the military security classification of the information in the paragraph, represented as *(TS)*, *(S)*, *(C)*, or *(U)*.

There is no limitation on the length of the abstract. However, the suggested length is from 150 to 225 words.

14. KEY WORDS: Key words are technically meaningful terms or short phrases that characterize a report and may be used as index entries for cataloging the report. Key words must be selected so that no security classification is required. Identifiers, such as equipment model designation, trade name, military project code name, geographic location, may be used as key words but will be followed by an indication of technical context. The assignment of links, rules, and weights is optional.

SEMIANNUAL TECHNICAL REPORT

ARPA Order Number:	1579, Amendment No. 3
Program Code Number:	2F10
Name of Contractor:	Agbabian Associates
Effective Date of Contract:	1 March 1972
Contract Expiration Date:	1 May 1973
Amount of Contract:	$152,549
Contract Number:	H0220035
Principal Investigator:	Jeremy Isenberg
Phone Number:	(213) 776-6870
Title of Work:	Analytic Modeling of Rock-Structure Interaction, Semiannual Report

This research was supported by the Advanced Research Projects Agency of the Department of Defense and was monitored by the Bureau of Mines under Contract No. H0220035.

TECHNICAL REPORT SUMMARY

The objective of this project is to combine a number of recent advances in finite element theory and computer technology for analyzing cavities and structures in rock. This computer program applies to general three-dimensional structures, considers nonlinear material properties including homogeneous deformations and inhomogeneous deformations due to joints, anisotropic and time-dependent material propertoes, gravity loading, and sequence of construction or excavation.

During the first half of this contract, work has been aimed at producing a user-oriented computer program. The work of writing the program was divided into three areas:

a. Input

b. Execution and output

c. Material properties

The Input Section automatically generates the continuum part of the finite element mesh, including joint elements, allows the user to add other elements (beam, shell, truss) to the mesh, plots the result, reduces the bandwidth and reads loads, material properties, and other quantities necessary to the calculation. The Execution Section forms the global stiffness matrix and solves equations of equilibrium for displacements by an implicit method. The material properties are represented by subroutines within the Execution Section, which are written in a modular form so that if the general equations of nonlinear elasticity, viscoelasticity, viscoplasticity, or plasticity do not suit a particular problem they may be easily modified. This work is now complete except for linkage among the various sections to be checked out and for the efficiency of some operations to be improved.

One of the guidelines for this project was that no major new research was to be done. Accordingly, the program uses existing finite elements, a proven form of the equation of equilibrium, existing material property descriptions, and an existing bandwidth reducer. However, a small amount of new work was done. A new joint element was developed and an existing concept for automatic mesh generation was greatly extended. Also, a form of Choleski decomposition was modified for efficient use of multibuffering, resulting in substantial improvement in efficiency of solving equations of equilibrium using peripheral storage.

During the first six months of this study, some new work was reported by other ARPA/Bureau of Mines contractors which has been incorporated in the program. Among these are some creep data obtained by W. A. Wawersik of the University of Utah and strength/deformability data for faults by R. E. Goodman, F. E. Heuze, and Y. Ohnishi of the University of California, Berkeley.

The technical work reported below is divided into four main parts. Section 3 describes the equations of equilibrium and the types of finite elements available in the program, including the new joint element. Section 4 describes the properties of rock including anisotropy, rate effects, joints, and homogeneous inelasticity. Section 5 describes the computer program. Most attention is given to the processing of input data and to options available to the user for mesh generation, sequential excavation, or construction, automatic bandwidth reduction and plotting of the mesh. Some logical flow diagrams are given. Section 6 describes some example problems which have been solved during the checkout of the program.

During the second half of this project work will concentrate on applications of the program to field situations in which measurements are available for comparison with results of analysis.

FOREWORD

The principal contributors to the work reported here are listed below. All are members of the technical staff of Agbabian Associates.

A. K. Bhaumik

K. P. Chuang

J. M. Clark

K. T. Dill

J. Ghaboussi

J. Isenberg

E. M. Raney

CONTENTS

ILLUSTRATIONS

ILLUSTRATIONS (CONTINUED)

ILLUSTRATIONS (CONTINUED)

ILLUSTRATIONS (CONTINUED)

ILLUSTRATIONS (CONTINUED)

TABLES

SECTION 1

INTRODUCTION

The purpose of this contract is to combine a number of recent advances in finite element theory and computer technology into a computer program for analyzing structures and cavities in rock. This computer program applies to general three-dimensional structures, considers nonlinear material properties including homogeneous deformation and inhomogeneous deformation due to joints, anisotropic and time-dependent material properties, gravity loading, and sequence of construction or excavation. Since the program is intended for practical analysis and design, great effort has been made to foresee difficulties in using it. For example, much tedious work, which formerly was done by the user, has been eliminated by sophisticated mesh generators and a bandwidth reducer. Also, since many prospective users may have access to small or medium-sized computers but may still wish to solve large problems (4000-6000 equations), the program uses up-to-date multibuffering techniques for accessing peripheral storage units, thus dramatically reducing computer run time for out-of-core problems. Finally, an attempt is made to lengthen the useful life of the program by making it simple to add new elements and to expand the material property description and by making the program efficient for and compatible with a wide variety of computers.

The purpose of this report is to discuss what the computer program now does and what it will do when the present contract is complete. Most of the description is given from the standpoint of a prospective user. Mesh generation, the types of elements available, the types of loading and construction which may be done, and the material properties and joints which are available are described. Assurance that the program is working properly is given by comparing analytic solutions for one-, two-, and three-dimensional problems with the finite element solutions to the same problems. The theory underlying the present finite element formulation is also described. Also, the structure of the code is indicated by logic diagrams.

The work which will be done in the second half of the contract period involves application of the code to actual mining situations. During this phase, general features of the program such as the joint element and the material property representations will be refined. Parameters will be selected for specific field conditions and an attempt will be made to match field data with calculations. The sites have not yet been selected.

To summarize, this report describes a finite element computer program which incorporates a number of good features which are not all available in any other program. By means of comparison with analytic solutions, evidence is given that the program is consistent with the assumptions under which it was formulated and written, and that it contains no programming errors. The task of demonstrating that it accurately represents field conditions is left to the second phase of the contract.

SECTION 2

PHYSICAL ASPECTS OF ROCK AND SUPPORT SYSTEMS WHICH THIS PROGRAM REPRESENTS

This section describes the scope and specific goals of the present computer program. These are representation of gravity and live loading, properties of homogeneous rock including anisotropic, inelastic and viscous effects, properties of jointed rock, excavation and construction, and geometry of cavities and support systems.

To illustrate the capability of the program three typical problems are described below. These problems have not actually been solved with the present program, but they could be solved at any time. The first is illustrated in Figure 2-1. A section of tunnel is to be excavated in a region containing a major joint. The properties of the joint are assumed to be known. The rock adjacent to the joint is assumed to be homogeneous and to have viscous properties which can be represented by a visco-plastic model. In Step 1, the tunnel has not yet been excavated. Stress in the rock is computed by applying static overburden to the edges of the finite element mesh. Then the tunnel is excavated by removing appropriate elements. At each stage of the excavation, the tunnel roof is propped by truss and beam elements. Eventually, the tunnel is fully open and the final supports are installed. Each stage is associated with an elapsed time, during which the rock flows in a visco-plastic manner. At each intermediate stage and at a stage the user defines to be final, the stresses in the rock and in the support elements are printed.

The second problem is illustrated in Figure 2-2. A bank is to be excavated in a rock such as shale having nonlinear, anisotropic stress/strain properties and an anisotropic fracture criterion. In Step 1, the in situ states of stress are computed by applying gravitational forces in a step-by-step fashion throughout the grid. In subsequent steps, elements are removed in any sequence the user desires. Between excavation steps the remaining rock will be checked for fracture which would correspond to spall and sliding in an actual field situation.

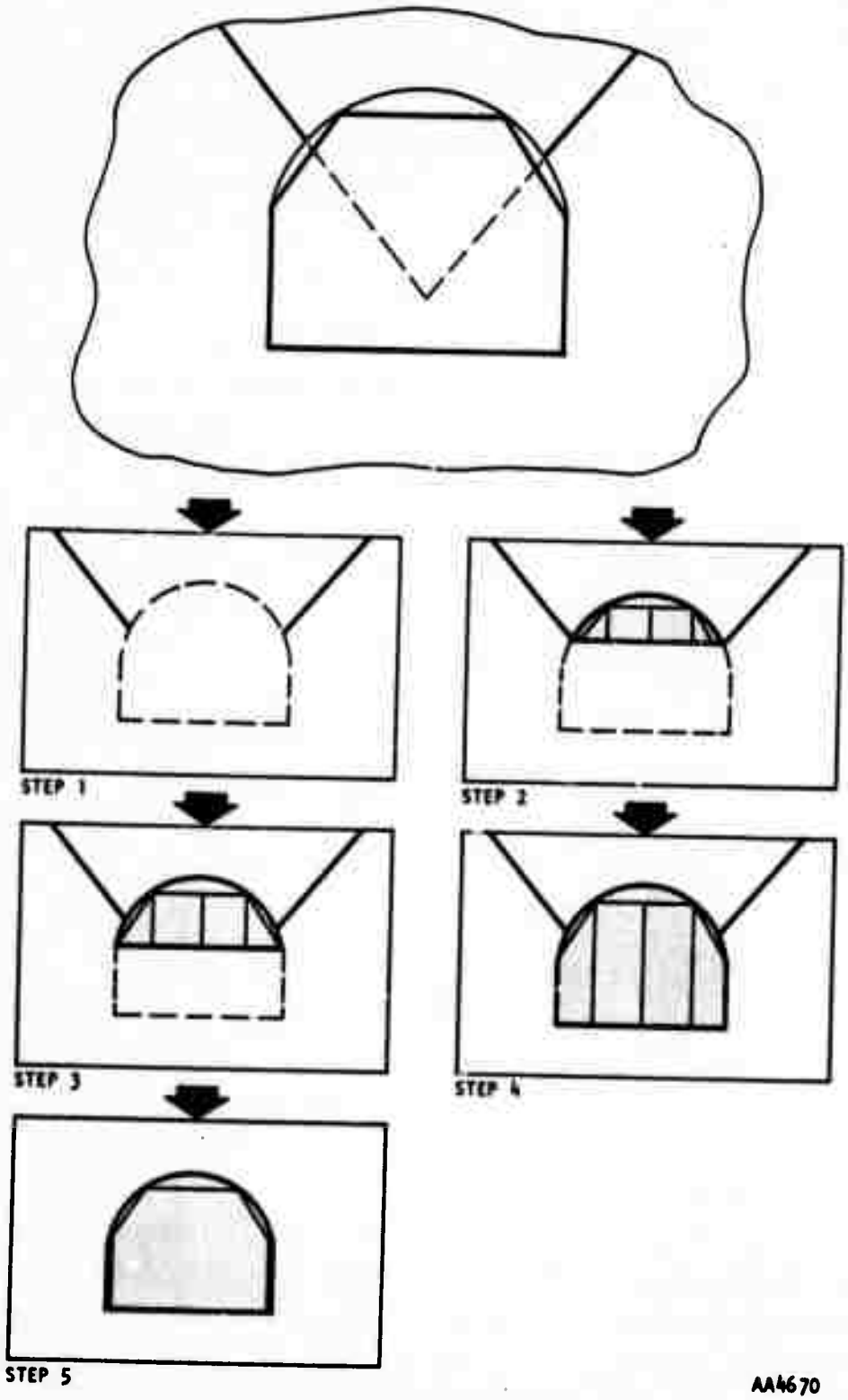

FIGURE 2-1. TWO-DIMENSIONAL TUNNEL WITH EXCAVATION, TEMPORARY BRACING AND JOINTS

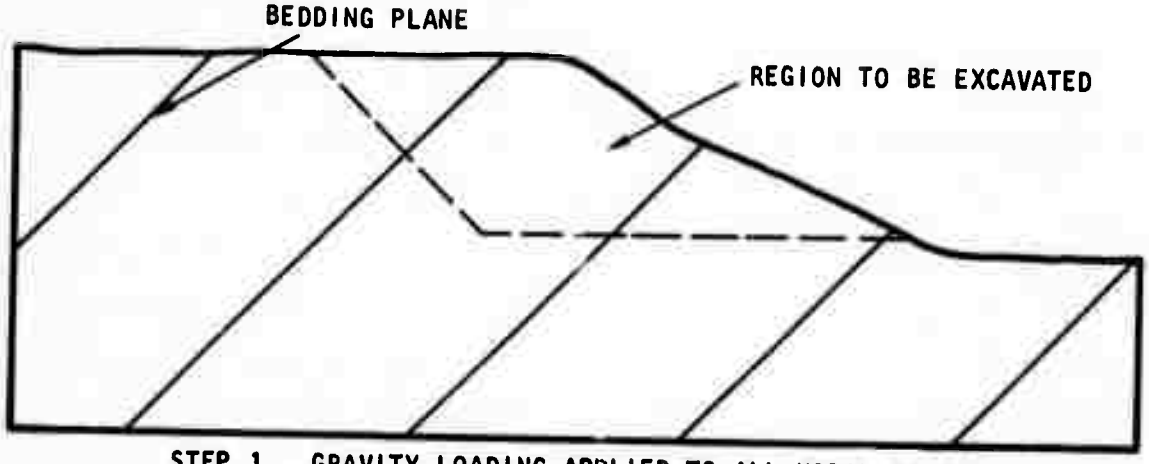

STEP 1. GRAVITY LOADING APPLIED TO ALL NODAL POINTS

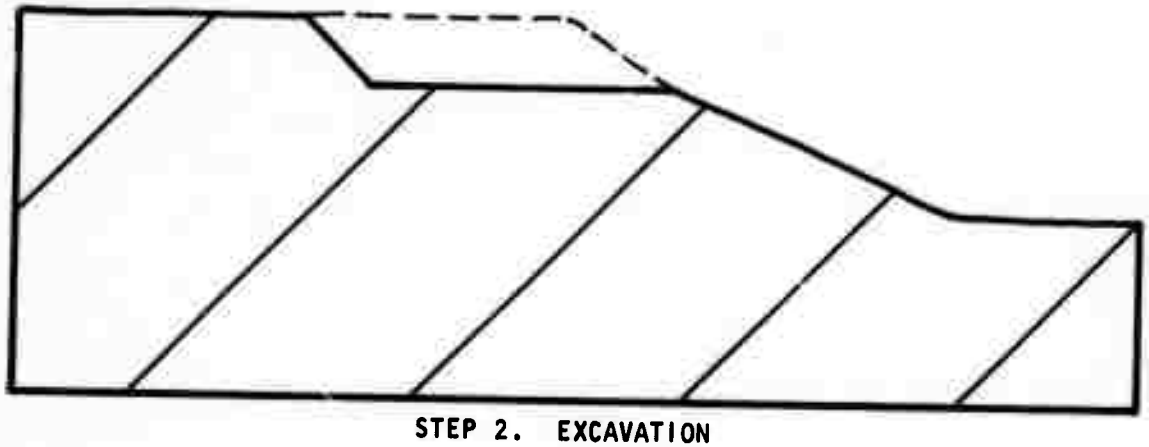

STEP 2. EXCAVATION

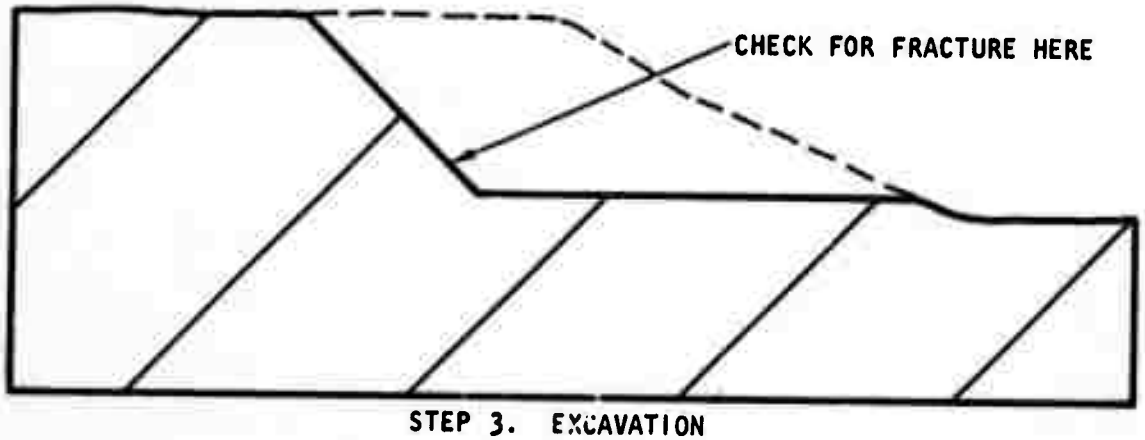

STEP 3. EXCAVATION

FIGURE 2-2. EXCAVATION OF BANK

The third example is an extension to three dimensions of the first example. The final stage in the calculation, at which the section of tunnel under consideration is fully excavated, is illustrated in Figure 2-3. Notice that the plane of the joint is not parallel to the axis of the tunnel. This problem is one of the largest and most difficult which the code is intended to handle.

Several important questions remain unanswered. First, how much do such analyses cost in terms of computing time and engineering preparation and interpretation? Second, are sufficient field data available for nonlinear and anisotropic properties of the rock and for the properties of the joints to be accurately modeled? Part of the answer to the first question can be found in Section 6 of the present report in which the computer times for solving simple checkout problems are given. More information on costs will be forthcoming at the end of this project. It appears at present that sufficient field data are not available for accurate modeling. Hopefully, the development of analytic tools such as the present program will stimulate the necessary measurements.

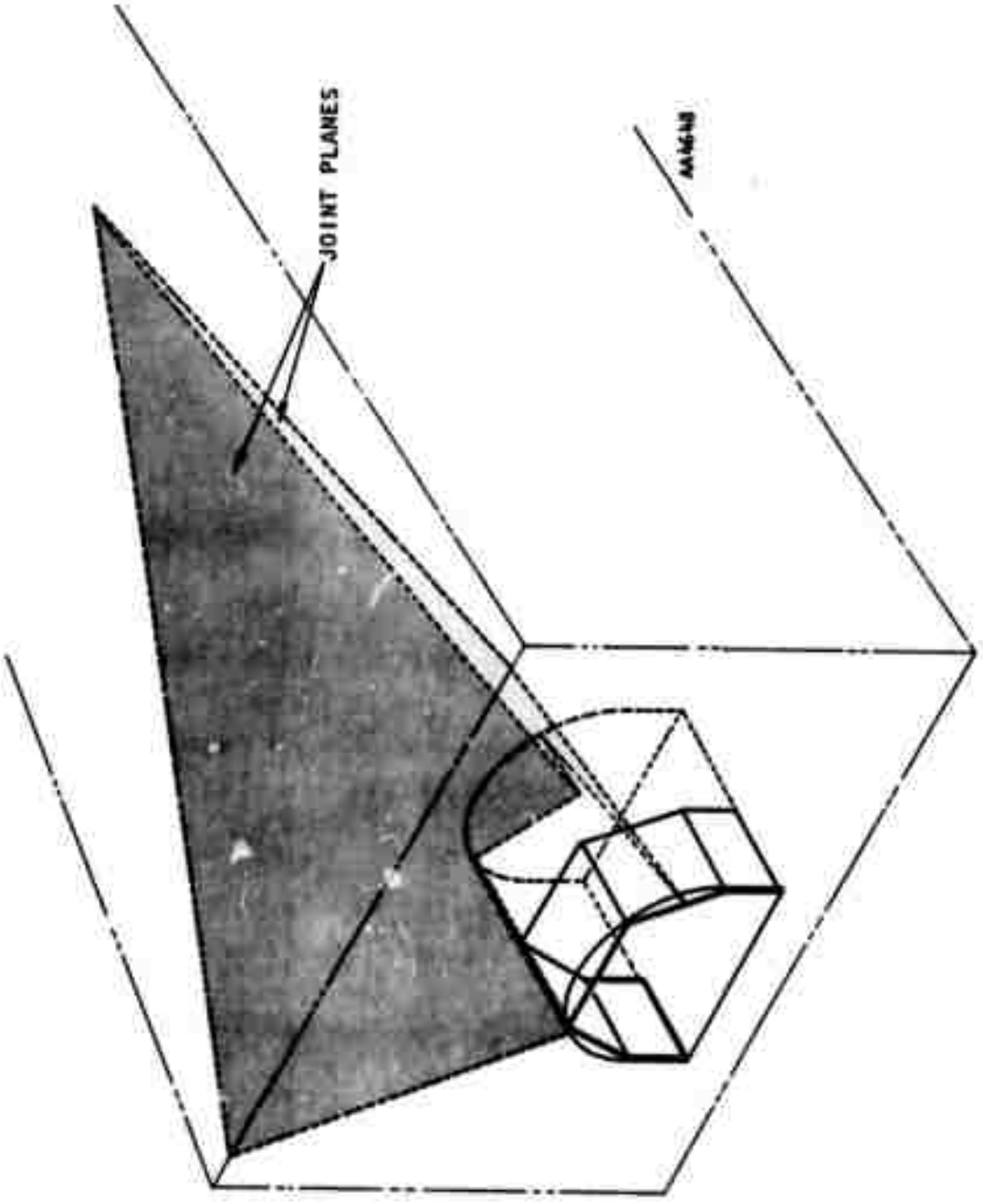

FIGURE 2-3. THREE-DIMENSIONAL TUNNEL ANALYSIS WITH JOINTS

SECTION 3

APPLICATION OF FINITE ELEMENT THEORY

This section discusses the present formulation of equations of equilibrium. The provisions to extend this formulation to large deformations is also described. Then the types of elements, including truss, beam, plane strain and axisymmetric, three-dimensional and thick shell elements are described. In addition, a new element for representing slip and debonding along planar joints is described.

3.1 SOLUTION OF NONLINEAR EQUATIONS OF EQUILIBRIUM

The matrix equation of equilibrium for a structural system with material nonlinearity is:

$$\underline{K}\,(\underline{u})\,\underline{u} = \underline{P} \qquad (3\text{-}1)$$

where the instantaneous stiffness matrix (K) is a nonlinear function of the displacement vector (u). P is the vector containing external loads. There exist numerous methods of solving the above system of nonlinear equations. In general, these methods can be divided into two classes: iterative methods and incremental methods.

Iterative methods apply the total load initially and approach the solution by modifying the stiffness matrix and/or modifying the load vector. Modification of the stiffness matrix in general accelerates the convergence but is computationally costly. The optimum may be achieved by occasional stiffness reformulation.

In incremental methods the loads are applied in several steps and an incremental form of the Equation 3-1 is solved.

$$\underline{\underline{K}}_n \, \underline{\underline{\Delta u}}_{n+1} = \underline{\underline{\Delta P}}_{n+1} \qquad (3\text{-}2)$$

where

$$\underline{\underline{\Delta u}}_{n+1} = \underline{u}_{n+1} - \underline{u}_n$$

$$\underline{\underline{\Delta P}}_{n+1} = \underline{P}_{n+1} - \underline{P}_n$$

It is important to note that the stiffness matrix K_n can only be formed based on the displacement vector from the previous step $\underline{u}_n$ which creates some step-wise error. In this simple incremental technique the step-wise errors can accumulate and lead to considerable total error. To prevent this accumulation of the step-wise error, a modified form of the load vector is used.

$$\underline{\underline{K}}_n \, \underline{\underline{\Delta u}}_{n+1} = \underline{P}_{n+1} - \underline{F}_n \qquad (3\text{-}3)$$

where

$\underline{P}_{n+1}$ = Total load vector at the end of the $(n+1)^{th}$ step

$\underline{F}_n$ = Vector of the internal resisting forces at the end of the n^{th} step

By using this method of load vector correction the equilibrium is satisfied at the beginning of each incremental step and thereby the accumulation of the step-wise error is prevented. Satisfaction of equilibrium is assured in spite of errors or approximations in the stiffness matrix and, therefore, the reformulation of the stiffness matrix is not required at every step. However, the error in each step is directly dependent on the approximation of instantaneous stiffness matrix.

An alternative method is to apply the total force from the beginning, in which case the load in Equation 3-3 will be

$$P_n = P_{total} \qquad (n=1,\ldots,N)$$

It should be noted that the application of the total loads makes this method equivalent to an iterative scheme with load vector correction which was previously discussed. However, the loads in general have a specified history dictated by the sequence of application, sequence of construction and excavation, and the time phenomenon associated with the viscous material properties. In most practical problems, the specified history of loading is a series of step functions. This is true in case of construction and excavation which can be considered as a discontinuity in force-displacement relation and an abrupt change in the instantaneous stiffness matrix.

An efficient scheme is to apply the total of the step-wise loading at each stage and then carry out several iterations with occassional stiffness reformulation to accelerate the convergence. This scheme is summarized in the following steps.

For each step:

a. Compute $\underline{u}_n = \underline{u}_{n-1} + \Delta\underline{u}_n$ (for first step; $u_o = 0$)

b. Compute the strains ($\underline{\varepsilon}_n$) or strain increments ($\Delta\underline{\varepsilon}_n$) using the derivatives of the shape functions for each element which have been initially computed and stored

c. 1. For time-independent materials compute the stress ($\underline{\sigma}_n$) and the instantaneous stress-strain relations ($\underline{C}_n$) (see section on material properties)

   2. For visco-elastic elements

      i. Compute stresses $\underline{\sigma}_n = \underline{C}\,(\underline{\varepsilon}_n - \underline{\varepsilon}^{C}_{n-1})$ where $\underline{C}$ is the elastic stress-strain matrix, $\underline{\varepsilon}_n$ is the total strain and $\underline{\varepsilon}^{C}_{n-1}$ is the total creep strain

ii. Using the stresses, compute $\underline{\varepsilon}_n^c$ which is the total creep strain at the end of the time step (see section on material properties)

iii. Compute effective stress

$$\bar{\underline{\sigma}}_n = \underline{C}\,(\underline{\varepsilon}_n - \underline{\varepsilon}_n^c)$$

d. Compute the internal resisting forces from the stresses (effective stresses for viscoelastic elements). If it is stiffness update cycle, compute stiffness matrix.

e. Solve Equation 3-3 to obtain $\Delta\underline{u}_{n+1}$. Compute $\gamma = \|\Delta\underline{u}_{n+1}\|$.

f. If a specified number of iteration has been reached or if $\gamma \leq \varepsilon$ (ε is a specified quantity), go to Step *g*; otherwise, go to Step *a* and repeat the iteration.

g. Apply the next loading step and go to Step *a*.

3.2 EQUATIONS OF EQUILIBRIUM FOR LARGE DEFORMATIONS

The method of large deformation finite element analysis to be used in the present computer program was initially introduced by Sharifi and Yates, Reference 3-1.

The matrix equations of equilibrium (or motion) are derived from an incremental virtual work expression and the original configuration of the finite element system is taken as the reference configuration. This choice of the reference state eliminates the need for updating of the coordinates of the nodal points which is computationally a costly operation.

The incremental virtual work expression is

$$\int_{A_o} (t_n + \Delta t_n)\, \delta\Delta U_n dA_o - \int_{V_o} S_{ij}\, \delta\Delta\varepsilon_{ij} dV_o = \int_{V_o} S_{ij}\, \delta\Delta\eta_{ij} dV_o + \int_{V_o} \Delta S_{ij}\, \delta\Delta\varepsilon ij\, dV_o \tag{3-4}$$

where

u_k = Component of displacement vector

Δu_k = Incremental component of displacement vector

t_k = Component of traction vector

Δt_k = Incremental component of traction vector

S_{ij} = Component of Piola stress tensor

ΔS_{ij} = Incremental component of Piola stress tensor

$\Delta\varepsilon_{ij}$ = Linear component of incremental strain tensor

$\Delta\eta_{ij}$ = Nonlinear component of incremental strain tensor

The stresses and traction are referred to the area and the coordinates of the original configuration:

$$\Delta\varepsilon_{ij} = \Delta u_{i,j} + \Delta u_{j,i} + u_{k,i}\Delta u_{k,j} + u_{k,j}\Delta u_{k,i} \tag{3-5a}$$

$$\Delta\eta_{ij} = \Delta u_{k,i}\Delta u_{k,j} \tag{3-5b}$$

The total and incremental displacements within each element can be expressed in terms of the nodal point values of the displacements through shape functions

$$u_i = \underline{H}\,\underline{U}_i \tag{3-6a}$$

$$\Delta u_i = \underline{H}\,\underline{\Delta U}_i \tag{3-6b}$$

where $\underline{H}$ is the vector of the shape functions and $\underline{U}_i$ and $\underline{\Delta U}_i$ are the vectors of the total and incremental displacements of the element nodes.

Without loss of generality the remaining part of this section will be devoted to the derivation of the appropriate matrices for the two-dimensional quadrilateral element.

Substituting the Equation 3-6 into Equation 3-5 will result in the following expressions for the strain increments in terms of the nodal point displacements:

$$\begin{aligned}
\Delta\varepsilon_{xx} &= \underline{H}_{,x}\ \Delta\underline{U}_x + (\underline{H}_{,x}\ \underline{U}_x)\ \ (\underline{H}_{,x}\ \Delta\underline{U}_x) + (\underline{H}_{,x}\ \underline{U}_y)\ \ (\underline{H}_{,x}\ \underline{\Delta U}_y) \\
\Delta\varepsilon_{yy} &= \underline{H}_{,y}\ \Delta\underline{U}_y + (\underline{H}_{,y}\ \underline{U}_x)\ \ (\underline{H}_{,y}\ \Delta\underline{U}_x) + (\underline{H}_{,y}\ \underline{U}_y)\ \ (\underline{H}_{,y}\ \underline{\Delta U}_y) \\
\Delta\varepsilon_{xy} &= \underline{H}_{,x}\ \Delta\underline{U}_y + \underline{H}_{,y}\ \Delta\underline{U}_x + (\underline{H}_{y}\ \underline{U}_x)\ \ (\underline{H}_{,y}\ \Delta\underline{U}_x) + (\underline{H}_{,y}\ \underline{U}_y) \\
&\quad (\underline{H}_{,x}\ \Delta\underline{U}_y) + (\underline{H}_{,x}\ \underline{U}_x)\ \ (\underline{H}_{,y}\ \Delta\underline{U}_x) + (\underline{H}_{,y}\ \Delta\underline{U}_y)
\end{aligned} \tag{3-7}$$

The above equations can be written as matrix form

$$\Delta\underline{\varepsilon} = \underline{B}\,(\underline{I} + \underline{E})\,\Delta\underline{U} = \tilde{\underline{B}}\,\Delta\underline{U} \tag{3-8}$$

where $\underline{I}$ is the identity matrix and

$$\underline{\varepsilon} = \begin{Bmatrix} \varepsilon_{xx} \\ \varepsilon_{yy} \\ \varepsilon_{xy} \end{Bmatrix} \qquad \Delta\underline{U} = \begin{Bmatrix} \Delta\underline{U}_x \\ \Delta\underline{U}_y \end{Bmatrix} \tag{3-9}$$

$$\underline{B} = \begin{bmatrix} \underline{H},_x & \underline{0} \\ \underline{0} & \underline{H},_y \\ \underline{H},_x & \underline{H},_y \end{bmatrix} \qquad \underline{E} = \begin{bmatrix} \underline{U}_x\, H,_x & \underline{U}_y\, \underline{H},_x \\ \underline{U}_x\, H,y & \underline{U}_y\, \underline{H},_y \end{bmatrix} \tag{3-10}$$

$\underline{B}$ is the usual strain-displacement matrix for infinitesimal deformation and $\underline{E}$ is the large deformation contribution.

The linear and geometric stiffness matrices and the load correction vector are

$$\underline{k}_e = \int_{v_m} \tilde{\underline{B}}^T \underline{C}\, \tilde{\underline{B}}\, dv_m \tag{3-11}$$

$$\underline{k}_g = \int_{v_m} \underline{B}^T \underline{S}\, \underline{B}\, dv_m \tag{3-12}$$

$$\underline{f} = \int_{v_m} \tilde{\underline{B}}^T \underline{S}\, dv_m \tag{3-13}$$

where v_m is the area of each element in original configuration, and $\underline{C}$ is the instantaneous stress-strain relation

$$\Delta\underline{S} = \underline{C}\, \Delta\, \underline{\varepsilon} \tag{3-14}$$

Finally, the matrix equation of equilibrium is

$$(\underline{K}_e + \underline{K}_g)\, \Delta\underline{U} = \underline{R} - \underline{F} \tag{3-15}$$

It is important to note that for the computation of the above matrices only the derivatives of the shape functions H,x and H,y at original geometry of each element is required. Therefore, these derivatives at integration points, can be computed in the first part of the program.

3.3 STRUCTURAL FINITE ELEMENTS

A description of the structural elements incorporated in this computer program are given here. The beam and thick shell elements have linear elastic properties. All other elements are capable of representing nonlinear properties.

3.3.1 THREE-DIMENSIONAL TRUSS ELEMENTS

The truss element is the conventional space truss member which can resist compression or tension along its axis. It can also be used to model bolts. The truss member is subject to three translations at each end of the member as shown in Figure 3-1a. The member stiffness matrix is of order 6×6. The material and geometrical properties are defined by the tangent Young's modulus, and the cross-sectional area of the element.

3.3.2 THREE-DIMENSIONAL BEAM ELEMENTS

The three-dimensional beam element is subject to three translations and three rotations at each end of the member. The generalized forces and the generalized displacements associated with the six-degrees-of-freedom (DOF) at each end are shown in Figure 3-1b.

The geometrical properties of the beam element are specified by an axial and two shear areas and three principal moments of inertia, two associated with bending and one with torsion. Young's modulus and Poisson's ratio are required to define the material properties of the beam element.

The element stiffness matrix is of order 12×12 and is obtained from the classical beam theory including the effects of the shear deformations.

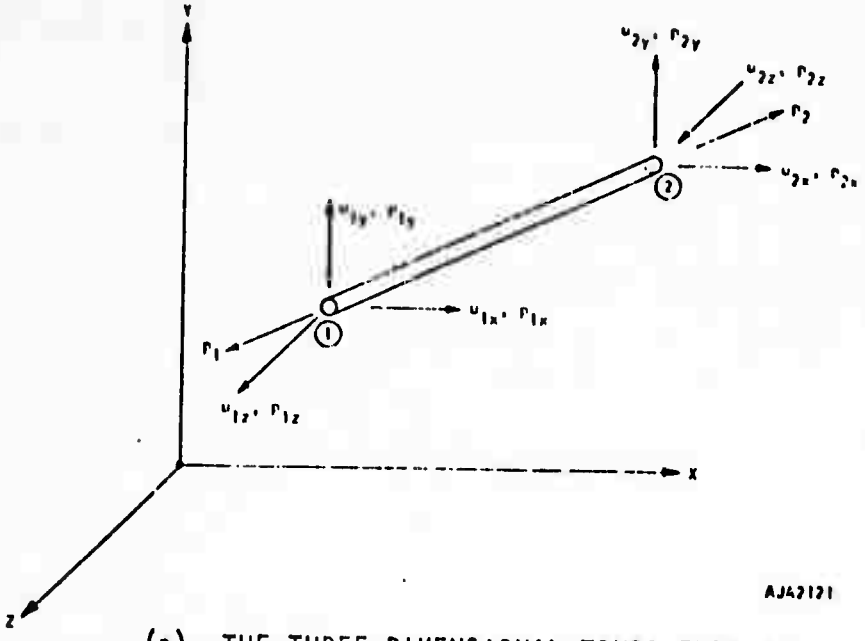

(a) THE THREE-DIMENSIONAL TRUSS ELEMENT

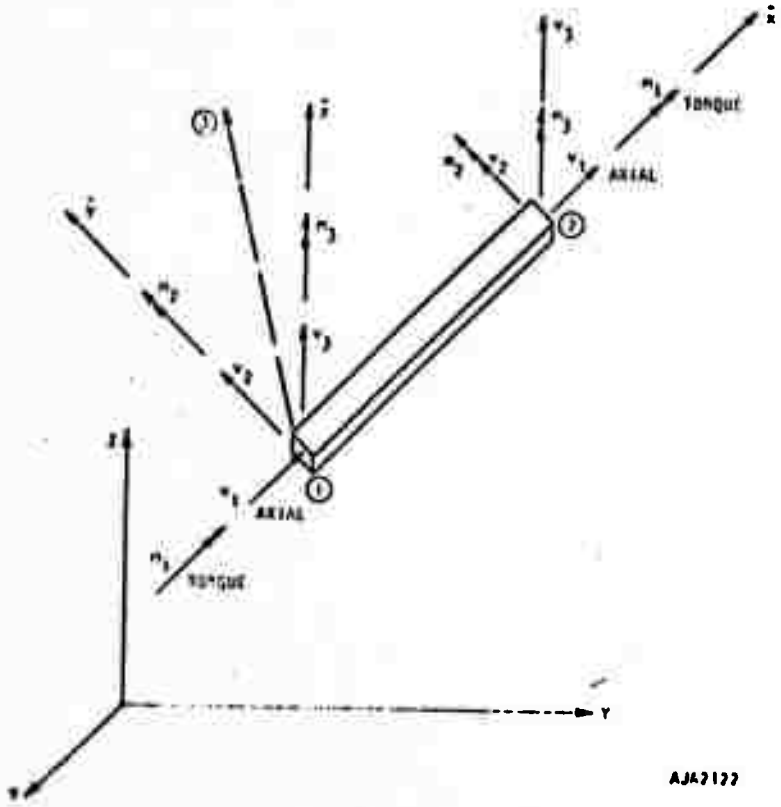

(b) THE THREE-DIMENSIONAL BEAM ELEMENT.

FIGURE 3-1. TRUSS AND BEAM ELEMENT

A provision for the member end boundary conditions accounts for hinges and other releases.

3.3.3 TWO-DIMENSIONAL PLANE STRAIN AND AXISYMMETRIC ELEMENTS

Quadrilateral isoparametric elements will be used in the computer program. For a general quadrilateral element, as shown in Figure 3-2, the local and global coordinate systems are related by

$$x = \sum_{i=1}^{4} h_i x_i$$
$$y = \sum_{i=1}^{4} h_i y_i \qquad (3\text{-}16)$$

where the interpolation functions are given by

$$h_1 = 1/4\ (1-s)\ (1-t)$$
$$h_2 = 1/4\ (1+s)\ (1-t)$$
$$h_3 = 1/4\ (1+s)\ (1+t) \qquad (3\text{-}17)$$
$$h_4 = 1/4\ (1-s)\ (1+t)$$

The same interpolation functions are used in the displacement approximation.

$$u_x\ (s,t) = \Sigma\ h_i\ u_{xi} + h_5\ \alpha_1 + h_6\ \alpha_2$$
$$u_y\ (s,t) = \Sigma\ h_i\ u_{yi} + h_5\ \alpha_3 + h_6\ \alpha_4 \qquad (3\text{-}18)$$

where

$$h_5 = (1-s^2)$$
$$h_6 = (1-t^2)$$

h_5 and h_6 are the incompatible interpolation functions.

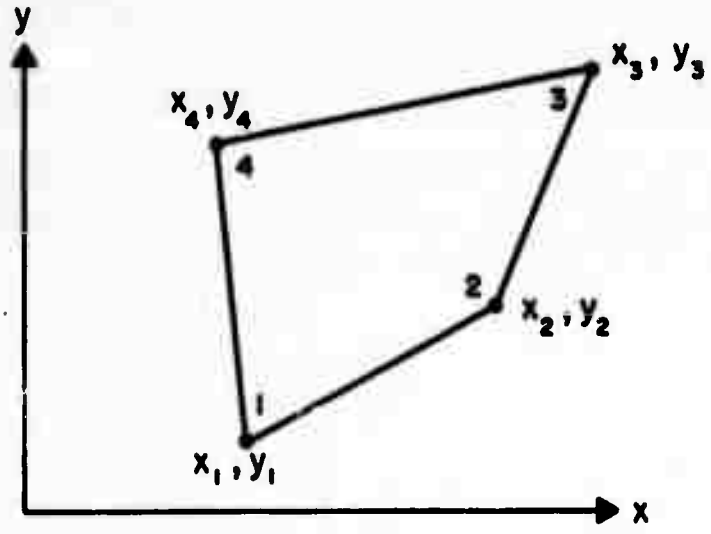

a. GLOBAL SYSTEM

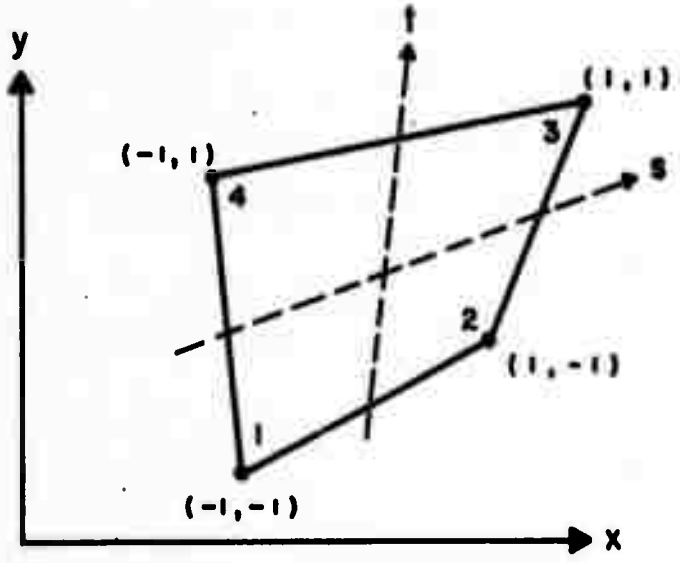

b. LOCAL SYSTEM

FIGURE 3-2. TWO-DIMENSIONAL ISOPARAMETRIC ELEMENT

For two-dimensional analysis the strain-displacement equations are

$$\varepsilon_{xx} = \frac{\partial u_x}{\partial x} = \Sigma\, h_{i,x}\, u_{xi} + h_{5,x}\,\alpha_1 + h_{6,x}\,\alpha_2$$

$$\varepsilon_{yy} = \frac{\partial u_y}{\partial y} = \Sigma\, h_{i,y}\, u_{yi} + h_{5,y}\,\alpha_3 + h_{6,y}\,\alpha_4$$

$$\varepsilon_{xy} = \frac{\partial u_x}{\partial y} + \frac{\partial u_y}{\partial x} = \Sigma\, h_{i,y}\, u_{xi} + \Sigma\, h_{i,x}\, u_{yi} + H_{5,y}\alpha_1 + h_{6,y}\alpha_2 + h_{5,x}\alpha_3 + h_{6,x}\alpha_4 \qquad (3\text{-}19)$$

Or Equation 3-19 can be written in matrix form as

$$\underline{\varepsilon} = \underline{B}\,\underline{U} = \begin{bmatrix} \underline{H},x & 0 \\ 0 & \underline{H},y \\ \underline{H},y & \underline{H},x \end{bmatrix} \begin{bmatrix} \underline{U}x \\ \underline{U}y \end{bmatrix} \qquad (3\text{-}20)$$

In this case the three strains are related to the eight nodal point displacements and four coefficients of incompatible displacement functions by a 3 x 12 matrix. The submatrices in Equation 3-20 are given by

$$\underline{H},_x = [h_{1,x}\ h_{2,x}\ h_{3,x}\ h_{4,x},\ h_{5,x},\ h_{6,x}]$$

$$\underline{H},_y = [h_{1,y}\ h_{2,y}\ h_{3,y}\ h_{4,y},\ h_{5,y},\ h_{6,y}] \qquad (3\text{-}21)$$

The element stiffness matrix is given by the following equation:

$$\underline{k} = \int_v \underline{B}^T\, \underline{C}\, B\, dv \qquad (3\text{-}22)$$

where $\underline{C}$ is the stress-strain matrix. The above equation is integrated numerically

$$\underline{k} = \sum_{l} \underline{B}_l^T \underline{C} B_l \qquad (3\text{-}23)$$

This stiffness matrix which is 12 x 12 is reduced to 8 x 8 by elimination of the four incompatible modes before assembling in the global stiffness matrix.

3.3.4 THREE-DIMENSIONAL ELEMENT

For an arbitrary eight-point brick element shown in Figure 3-3, the appropriate displacement approximations are

$$\begin{aligned} u_x &= \sum_{i=1}^{8} u_{xi} + h_9 \alpha_{x1} + h_{10} \alpha_{x2} + h_{11} \alpha_{x3} \\ u_y &= \sum_{i=1}^{8} u_{yi} + h_9 \alpha_{y1} + h_{10} \alpha_{y2} + h_{11} \alpha_{y3} \qquad (3\text{-}24) \\ u_z &= \sum_{i=1}^{8} u_{zi} + h_9 \alpha_{z1} + h_{10} \alpha_{z2} + h_{11} \alpha_{z3} \end{aligned}$$

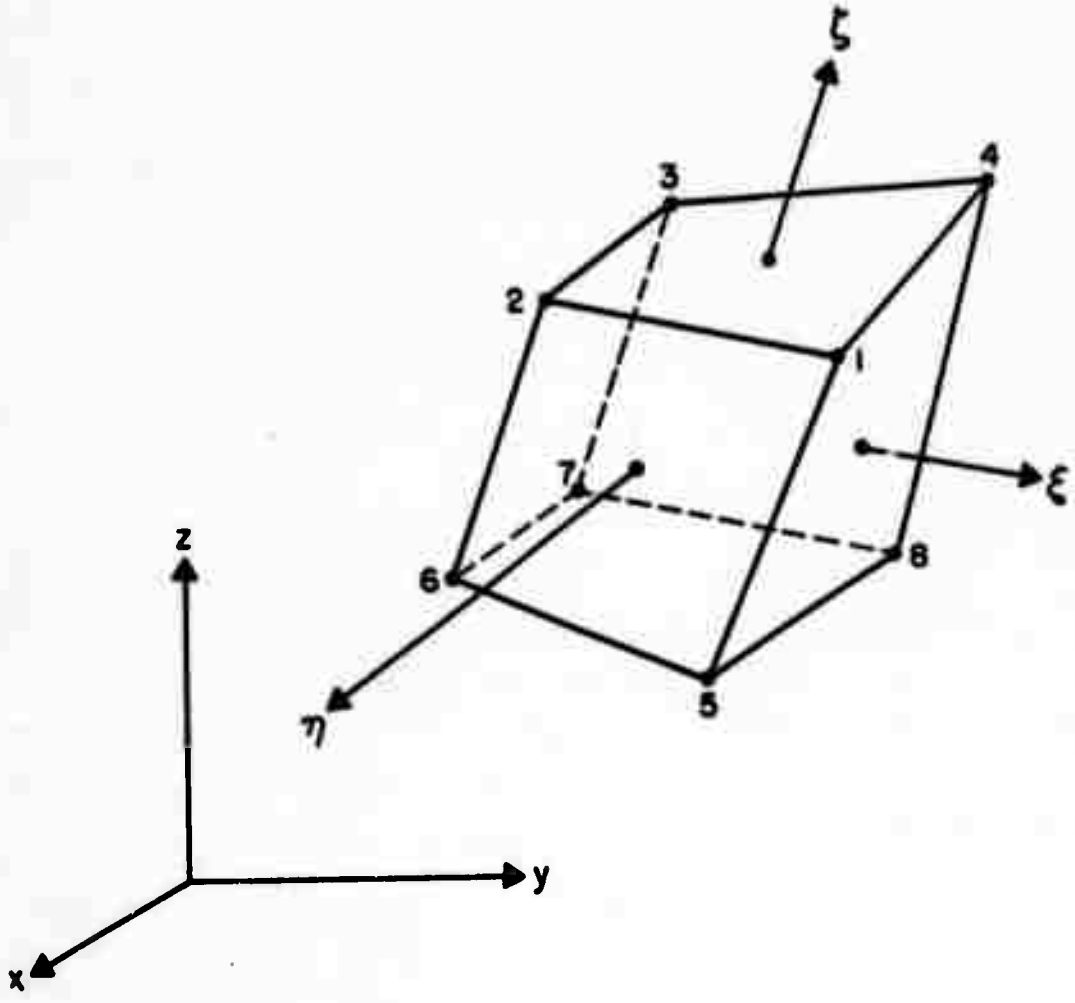

FIGURE 3-3. EIGHT-POINT THREE-DIMENSIONAL ELEMENT

where

$$
\begin{aligned}
h_1 &= 1/8\ (1 + \xi)\ (1 + \eta)\ (1 + \zeta) \\
h_2 &= 1/8\ (1 - \xi)\ (1 + \eta)\ (1 + \zeta) \\
h_3 &= 1/8\ (1 - \xi)\ (1 - \eta)\ (1 + \zeta) \\
h_4 &= 1/8\ (1 + \xi)\ (1 - \eta)\ (1 + \zeta) \\
h_5 &= 1/8\ (1 + \xi)\ (1 + \eta)\ (1 - \zeta) \\
h_6 &= 1/8\ (1 - \xi)\ (1 + \eta)\ (1 - \zeta) \\
h_7 &= 1/8\ (1 - \xi)\ (1 - \eta)\ (1 - \zeta) \\
h_8 &= 1/8\ (1 + \xi)\ (1 - \eta)\ (1 - \zeta) \\
h_9 &= (1 - \xi^2) \\
h_{10} &= (1 - \eta^2) \\
h_{11} &= (1 - \zeta^2)
\end{aligned}
\qquad (3\text{-}25)
$$

The first eight are the standard compatible interpolation functions. The last three are incompatible and are associated with linear shear and normal strains. The nine incompatible modes are eliminated at the element stiffness level by static condensation.

3.3.5 THICK SHELL ELEMENTS

The thick shell element described here was initially developed by Wilson, et al., Reference 3-3.

This shell element is a 16-node curved solid element shown in Figure 3-4. Each node has three unknown displacements. Therefore, if the shell is considered as a two-dimensional surface there are six unknowns per point. It is apparent that this type of formulation avoids the problems associated with the sixth degree of freedom--the normal rotation is set to zero when certain finite elements are used in the idealization of shells.

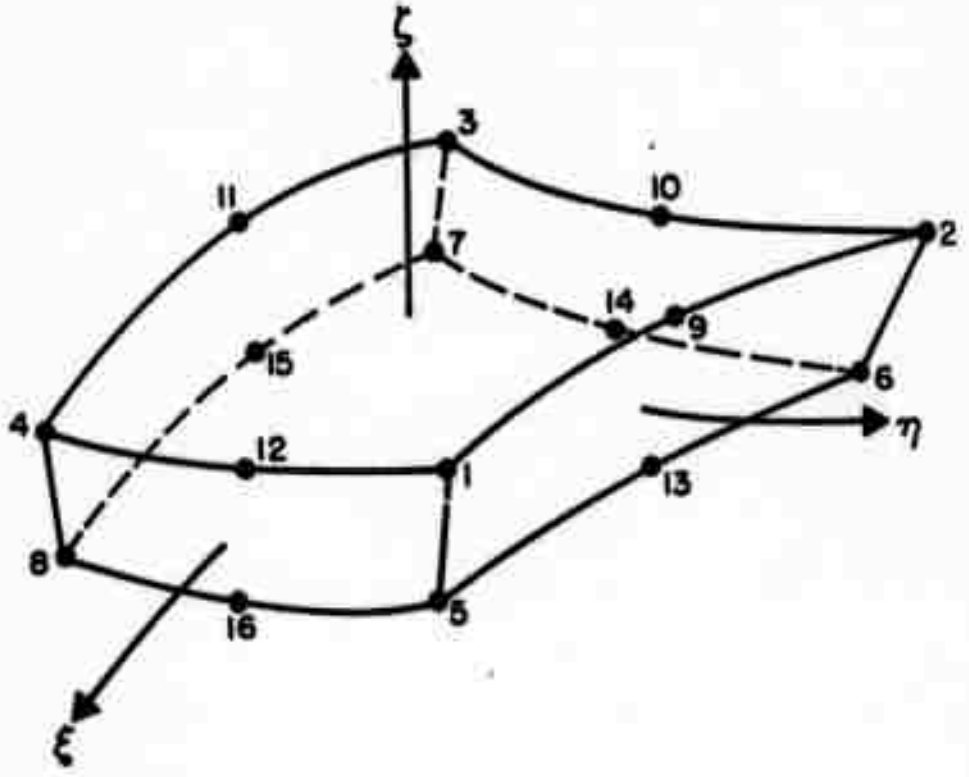

FIGURE 3-4. THREE-DIMENSIONAL THICK-SHELL ELEMENT

The locations of the nodes are defined by the orthogonal, right-handed coordinate system (x, y, z) which is referred to as a global system. Within the element a local coordinate system (ξ, η, ζ) has been chosen such that ξ, η, ζ vary from -1 to +1; (0, 0, 0) is located at the centroid of the element.

The local and global coordinate systems are related through a set of interpolating functions:

$$x = \sum_{i=1}^{16} h_i x_i$$

$$y = \sum_{i=1}^{16} h_i y_i \qquad (3\text{-}26)$$

$$z = \sum_{i=1}^{16} h_i z_i$$

where

$$
\begin{aligned}
h_1 &= 1/8\,(1+\xi)\,(1+\eta)\,(1+\zeta)\,(\xi+\eta-1)\\
h_2 &= 1/8\,(1-\xi)\,(1+\eta)\,(1+\zeta)(-\xi+\eta-1)\\
h_3 &= 1/8\,(1-\xi)\,(1-\eta)\,(1+\zeta)(-\xi-\eta-1)\\
h_4 &= 1/8\,(1+\xi)\,(1-\eta)\,(1+\zeta)\,(\xi-\eta-1)\\
h_5 &= 1/8\,(1+\xi)\,(1+\eta)\,(1-\zeta)\,(\xi+\eta-1)\\
h_6 &= 1/8\,(1-\xi)\,(1+\eta)\,(1-\zeta)(-\xi+\eta-1)\\
h_7 &= 1/8\,(1-\xi)\,(1-\eta)\,(1-\zeta)(-\xi-\eta-1)\\
h_8 &= 1/8\,(1+\xi)\,(1-\eta)\,(1-\zeta)\,(\xi-\eta-1)\\
h_9 &= 1/4\,(1-\xi^2)\,(1+\eta)\,(1+\zeta)\\
h_{10} &= 1/4\,(1-\xi)\,(1-\eta^2)\,(1+\zeta)\\
h_{11} &= 1/4\,(1-\xi^2)\,(1-\eta)\,(1+\zeta)\\
h_{12} &= 1/4\,(1+\xi)\,(1-\eta^2)\,(1+\zeta)\\
h_{13} &= 1/4\,(1-\xi^2)\,(1+\eta)\,(1-\zeta)\\
h_{14} &= 1/4\,(1-\xi)\,(1-\eta^2)\,(1-\zeta)\\
h_{15} &= 1/4\,(1-\xi^2)\,(1-\eta)\,(1-\zeta)\\
h_{16} &= 1/4\,(1+\xi)\,(1-\eta^2)\,(1-\zeta)
\end{aligned}
\qquad (3\text{-}27)
$$

The displacements within the element are assumed to be of the following form:

$$
\begin{aligned}
u_x &= \sum_{i=1}^{16} h_i\, u_{xi} + h_{17}\,\alpha_{x1} + h_{18}\,\alpha_{x2} + h_{19}\,\alpha_{x3} + h_{20}\,\alpha_{x4} + h_{21}\,\alpha_{x5}\\
u_y &= \sum_{i=1}^{16} h_i\, u_{yi} + h_{17}\,\alpha_{y1} + h_{18}\,\alpha_{y2} + h_{19}\,\alpha_{y3} + h_{20}\,\alpha_{y4} + h_{21}\,\alpha_{y5}\\
u_z &= \sum_{i=1}^{16} h_i\, u_{zi} + h_{17}\,\alpha_{z1} + h_{18}\,\alpha_{z2} + h_{19}\,\alpha_{z3} + h_{20}\,\alpha_{z4} + h_{21}\,\alpha_{z5}
\end{aligned}
\qquad (3\text{-}28)
$$

where

$$h_{17} = \xi (1 - \xi^2)$$

$$h_{18} = \eta (1 - \eta^2)$$

$$h_{19} = (1 - \zeta^2) \qquad (3\text{-}29)$$

$$h_{20} = \xi\eta (1 - \xi^2)$$

$$h_{21} = \eta\xi (1 - \eta^2)$$

The motivation for addition of the interpolation functions h_{17} to h_{21} is to increase the capability of the element in producing closer approximations to the exact displacements under simple loadings, thereby increasing the convergence to exact solution. The incompatible interpolation functions h_{17} to h_{21} have zero values at the nodes and produce incompatibilities in displacement field along the interelement boundaries.

3.4 JOINT FINITE ELEMENT

The joint element is intended to represent the rock joints, faults, interfaces and similar discontinuities in continuum systems. The joint element has the capability of representing the main characteristics of the deformation behavior of the rock joints such as debonding and slip. The term debonding means the ability of separation of the two blocks of continuum adjacent to the joint surface which were initially in contact. Subsequent contact can also develop by the movement of the two blocks towards each other. The term slip means the relative motion along the joint surface or fault when the shearing force exceeds the shear strength of the joint.

Previous attempts have been made to develop discrete elements to represent the joint behavior. Goodman, Taylor and Brekke (Reference 3-2) developed a simple rectangular, two-dimensional element with eight degrees of freedom. This element has no thickness, and therefore the adjacent blocks

of continuum elements can penetrate into each other. Zienkiewicz, et al., (Reference 3-4) advocate the use of continuum isoparametric elements with a simple nonlinear material property for shear and normal stresses, assuming uniform strain in the thickness direction. Numerical difficulties may arise from ill conditioning of the stiffness matrix due to very large off-diagonal terms or very small diagonal terms which are generated by these elements in certain cases.

To avoid such numerical problems a new joint element is developed below, which uses relative displacements as the independent degrees of freedom. The displacement degrees of freedom of one side of the slip surface are transformed into the relative displacements between the two sides of the slip surface. The transformation relations are as follows:

$$u^T_{xi} = u^B_{xl} + \Delta u_{xi}$$

$$u^T_{yi} = u^B_{yl} + \Delta u_{yi}$$

$$u^T_{xj} = u^B_{xk} + \Delta u_{xj}$$

$$u^T_{yj} = u^B_{yk} + \Delta u_{yj}$$

The superscripts T and B refer to the top and bottom elements with respect to the slip surface respectively. As shown in Figure 3-5, those degrees of freedom of the upper element which are on the slip surface are transformed but the degrees of freedom of the lower element are the original displacement quantities.

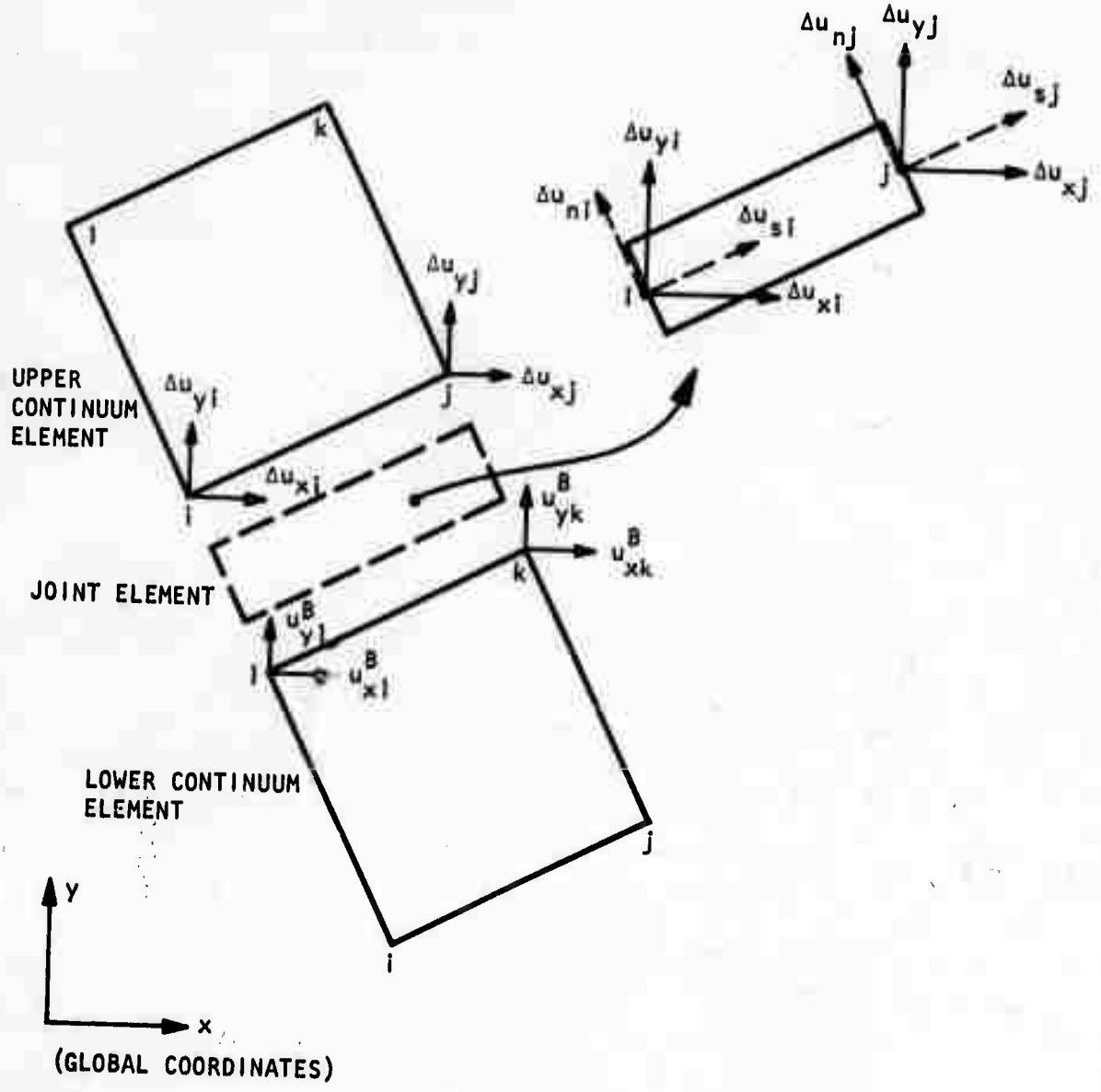

$$u^T_{xi} = u^B_{xl} + \Delta u_{xi}$$

$$u^T_{yi} = u^B_{yl} + \Delta u_{yi}$$

$$u^T_{xj} = u^B_{xk} + \Delta u_{xj}$$

$$u^T_{yj} = u^B_{yk} + \Delta u_{yj}$$

FIGURE 3-5. GEOMETRY OF JOINT ELEMENT

The joint element is assumed to have the relative displacements as the degrees of freedom. For example, in a two-dimensional problem the joint element will have four degrees of freedom (Figure 3-6). The relative normal and tangential displacements, Δu_n and Δu_s, are assumed to vary linearly along the element as follows

$$\begin{aligned} \Delta u_n &= h_i \Delta u_{ni} + h_j \Delta u_{nj} \\ \Delta u_s &= h_i \Delta u_{si} + h_j \Delta u_{sj} \end{aligned} \tag{3-30}$$

where the h_i and h_j are the linear interpolation functions

$$\begin{aligned} h_i &= \frac{1}{2}(1 - \xi) \\ h_j &= \frac{1}{2}(1 + \xi) \end{aligned} \tag{3-31}$$

and Δu_{ni}, Δu_{nj}, Δu_{si} and Δu_{sj} are the nodal point values of the relative displacements. The joint element is assumed to have only two strain components; ε_n = normal strain, and ε_s = shear strain. These two strain components are related to the relative displacements through the following relations.

$$\begin{aligned} \varepsilon_n &= \frac{1}{t} \Delta u_n \\ \varepsilon_s &= \frac{1}{t} \Delta u_s \end{aligned} \tag{3-32}$$

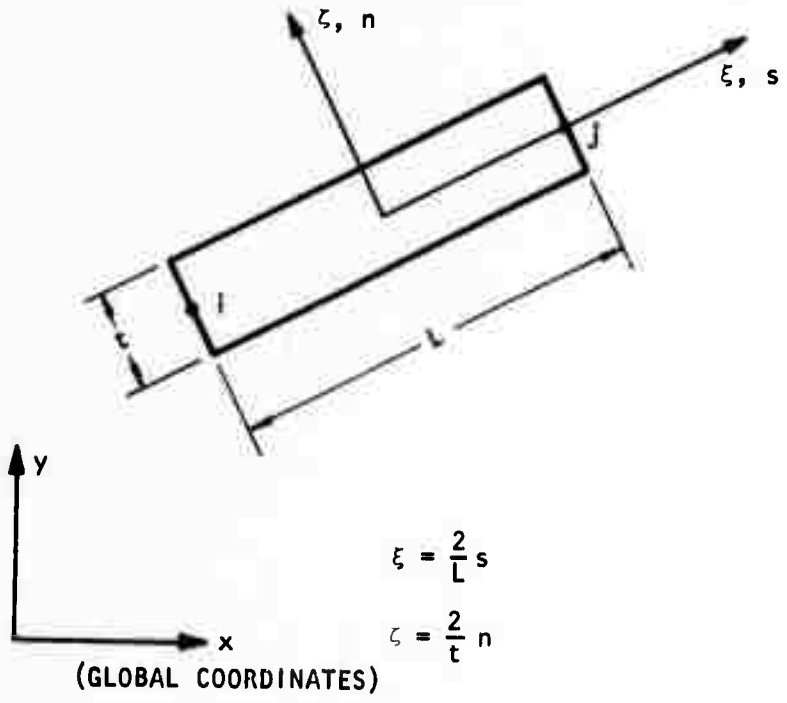

FIGURE 3-6. COORDINATE SYSTEMS FOR JOINT ELEMENT

The substitution of Equations 3-30 and 3-31 into Equation 3-32 results in the strain-displacement relation for the element

$$\begin{Bmatrix} \varepsilon_n \\ \varepsilon_s \end{Bmatrix} = \frac{1}{2t} \begin{bmatrix} (1-\xi) & 0 & (1+\xi) & 0 \\ 0 & (1-\xi) & 0 & (1+\xi) \end{bmatrix} \begin{Bmatrix} \Delta u_{ni} \\ \Delta u_{si} \\ \Delta u_{nj} \\ \Delta u_{sj} \end{Bmatrix} \tag{3-33}$$

$$\underline{\varepsilon} = \underline{B}\ \Delta\underline{U}$$

The stresses and the strains are related through the following material property matrix $\underline{C}$.

$$\begin{Bmatrix} \sigma_n \\ \sigma_s \end{Bmatrix} = \begin{bmatrix} C_{nn} & C_{ns} \\ C_{sn} & C_{ss} \end{bmatrix} \begin{Bmatrix} \varepsilon_n \\ \varepsilon_s \end{Bmatrix} \tag{3-34}$$

$$\underline{\sigma} = \underline{C}\ \underline{\varepsilon}$$

In general the above stress/strain relationship for rock joints is nonlinear, the details of which are given in Section 4.

The stiffness matrix for the joint element is formed in n-s coordinate system;

$$\underline{k}_{ns} = \int_v \underline{B}^T \underline{C}\ \underline{B}\ dv \tag{3-35}$$

and transformed to the x-y coordinate system as follows

$$\underline{k} = \underline{T}^T \underline{k}_{ns} \underline{T} \tag{3-36}$$

where $\underline{T}$ is the transformation matrix containing the direction cosines.

$$\underline{k} = \frac{L}{6t} \begin{bmatrix} 2(A_1 - 2B_1) & 2(A_3 + B_2) & (A_1 - 2B_1) & (A_3 + B_2) \\ & 2(A_2 + 2B_1) & (A_3 + B_2) & (A_2 + 2B_1) \\ & \text{Symmetric} & 2(A_1 - 2B_1) & 2(A_3 + B_2) \\ & & & 2(A_2 + 2B_2) \end{bmatrix} \tag{3-37}$$

where

$$A_1 = C_{ss}a^2 + C_{nn}b^2 \qquad B_1 = C_{ns}ab$$

$$A_2 = C_{ss}b^2 + C_{nn}a^2 \qquad B_2 = C_{ns}(a^2 - b^2)$$

$$A_3 = (C_{nn} - C_{ss})\, ab$$

$$a = \frac{1}{L}(x_j - x_i)$$

$$b = \frac{1}{L}(y_j - y_i)$$

REFERENCES

3-1. Sharifi, F., and D. Yates, *Nonlinear Thermo-Elastic-Plastic and Creep Analysis by the Finite Element Method*, Missile Systems Division, Lockheed Missile and Space Company.

3-2. Goodman, R. E., R. L. Taylor, and T. L. Brekke, "A Model for the Mechanics of Jointed Rock," *J. Soil Mech., ASCE*, Vol. 94, SM3, 1968.

3-3. Wilson, E. L., et al., *Incompatible Displacement Models*, ONR Symposium on Matrix Methods in Structural Mechanics, Univ. of Illinois, Urbana, Illinois.

3-4. Zienkiewicz, O. C., et al., "Analysis of Nonlinear Problems in Rock Mechanics with Particular Reference to Jointed Rock Systems," *Proc. of 2nd Cong. of Int. Soc. for Rock Mech.*, Belgrade, 1970.

SECTION 4

REPRESENTATION OF PROPERTIES OF ROCK, INCLUDING ANISOTROPY, INELASTICITY, RATE EFFECTS AND PROPERTIES OF FAULTS OR JOINTS

The first part of this section describes homogeneous properties of rock which are available in the AA computer program. As used here, "homogeneous" refers to properties which can reasonably be averaged over several feet, which is a typical dimension of a finite element in applications to mining engineering. Inhomogeneous properties of rock masses, such as those caused by faulting, are treated by a separate procedure which is described in the second part.

The topics which are covered below include the following:

a. Inelasticity

   1. Variable modulus
   2. Variable modulus with perfect plasticity
   3. Variable modulus with perfectly plastic fracture criterion and strain hardening cap

b. Anisotropy

   1. Variable modulus with anisotropic fracture criterion based on the hypothesis of Jaeger (plane geometry only)
   2. Variable modulus with anisotropic yield criterion based on the hypothesis of Hill

c. Rate Effects (Isotropic Only)

   1. Creep (series of Kelvin elements)
   2. Viscoplasticity (based on work of Perzyna)

d. Joint Properties

1. Dilatant

2. Nondilitant

4.1 HOMOGENEOUS PROPERTIES

These models, which are also summarized in Table 4-1, afford some material descriptions which probably cannot be effectively used at present owing to the lack of experimental data on rock from particular mines. As analysis increases in effectiveness, it is expected that more data will be routinely obtained, thus enabling more sophisticated material models to be used. Advantages and disadvantages of these models are summarized in Table 4-2. Typical laboratory properties for rocks are shown in Figure 4-1.

TABLE 4-1. SUMMARY OF AVAILABLE MATERIAL PROPERTIES

Type of Model	Material Characteristics				
	Isotropic	Anisotropic	Viscoelastic	Viscoplastic	Inviscid
Constant elastic moduli	X	0	X		0
Variable moduli	X	0			X,0
Elastic/plastic (fixed static yield surface)					
Constant moduli	X	0		X	0
Variable moduli	X	0		X	0
Cap model	X				X

X options or 0 options may be used simultaneously, but X and 0 options may not be mixed, except where noted.

TABLE 4-2. ADVANTAGES AND DISADVANTAGES OF EACH MODEL

Advantages	Disadvantages
A. Elastic-ideally Plastic	
Simple to fit to data	May not fit all available data
Approximates most features of data	Cannot match triaxial test
G = Const. G = $G(P_m)$ and associated flow rule theoretically correct	Other treatments of G can lead to possible paths of energy generation
	For nonassociated flow rule no general uniqueness theorem
B. Variable Moduli	
Best fit of data	Restricted to near-proportional loading (in shear)
Only model with repeated hysteresis within failure envelope	For nonproportional loading paths no uniqueness theorem
Ideal for finite element	Additional quantity must be stored at each grid point
Computationally simple	
Relatively easy to fit	
C. Cap Model	
Satisfies all rigorous theoretical requirements	Indirect approach needed to fit data
Reasonably good fit of data	Relatively complicated
Effective control of dilatancy	Additional quantity, the strain hardening parameter, must be stored at each grid point
D. Viscoelastic	
Simple to fit to data	Requires sophisticated testing to define viscous coefficients for multi-axial loading.
Approximates features of data for some rocks	Does not account for deterioration in strength with time
E. Viscoplastic	
Approximates some features of data including shear strength, stick-slip phenomenon	Requires sophisticated testing

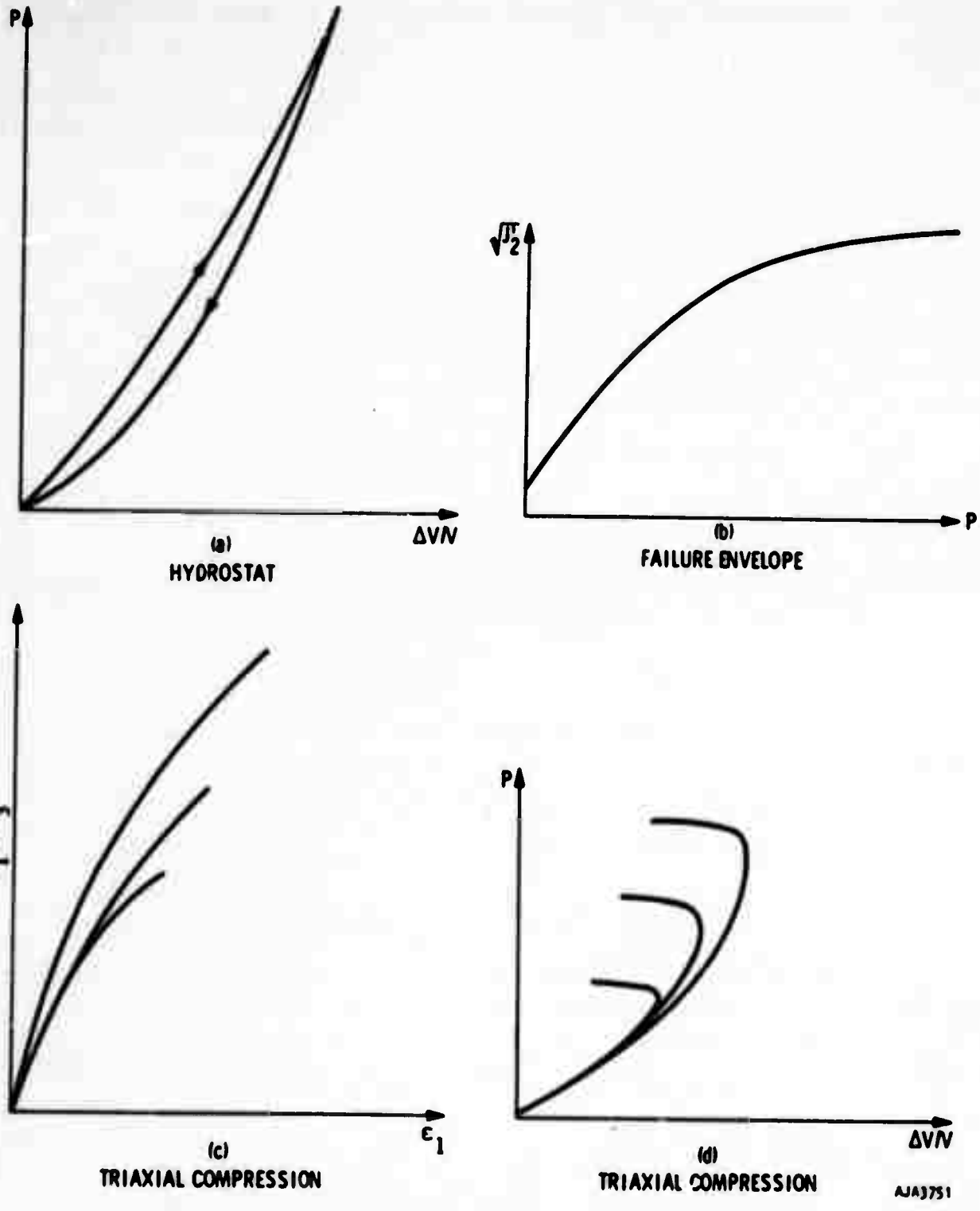

FIGURE 4-1. TYPICAL LABORATORY DATA ON ROCK FROM WHICH CONSTITUTIVE EQUATIONS ARE DERIVED

The programming of the material property subroutines is arranged to provide maximum flexibility and ease in changing properties. This is done by performing each separate function in the material properties description by a separate subroutine. Thus separate subroutines are provided for the following purposes:

Computing variable moduli

Computing derivatives of the yield functions with respect to its arguments.

Testing for yielding or fracture

Adjusting stresses for viscoelastic relaxation.

Adjusting stresses for viscoplastic relaxation.

Transforming strain increments to principal axes of orthotrophy and transforming the matrix of stress/strain coefficients to the global axes.

There is considerable interdependence between the inelastic and anisotropic capabilities. Wherever possible this interdependence is used to economize on programming. Logic diagrams for each subroutine in the homogeneous material property package, are given in Appendix A.

4.1.1 INELASTICITY FOR ISOTROPIC MATERIALS--VARIABLE MODULUS

Inelasticity in isotropic materials is represented through variable bulk and shear moduli and through plasticity theory. The bulk modulus B is assumed to depend on the current value of elastic volumetric strain μ and its previous maximum value μ_{max}.

FOR LOADING ($0 > \mu \geq \mu_{max}$)

$$B = (B_m - B_o) \exp\left(\frac{-\mu}{\mu_1}\right) \qquad (4\text{-}1)$$

FOR UNLOADING OR RELOADING ($0 < \mu < \mu_{max}$)

$$B = B_u + (B_m - B_u)\left(\frac{\mu}{\mu_2}\right) \tag{4-2}$$

where

$$B_u = \text{the lesser of} \begin{cases} B_o + (B_m - B_o)\left(\frac{\mu_{max}}{\mu}\right) \\ B_m \end{cases}$$

FOR LOADING OR UNLOADING/RELOADING IN TENSION ($\mu < 0$)

$$B = B_t \tag{4-3}$$

Application of this model to a granitic rock is illustrated in Figure 4-2. Specific parameters for this rock are

$B_m = 7.6 \times 10^6$ psi

$B_o = 1.205 \times 10^6$ psi

$\mu_1 = 0.0275$

$\mu_2 = 0.05$

The shear modulus G is also assumed to depend on μ and μ_{max}

FOR LOADING ($0 \leq \mu_{max} \leq \mu$)

$$G = G_m - (G_m - G_o) \exp\left(\frac{-\mu}{\mu_3}\right) \tag{4-4}$$

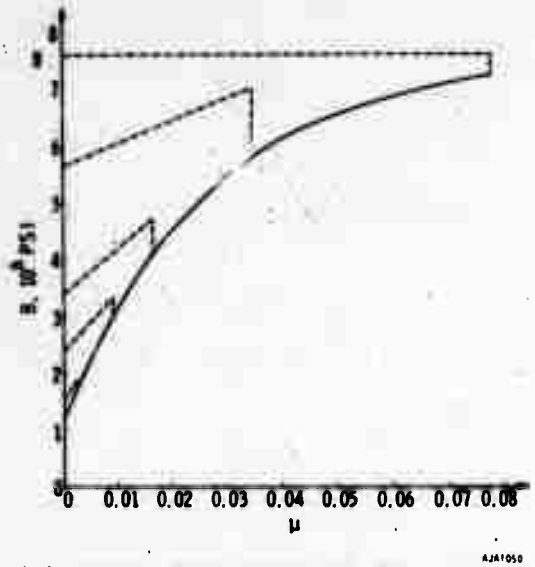

(a) MODEL BULK MODULUS FOR LOADING AND UNLOADING

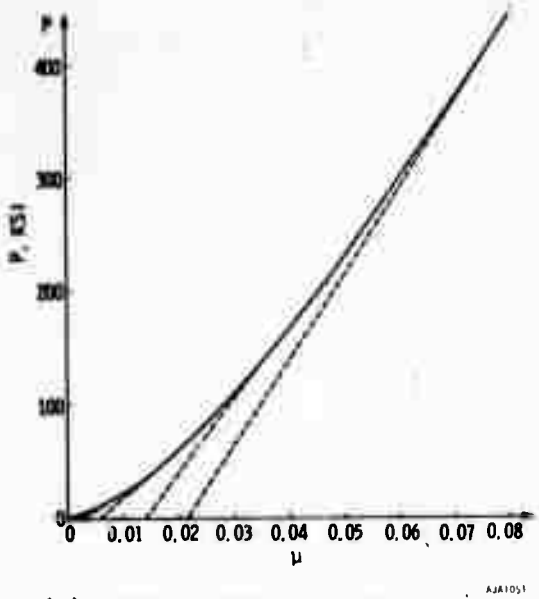

(b) MODEL HYDROSTAT FOR LOADING AND UNLOADING

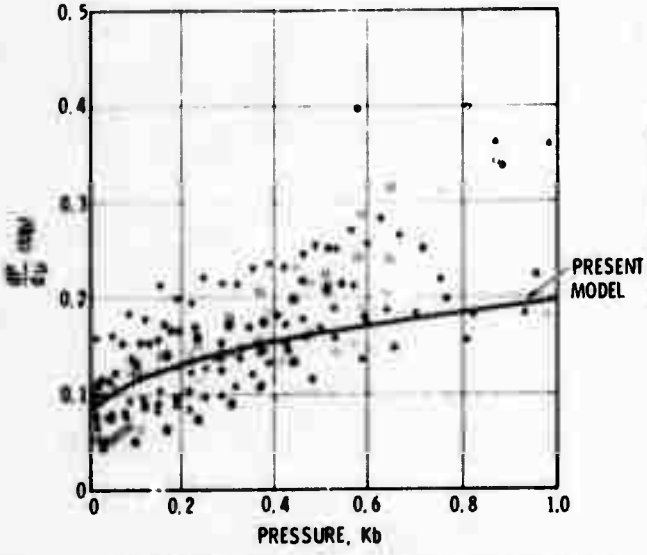

(c) LOW PRESSURE BULK MODULUS COMPARED WITH DATA (REFERENCE 4-1)

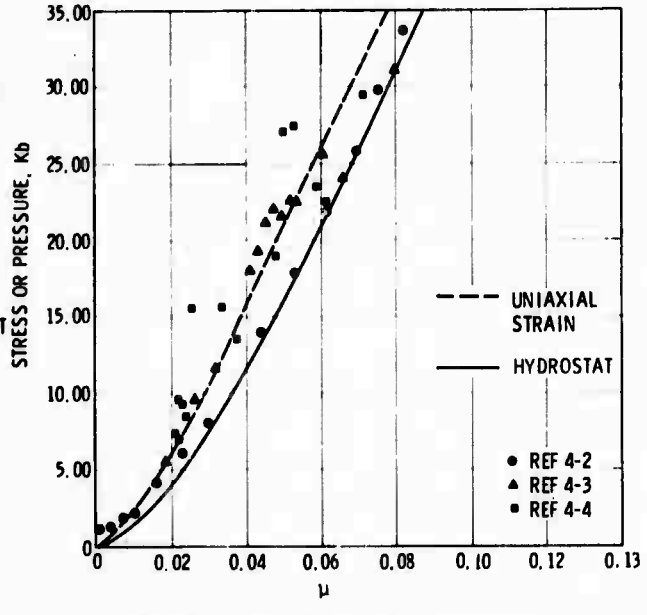

(d) MODEL HUGONIOT AND HYDROSTAT COMPARED WITH DATA

FIGURE 4-2. MODEL BULK MODULUS, HYDROSTAT AND YIELD POINT IN UNIAXIAL STRAIN COMPARED WITH DATA

FOR UNLOADING/RELOADING ($0 \leq \mu < \mu_{max}$)

$$G = \text{Maximum previous value of } G \tag{4-5}$$

FOR LOADING OR UNLOADING/RELOADING IN TENSION ($\mu < 0$)

$$G = G_t \tag{4-6}$$

Application of this model to cracked and uncracked granitic rocks is illustrated in Figure 4-3. Specific parameters for these rocks are:

$$G_m = 4.35 \times 10^6 \text{ psi}$$

$$G_o = 0$$

$$\mu_3 = 0.005$$

The incremental stress $d\sigma_{ij}$ is related to the incremental component of elastic strain de^e_{ij} by the following expression:

$$d\sigma_{ij} = \left(B - \frac{2}{3}G\right) d\varepsilon^e_{kk}\,\delta_{ij} + 2G\left(d\varepsilon^e_{ij}\right) \tag{4-7}$$

where

$$\delta_{ij} = 0 \text{ if } i \neq j; = 1 \text{ if } i = j$$

Theoretical guidance on the appropriate functions for B and G is provided by Walsh (References 4-7, 4-8), who postulates that the effective modulus differs from the intrinsic modulus due to cracks and pores. As these are closed by increasing pressure, the effective modulus tends toward the consolidated value. Walsh's work contains parameters which are not retained

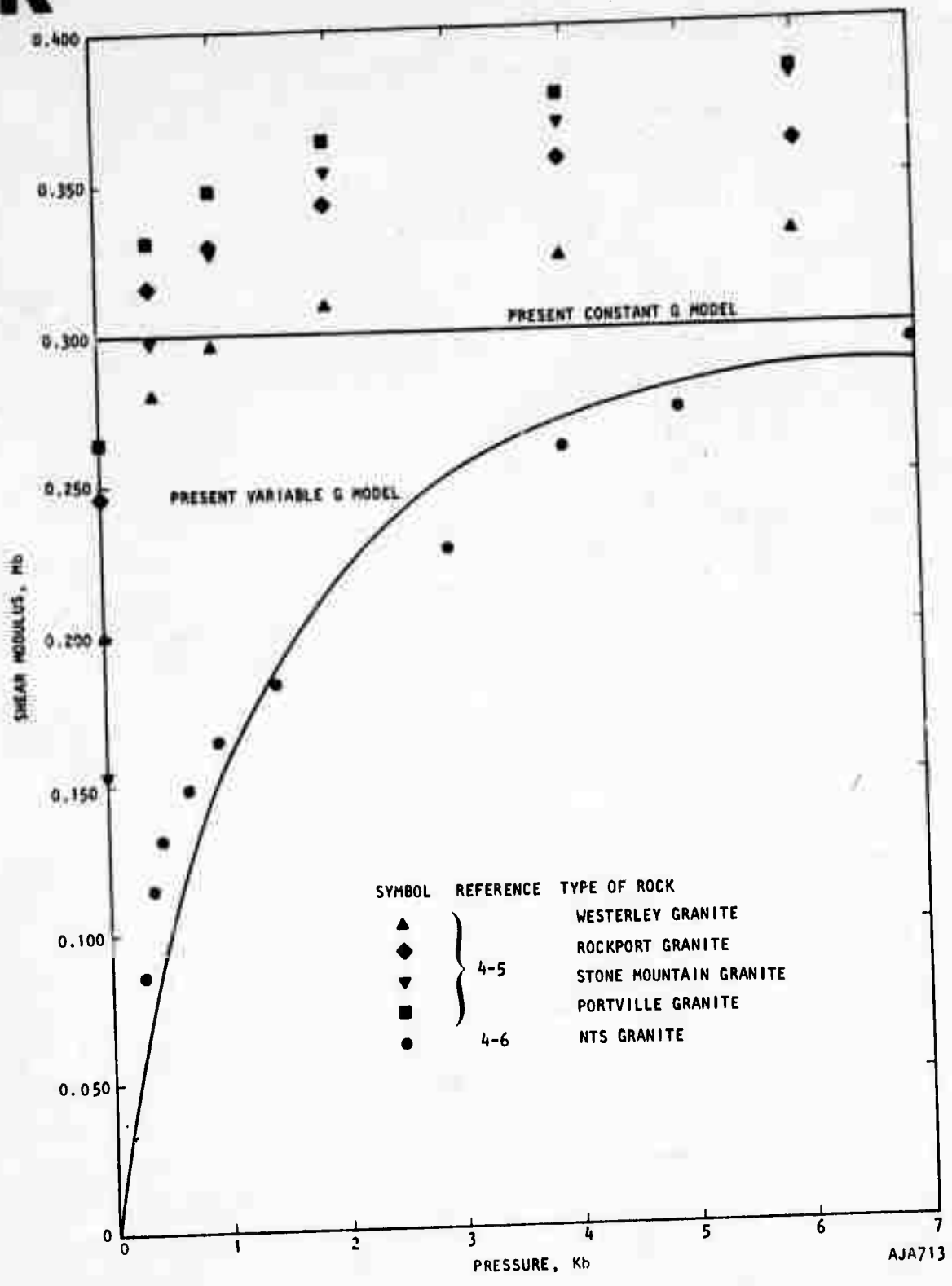

FIGURE 4-3. SHEAR MODULUS VERSUS PRESSURE FOR NTS GRANITE

in the following empirical expressions for the effective bulk modulus. However, the basic concept is retained. Also, the present model for the effective shear modulus merely follows Walsh's concept. The idea of coupling the shear stiffness to volumetric strain is proposed in Reference 4-9 and carries the danger that energy might be extracted from the model by hydrostatic compression, followed by shearing, followed by releasing the pressure and finally by releasing the shear. This danger is avoided by assuming that friction prevents cracks from reopening during unloading so that the largest value of G reached on loading is retained during subsequent unloading/reloading. Under these conditions a material may dissipate energy in shear during loading and unloading cycles but can never produce additional energy.

4.1.2 INELASTICITY FOR ISOTROPIC MATERIALS--VARIABLE MODULI WITH PLASTICITY

The present adaptation of plasticity theory is based on work of References 4-9 through 4-13. The model consists of a yield criterion

$$f(\sigma_{ij}, L) = 0 \qquad (4\text{-}8)$$

where L is a function of plastic strain,

and a plastic flow rule in which f is regarded as a potential function

$$d\varepsilon^{p}_{ij} = \Lambda \frac{\partial f}{\partial \sigma_{ij}} \qquad (4\text{-}9)$$

The incremental stress is related to the elastic component of incremental strain by Equation 4-7. Defining

$$d\varepsilon^{e}_{ij} = d\varepsilon_{ij} - d\varepsilon^{p}_{ij} \qquad (4\text{-}10)$$

Substituting Equations 4-9 and 4-10 into Equation 4-7 leads to

$$d\sigma_{ij} = \lambda\left(d\varepsilon_{kk} - \Lambda \frac{\partial f}{\partial \sigma_{\ell\ell}}\right)\delta_{ij} + 2G\left(d\varepsilon_{ij} - \Lambda \frac{\partial f}{\partial \sigma_{ij}}\right) \qquad (4\text{-}11)$$

where

$$\lambda = B - \frac{2}{3}G$$

If the yield criterion is satisfied, the stress state must lie on the surface defined by f in Equation 4-8. The mathematical statement of this constraint is

$$df = \frac{\partial f}{\partial \sigma_{ij}} d\sigma_{ij} + \frac{\partial f}{\partial L} dL = 0 \qquad (4\text{-}12)$$

Substituting Equation 4-11 into 4-12 permits solutions for Λ

$$\Lambda = \frac{\lambda(d\varepsilon_{kk})\, f_{\ell\ell} + 2G\, d\varepsilon_{ij} f_{ij}}{\lambda f_{kk} f_{\ell\ell} + 2G\, f_{ij} f_{ij} + R} \qquad (4\text{-}13)$$

where R is a strain-hardening function to be defined below.

Substitution of Equation 4-13 into 4-11 expresses the stress increment in terms of the strain increment.

Specific functional forms have been assumed for f. These contain empirical constants whose values can be selected to match data for a specific material. The forms are

Polynomial 1 in σ_{ij}

$$f_1(\sigma_{ij}) = \begin{cases} \sqrt{J_2'} - \sum_{n=1}^{4} a_n J_1^{n-1} = 0 & J_1 > b \\ \sqrt{J_2'} - a_5 = 0 & J_1 \leq b \end{cases} \tag{4-14}$$

Polynomial 2 in σ_{ij}

$$f_1(\sigma_{ij}) = \begin{cases} \sqrt{J_2'} - \left\{ a_1 \left[1 - \left(1 - \frac{J_1}{b} \right)^2 \right] + a_2 \right\} = 0 & J_1 > b \\ \sqrt{J_2'} - (a_1 + a_2) = 0 & J_1 \leq b \end{cases} \tag{4-15}$$

Cap (to be used with Polynomial 2)

$$f_2 = (J_1 - V)^2 + P^2 (J_2' - Q) = 0 \tag{4-16}$$

in which

$$V = L + P^2 X(L)\, X'(L) \tag{4-17}$$

$$Q = [X(L)]^2 \left\{ 1 + P^2 [X'(L)]^2 \right\} \tag{4-18}$$

and

$$X(L) = \begin{cases} A \left[1 - \left(1 - \frac{L}{B} \right)^2 \right] + C & L \leq B \\ A + C & L > B \end{cases} \tag{4-19a}$$

$$X'(L) = \begin{cases} \frac{2A}{B}\left(1 - \frac{L}{B}\right) & L \leq B \\ 0 & L > B \end{cases} \qquad (4\text{-}19b)$$

The hardening parameter, L, is

$$L = \int_0^t g\left(J_1, \sqrt{J_2'}\right) \sqrt{\dot{i}_2^P}\, dt \qquad (4\text{-}20)$$

where

$$g = W\left[1 - \frac{\sqrt{J_2'}}{\sqrt{J_2'} - f_1}\right]^2 \qquad (4\text{-}21)$$

$$\dot{i}_2^P = \left(\dot{\varepsilon}_1^P\right)^2 + \left(\dot{\varepsilon}_2^P\right)^2 + \left(\dot{\varepsilon}_3^P\right)^2 \qquad (4\text{-}22)$$

The hardening parameter R is

$$R = \left(\frac{f_1^2}{\left(f_1 - \sqrt{J_2'}\right)^2}\right)\left(\frac{\partial f_2}{\partial L}\right)\sqrt{\left(\frac{\partial f_2}{\partial \sigma_1}\right)^2 + \left(\frac{\partial f_2}{\partial \sigma_2}\right)^2 + \left(\frac{\partial f_2}{\partial \sigma_3}\right)^2} \qquad (4\text{-}23)$$

where

σ_1, σ_2, σ_3 are principal stresses

and

$R = 0$ if $f = f_1$.

The cap parameters and stress/strain relations produced by the cap model are shown in Figures 4-4 through 4-6. Data on strength for granite containing various degrees of cracking are shown in Figure 4-7, which illustrate the adequacy of the assumed fracture criteria.

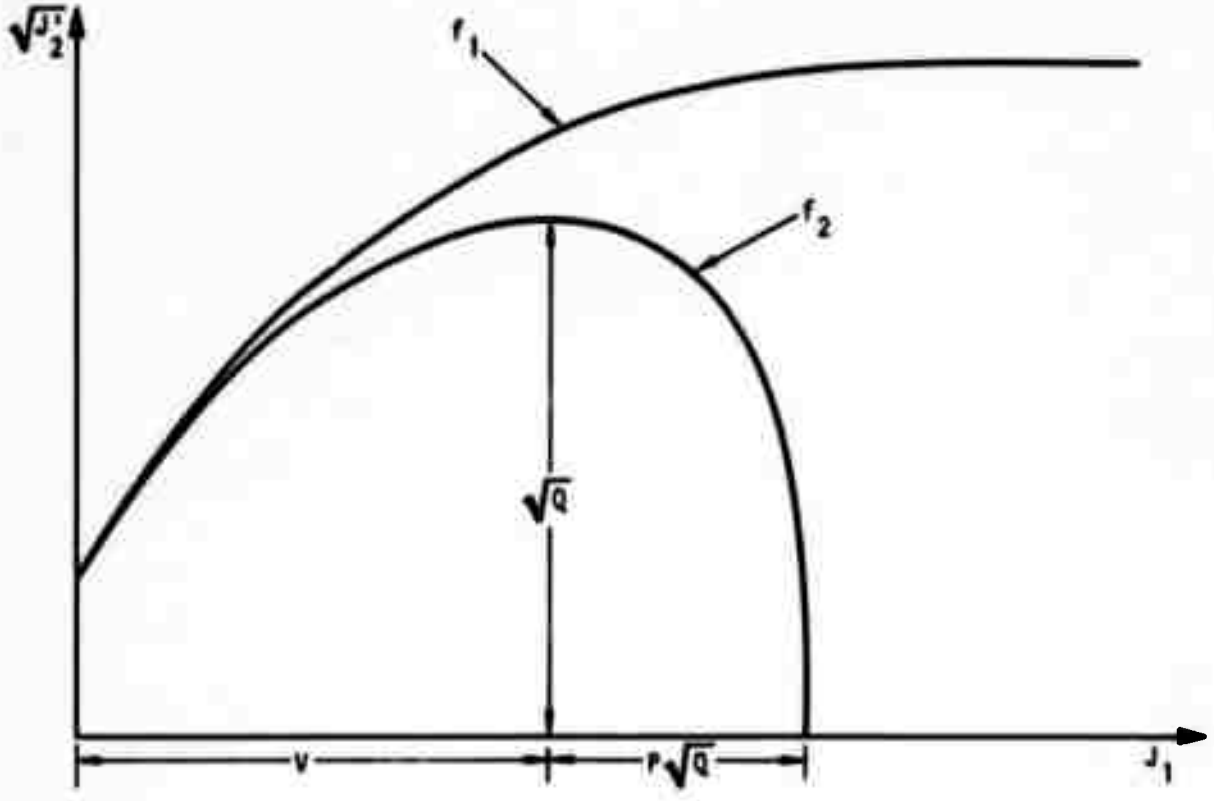

FIGURE 4-4. CAP MODEL

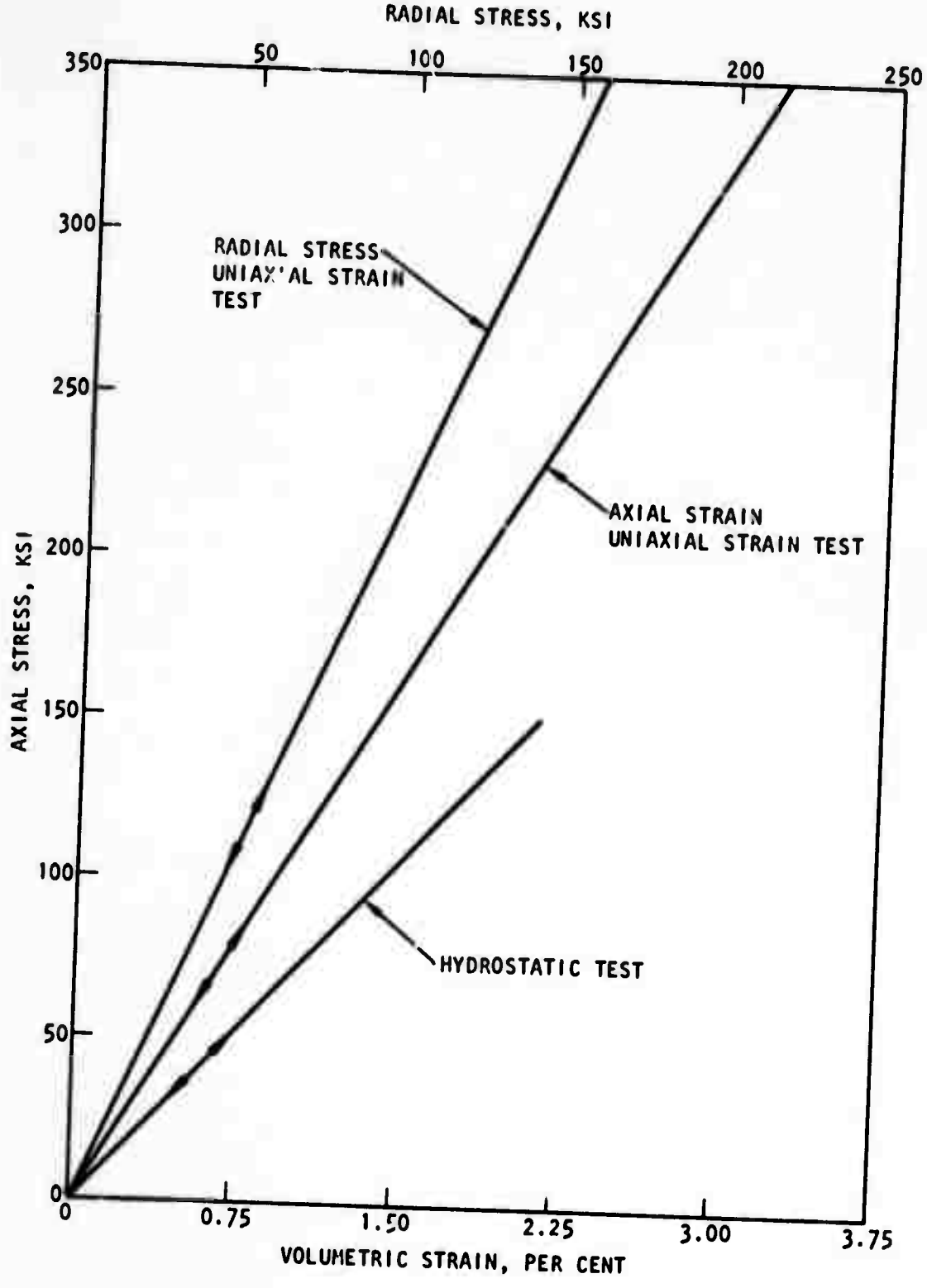

FIGURE 4-5. HYDROSTATIC AND UNIAXIAL STRAIN BEHAVIOR CAP MODEL FIT FOR GRANITIC MATERIAL

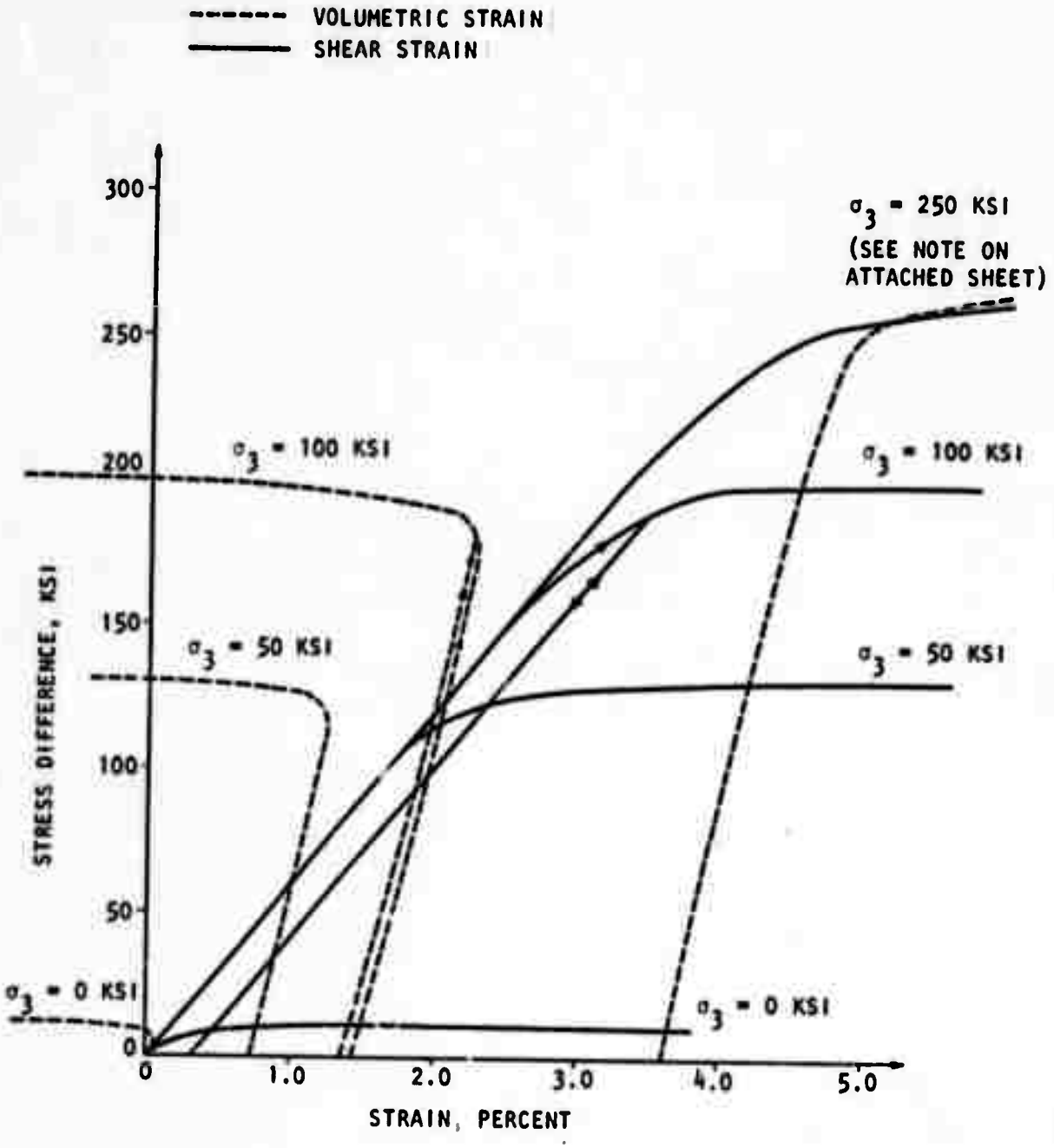

FIGURE 4-6. TRIAXIAL STRESS BEHAVIOR, CHAMBER PRESSURE = 0, 50, 100, 200 KSI, CAP MODEL FIT FOR GRANITIC MATERIAL

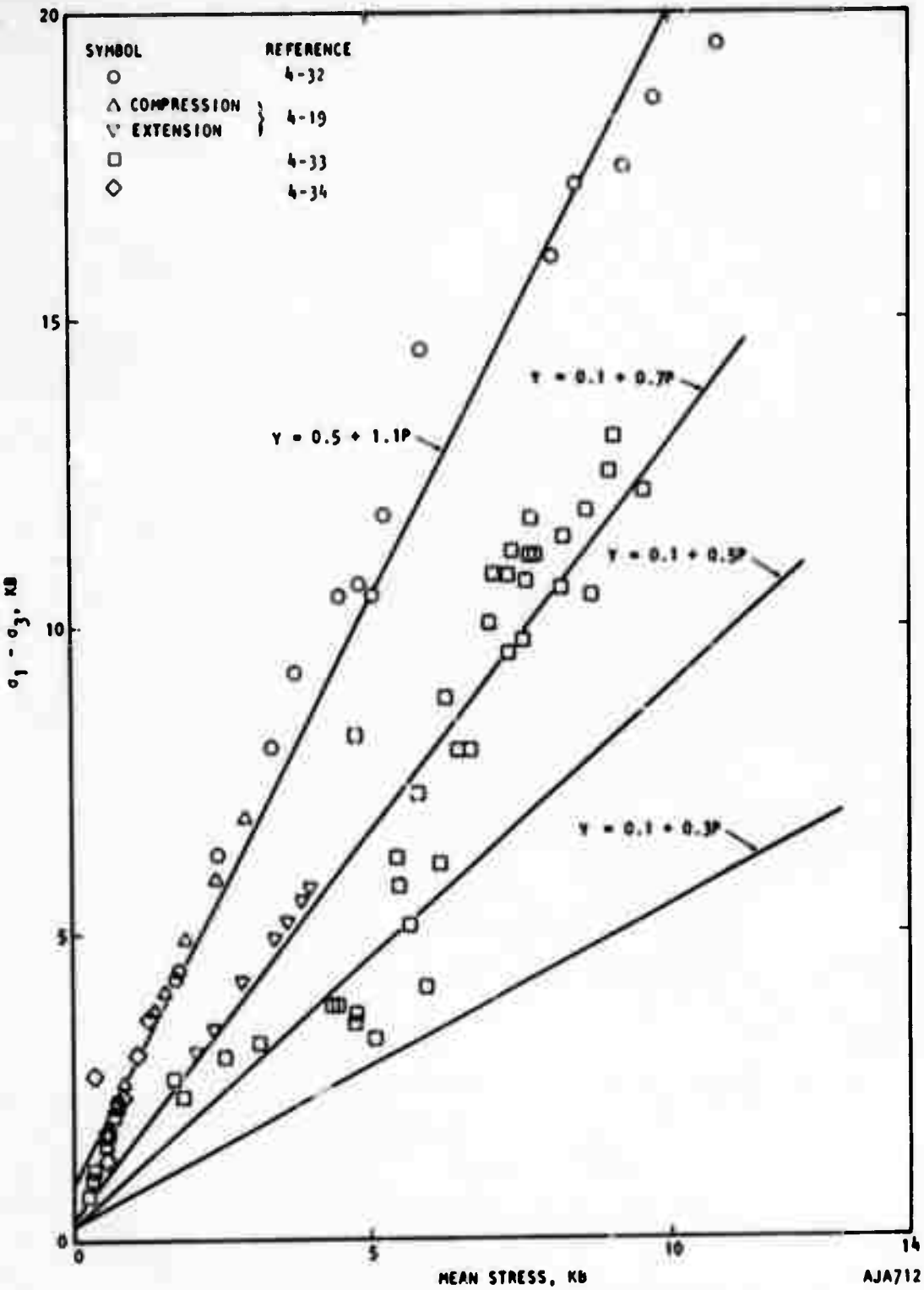

FIGURE 4-7. YIELD STRENGTH VERSUS MEAN STRESS FOR NTS GRANITE

The incremental stress/strain equations are expressed in matrix form as follows:

$$\{d\sigma\} = [C]\{d\varepsilon\} \qquad (4\text{-}24)$$

where $d\varepsilon$ is the total increment of strain. The C matrix thus contains generalized tangent moduli and can be used in forming the element stiffness matrices. For the models described above, the C matrix is as follows:

C =

$$
\begin{bmatrix}
\cdot + 2G - \frac{(\lambda G + 2Gf_{11})^2}{D} & \cdot - \frac{(\lambda F + 2Gf_{22})(\lambda F + 2Gf_{11})}{D} & \cdot - \frac{(\lambda F + 2Gf_{33})(\lambda F + 2Gf_{11})}{D} & -2Gf_{12}\frac{\lambda F + 2Gf_{11}}{D} & -2Gf_{13}\frac{\lambda F + 2Gf_{11}}{D} & -2Gf_{23}\frac{\lambda F + 2Gf_{11}}{D} \\
 & \cdot + 2G - \frac{(\lambda + 2Gf_{22})^2}{D} & \cdot - \frac{(\lambda F + 2Gf_{22})(\lambda F + 2Gf_{33})}{D} & -2Gf_{12}\frac{\lambda F + 2Gf_{22}}{D} & -2Gf_{13}\frac{\lambda F + 2Gf_{22}}{D} & -2Gf_{23}\frac{\lambda F + 2Gf_{22}}{D} \\
 & & \cdot + 2G - \frac{(\lambda + 2Gf_{33})^2}{D} & -2Gf_{12}\frac{\lambda F + 2Gf_{33}}{D} & -2Gf_{13}\frac{\lambda F + 2Gf_{33}}{D} & 2Gf_{23}\frac{\lambda F + 2Gf_{33}}{D} \\
 & & & G - \frac{4G^2f_{12}^2}{D} & \frac{-4G^2f_{13}f_{12}}{D} & \frac{-4G^2f_{23}f_{12}}{D} \\
 & & & & G - \frac{4G^2f_{13}^2}{D} & \frac{-4G^2f_{13}f_{23}}{D} \\
 & & & & & G - \frac{4G^2f_{23}^2}{D}
\end{bmatrix}
\qquad (4\text{-}25)
$$

Symmetric

where

$$D = F^2 + 2G\lambda - R$$

$$F = \frac{\partial f}{\partial \sigma_{11}} + \frac{\partial f}{\partial \sigma_{22}} + \frac{\partial f}{\partial \sigma_{33}} = f_{11} + f_{22} + f_{33}$$

$$R = f_{11}^2 + f_{22}^2 + f_{33}^2 + 2f_{13}^2 + 2f_{12}^2 + 2f_{23}^2$$

The C matrix is clearly composed of elastic and inelastic parts

$$C = C^e - C^p \tag{4-26}$$

The C^e and C^p matrices are computed separately. The reason for this is efficiency in treating isotropic and anisotropic materials with the same Fortran statements.

In weakly nonlinear problems it is possible to avoid time-consuming reformulation of the stiffness matrix by introducing nonlinearity through the load vector. The method is an extension of the equilibrium equations given in Reference 4-29. In the following equation, time is used as a parameter. Number of load step could be used instead.

At time τ, the total change in complimentary strain energy is equal to the change in complimentary work done by nodal point forces.

$$\sum_{\tau=0}^{\tau=t} \int_{vol} \langle \varepsilon \rangle_\tau \{d\sigma\}_\tau \, dV = \sum_{\tau=0}^{\tau=t} \langle u \rangle_\tau \{dP\}_\tau \tag{4-27}$$

where

$\langle \varepsilon \rangle$, $\{d\sigma\}$ = Element strain and stress increment

$\langle u \rangle$, $\{dP\}$ = Nodal displacement and force vector

V = Volume of finite element

τ = Arbitrary instant of time

The strain/displacement relation is

$$\{\varepsilon\} = [B]\{u\}$$

or

$$\langle \varepsilon \rangle = \langle u \rangle [B]^T \tag{4-28}$$

The stress increment in an elastic/plastic material may be expressed by rewriting Equation 4-24 as follows.

$$\{d\sigma\} = [C]\{d\varepsilon\} - \{d\sigma_p\} \qquad (4\text{-}29)$$

elastic correction

where now $C = C^e$

Substituting Equations 2-28 and 2-29 into Equation 2-27,

$$\sum_{\tau=0}^{\tau=t} \int_{vol} \langle u \rangle_\tau [B]^T \left\{ [C][B]\{du\}_\tau - \{d\sigma_p\}_\tau \right\} dV = \sum_{\tau=0}^{\tau=t} \langle u \rangle_\tau \{dP\}_\tau \qquad (4\text{-}30)$$

Noting that $\langle u \rangle_\tau$ may be eliminated from both sides and that

$$\int_{vol} [B]^T [C][B] dV = [K] \qquad (4\text{-}31)$$

where $[K]$ is the elastic stiffness matrix, Equation 2-30 may be rewritten as

$$\sum_{\tau=0}^{\tau=t-\Delta t} \left([K]\{du\}_\tau - \int_{vol} [B]^T \{d\sigma_p\}_\tau \, dV \right)$$

$$+ [K]\{du\}_{\Delta t} - \int_{vol} [B]^T \{d\sigma_p\}_{\Delta t} \, dV = \sum_{\tau=0}^{\tau=t} \{P\}_\tau \qquad (4\text{-}32)$$

where $\{du\}_{\Delta t}$, $\{d\sigma_p\}_{\Delta t}$ equal change in u and σ_p during the interval $t - \Delta t$ to t.

Performing the indicated summation, assuming stress to be constant throughout the element and defining

$$E_\tau = \sum_{\tau=0}^{\tau} [K]\{du\}_\tau \qquad (4\text{-}33)$$

we have

$$[K]\{du\}_{\Delta t} - [B]^T\{d\sigma_p\}_{\Delta t} V = \{P\}_t - \{E\}_{t-\Delta t} + [B]^T\{\sigma_p\}_{t-\Delta t} V \quad (4\text{-}34)$$

For small increments of stress and time in a step-by-step integration, the second term on the left hand side is neglected.

The expression which is used for {E} in the computer program is derived as follows. The recoverable work done on an element is equated to the elastic strain energy stored in the element by the following equation.

$$\frac{1}{2} <u>\{E\} = \frac{1}{2} <\varepsilon>[C]\{\varepsilon\}V \quad (4\text{-}35)$$

or

$$\{E\} = [B^T][C]\{\varepsilon\}V \quad (4\text{-}36)$$

Thus Equation 4-34 may be rewritten

$$[K]\{du\}_{\Delta t} = \{P\}_t - [B^T]\left\{[C]\{\varepsilon\}_{t-\Delta t} - \{\sigma_p\}_{t-\Delta t}\right\}V \quad (4\text{-}37)$$

Following Equation 4-29

$$d\sigma_{ij} = \left(\lambda d\varepsilon_{kk}\delta_{ij} + 2G\, d\varepsilon_{ij}\right) - \left(\lambda \frac{\partial f}{\partial \sigma_{kk}} \delta_{ij} + 2G \frac{\partial f}{\partial \sigma_{ij}}\right) \Lambda \quad (4\text{-}38)$$

or

$$d\sigma_{ij} = \lambda d\varepsilon_{kk}\delta_{ij} + 2G\, d\varepsilon_{ij} - d\sigma^p_{ij} \quad (4\text{-}39)$$

where

$$d\sigma^{p}_{ij} = \left(\lambda \frac{\partial f}{\partial \sigma_{kk}} \delta_{ij} + 2G \frac{\partial f}{\partial \sigma_{ij}}\right) \frac{\lambda d\varepsilon_{kk} \frac{\partial f}{\partial \sigma_{\ell\ell}} + 2G\, d\sigma_{ij} \frac{\partial f}{\partial \sigma_{ij}}}{\lambda \frac{\partial f}{\partial \sigma_{kk}} \frac{\partial f}{\partial \sigma_{\ell\ell}} + 2G \frac{\partial f}{\partial \sigma_{ij}} \frac{\partial f}{\partial \sigma_{ij}}} \quad \text{if } f = 0$$

$$= 0 \quad \text{if } f < 0 \qquad (4\text{-}40)$$

After each integration step, Δu_i is given; $d\varepsilon_{ij}$ is found.

Based on $d\varepsilon_{ij}$ and stress at previous time, f is checked and $d\sigma_{ij}$ is calculated according to whether material is elastic or plastic by adding contribution for elastic part to contribution from plastic part.

Stiffness is always based on elastic, parameters, i.e., λ, G. Plasticity is introduced through updating of stress increment. Hence, there is need to update stiffness matrix.

4.1.3 INELASTICITY FOR ANISOTROPIC MATERIALS--THEORY OF JAEGER

The fracture of anisotropic rocks is the subject of several failure theories. The Walsh-Brace theory (Reference 4-14) assumes that failure is tensile in nature and that it is influenced by the presence of preexisting cracks. Some of the cracks are assumed to be small and randomly oriented while others are long and have preferred directions. Extension of the cracks is postulated to occur when the Griffith criterion (Reference 4-15), as modified by McClintock and Walsh (Reference 4-16) to account for friction on the crack faces, is satisfied.

In contrast, Jaeger (Reference 4-17) assumes the material to fail in shear either along a single plane of weakness or within the matrix material according to a Mohr-Coulomb type of failure criterion of the form

$$\tau = a_o - \sigma a_1 \qquad (4\text{-}38)$$

where

τ = Shear stress on plane of fracture

σ = Normal stress on plane of fracture

a_o, a_1 = Cohesion, angle of friction

The theory is expressed in terms of principal stresses by an axis rotation as follows

$$\sigma_1 - \sigma_3 = \frac{2a_o - 2a_1\sigma_3}{a_1 - \sqrt{a_1^2 + 1}} \qquad (4\text{-}39)$$

Improved agreement with experiment is obtained if a_o is assumed to vary

$$a_o = a_2 - a_3 \cos\left(2(\xi - \beta)\right) \qquad (4\text{-}40)$$

where

β = Counterclockwise angle from the direction of the major principal stress (σ_1) to the direction of the bedding planes

ξ = The orientation of β at which a_o is minimum. Usually assumed to be equal to 30 deg

The angle β is shown in Figure 4-8 along with angles relating it to global directions in the finite element formulation. McLamore and Grey (Reference 4-18) have obtained satisfactory agreement between experimental data on strengths of slates and shales using a modification of Equation 4-25 as follows:

$$a_o = a_2 - a_3[\cos 2(\xi - \beta)]^n \quad \text{for} \quad 0 < \xi < \beta$$
$$a_o = a_4 - a_5[\cos 2(\xi - \beta)]^n \quad \text{for} \quad \beta < \xi < 90^o \qquad (4\text{-}41)$$

Some of their results and those of Brace and Walsh are illustrated in Figure 4-9.

X - Y - Z = GLOBAL AXES

1 - 2 - 3 = PRINCIPAL STRESS AXES

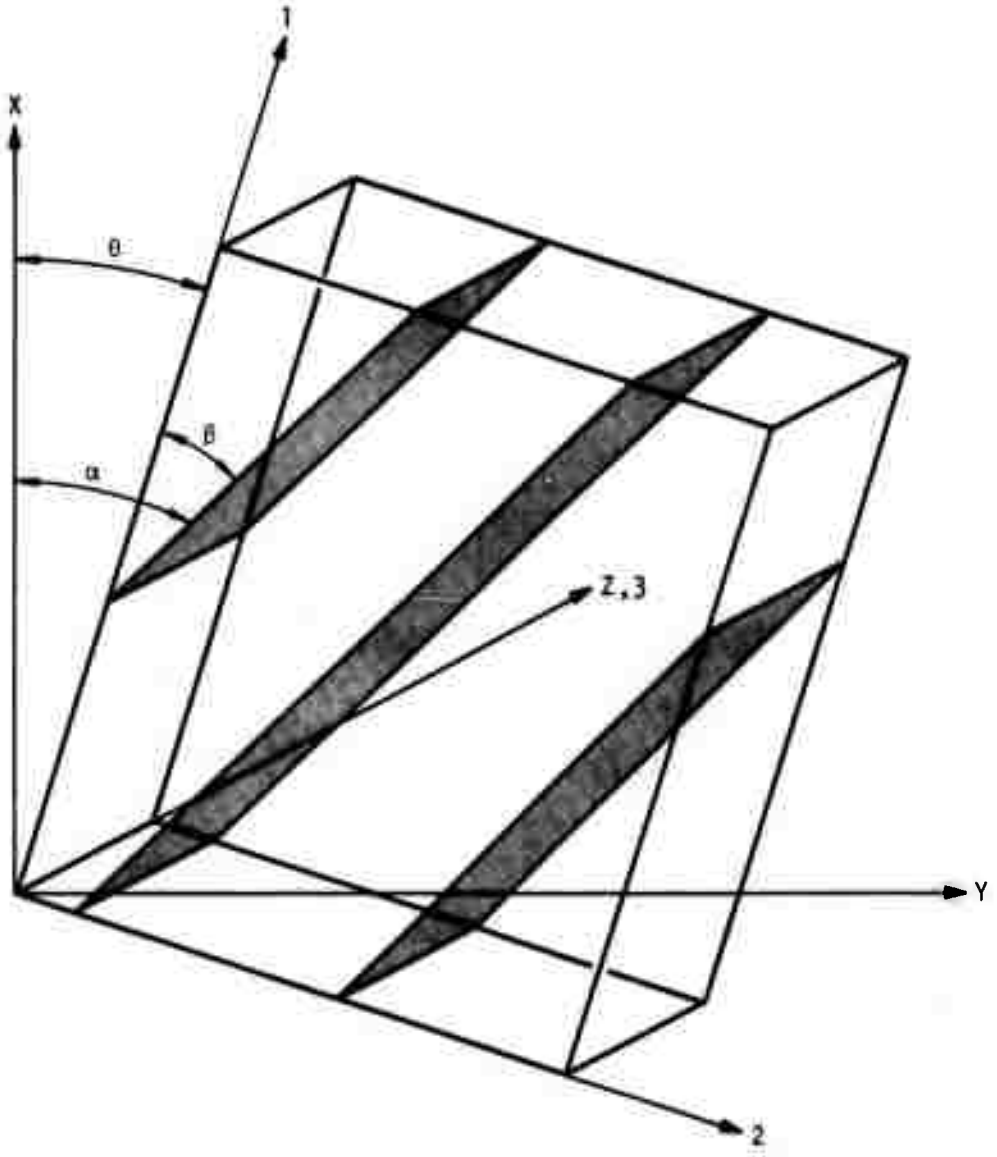

FIGURE 4-8. ORIENTATION OF PLANES OF WEAKNESS DEFINING ANISOTROPIC BEHAVIOR ACCORDING TO JAEGER

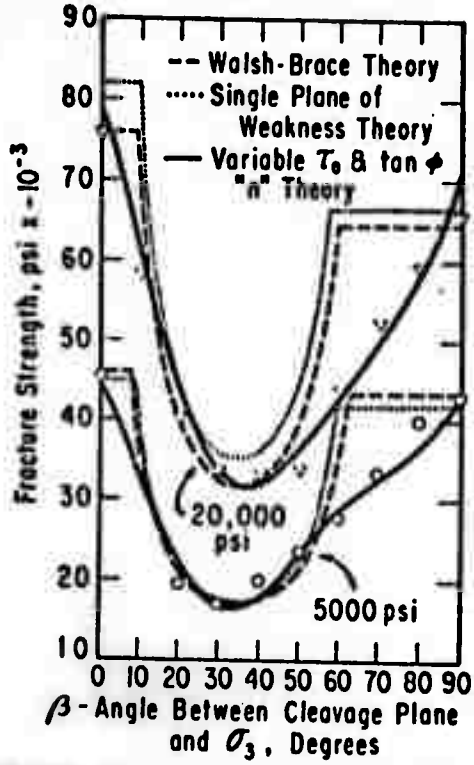

COMPARISON OF VARIOUS FAILURE THEORIES WITH SLATE DATA FOR CONFINING PRESSURES OF 5000 PSI AND 20,000 PSI

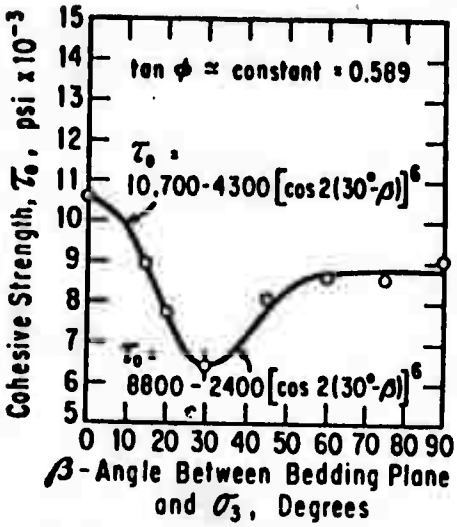

VARIATION OF τ_o WITH RESPECT TO β FOR GREEN RIVER SHALE-1

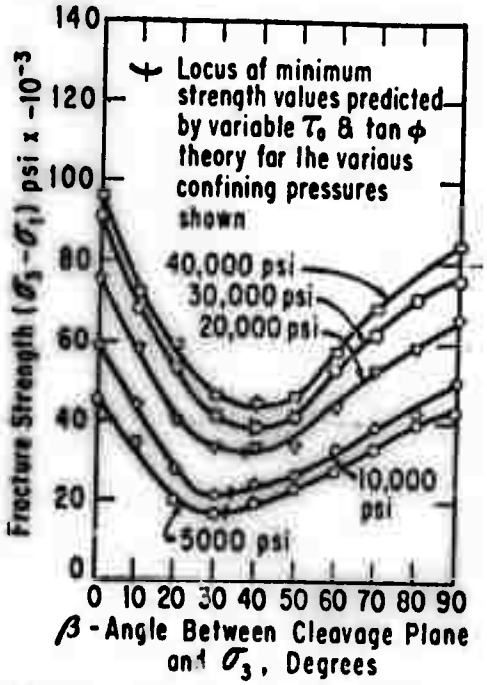

FRACTURE STRENGTH VERSUS ORIENTATION ANGLE β FOR SLATE AT VARIOUS CONFINING PRESSURES

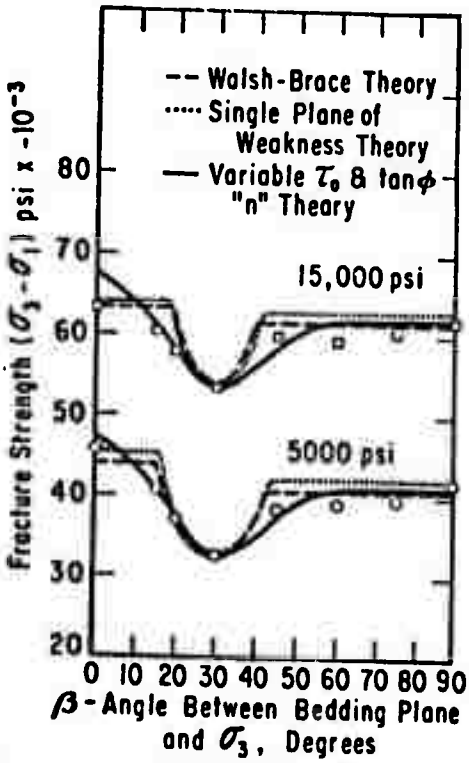

COMPARISON OF VARIOUS FAILURE THEORIES WITH GREEN RIVER SHALE-1 DATA FOR CONFINING PRESSURES OF 5000 PSI AND 15,000 PSI

FIGURE 4-9. COMPARISON BETWEEN FAILURE THEORIES AND EXPERIMENTAL DATA FOR ANISOTROPIC ROCK (REFERENCE 2-18)

The present application of the hypotheses in Reference 4-18 is limited to plane geometry. It does not take into account the effect of the intermediate principal stress which is shown in Reference 4-19 to play an important role in fracture of some types of rocks. More work is needed to remove these restrictions.

The first step is to determine the magnitude of the principal stresses σ_1, σ_2 and their direction as specified by θ, the counter-clockwise angle from the +X global axis.

$$\sigma_{1,2} = \frac{\sigma_{xx} + \sigma_{yy}}{2} \pm \sqrt{\left(\frac{\sigma_{xx} - \sigma_{yy}}{2}\right)^2 + \sigma_{xy}^2} \qquad (4\text{-}42)$$

$$\theta = \frac{1}{2} \text{Arctan} \left(\frac{-2\sigma_{xy}}{\sigma_y - \sigma_x}\right) \qquad (4\text{-}43)$$

Bilinear stress/strain relations are specified by the user in terms of Young's moduli and Poisson's ratio in directions parallel and perpendicular to the bedding planes (oriented at α relative to global axes). Thus, experimental data is required from specimens cut orthogonal to bedding plane and at angles other than 90^o. The computer program transforms the various E and ν to the principal directions of stress and modifies them to account for fracture. These parameters, E_1, ν_{12}, ν_{13}, E_2, ν_{21}, ν_{23}, etc., are assembled into a matrix relating incremental stress and strain in principal stress axes. The relationship between incremental stress and incremental strain expressed in the principal axes of anisotropy (principal stress axes) is shown in Equation 2-24 where C is given by Equation 4-44. The matrix is then transformed through the angle θ into global coordinates for inclusion in the element stiffness matrix. An illustration of the bilinear Young's modulus approach is superposed on data in Figure 4-10.

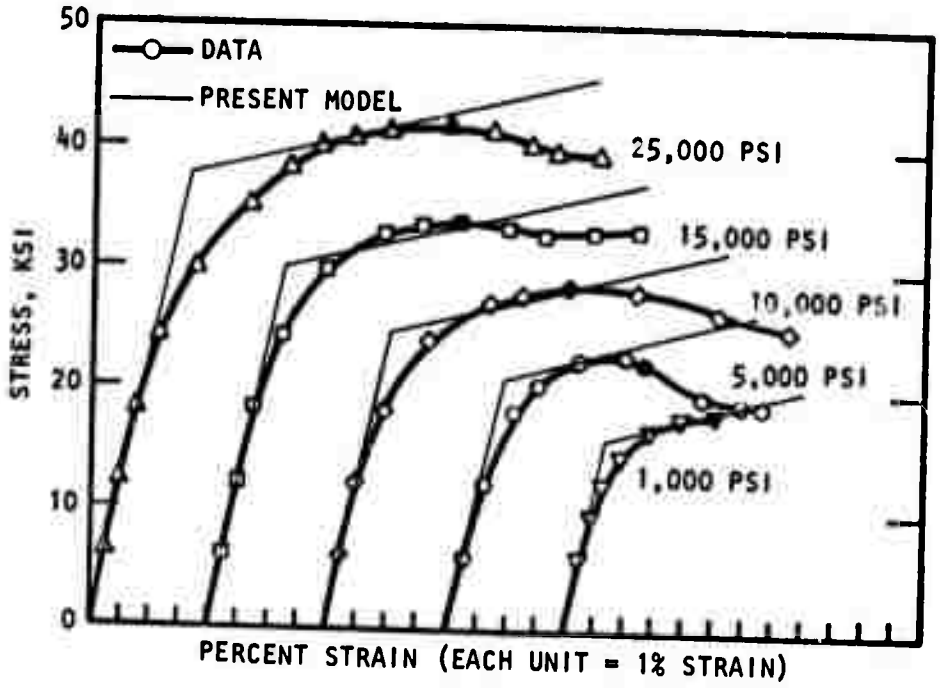

FIGURE 4-10. STRESS-STRAIN CURVES FOR GREEN RIVER SHALE-2 FOR VARIOUS CONFINING PRESSURES, β = 10 DEG (REFERENCE 2-18)

$$[c] = \frac{1}{D}\begin{bmatrix} E_1(1 - \nu_{23}\nu_{32}) & E_1(\nu_{12} + \nu_{13}\nu_{32}) & E_1(\nu_{13} + \nu_{12}\nu_{23}) & & & \\ E_2(\nu_{21} + \nu_{23}\nu_{31}) & E_2(1 - \nu_{13}\nu_{31}) & E_2(\nu_{23} + \nu_{21}\nu_{13}) & & & \\ E_3(\nu_{13} + \nu_{32}\nu_{21}) & E_3(\nu_{32} + \nu_{31}\nu_{12}) & E_3(1 - \nu_{12}\nu_{21}) & & & \\ & & & DG_{12} & & \\ & & & & DG_{13} & \\ & & & & & DG_{23} \end{bmatrix} \quad (4\text{-}44)$$

where

$$D = 1 - \nu_{23}\nu_{32} - \nu_{12}\nu_{21} - \nu_{13}\nu_{31} - \nu_{12}\nu_{23}\nu_{31} - \nu_{13}\nu_{21}\nu_{32}$$

4.1.4 INELASTICITY FOR ANISOTROPIC ROCK--THEORY OF HILL

Hill (Reference 4-9) has proposed a yield criterion for anisotropic materials whose form is compatible with the isotropic plasticity theory described above. If the stress components are expressed in the principal axes of anisotropy (not necessarily principal stress axes), the yield criterion can be expressed by

$$f\left(\sqrt{J_2'^*},\ J_1^*\right) = 0 \quad (4\text{-}45)$$

where

$$\sqrt{J_2'^*} = C_1(\sigma_{\zeta\zeta} - \sigma_{\eta\eta})^2 + C_2(\sigma_{\eta\eta} - \sigma_{\xi\xi})^2 + C_3(\sigma_{\zeta\zeta} - \sigma_{\xi\xi})^2$$

$$C_4\sigma_{\zeta\xi}^2 + C_5\sigma_{\eta\xi}^2 + C_6\sigma_{\zeta\xi}^2$$

$$J_1^* = C_7\sigma_{\zeta\zeta} = C_8\sigma_{\eta\eta} + C_9\sigma_{\xi\xi}$$

in which it is assumed that the ζ, η, ξ axis system coincides with the principal direction of anisotropy. f may be used as the potential function described above. Adaptation of this theory to rock is described in Reference 4-20.

The elastic behavior of the material may be prescribed to be either isotropic or anisotropic. If it is isotropic, the quantities B and G may be used. If it is anisotropic, Young's moduli and Poisson ratios E_1, ν_{12}, ν_{13}, etc. are specified in the principal directions of anisotropy. The C matrix (Equation 4-24) which relates incremental stress to incremental strain is thus initially expressed in the principal axes of anisotropy and is subsequently transformed to global directions of the finite element mesh.

4.1.5 RATE EFFECTS--VISCOPLASTICITY

This method of incorporating rate sensitivity equations is based on Perzyna's elastic-viscoplastic model (Reference 4-21) which is a generalization of an earlier model proposed by Hohenemser and Prager (Reference 4-22). An adaptation of the cap model described above for viscoplasticity is described in Reference 4-23. The present model is taken from Reference 4-24.

A linear elastic, rate independent region is bounded by a static yield criterion

$$f(J_1, J_2') < 0 \qquad (4\text{-}46)$$

within which Hooke's Law applies. If the static yield criterion is satisfied or exceeded

$$f(J_1, J_2') \geq 0 \qquad (4\text{-}47)$$

A viscoplastic strain rate is assumed to develop according to the following flow rule.

$$\dot{\varepsilon}_{ij}^{P} = \gamma\phi(f)\frac{\partial F}{\partial \sigma_{ij}} \qquad (4\text{-}48)$$

where

$\phi(f)$ = A function of the static yield criterion f

F = Assumed potential function. Presently, a nonassociated flow rule is used in which $F = J_2'$ and differentiation is performed with respect to the stress deviators σ'_{ij}

γ = Empirical viscoplastic parameter

It is assumed in the present work that

$$\phi(f) = \begin{cases} \dfrac{\sqrt{J_2'}}{\sum_{n=1}^{4} a_n J_1^{n-1}} - 1. & J_1 > b \\ \dfrac{\sqrt{J_2'}}{a_5} - 1. & J_1 \leq b \end{cases} \tag{4-49}$$

for

$$f = \begin{cases} \sqrt{J_2'} - \sum_{n=1}^{4} a_n J_1^{n-1} \geq 0 & J_1 > b \\ \sqrt{J_2'} - a_5 \geq 0 & J_1 \leq b \end{cases} \tag{4-50}$$

If $f < 0$, elastic inviscid stress/strain relations apply.

Making use of Hooke's law

$$\dot{\sigma} = \lambda \dot{\varepsilon}_{kk} \delta_{ij} + 2G \dot{\varepsilon}^e_{ij} \tag{4-51}$$

and expressing the elastic deviatoric strain rate by

$$\dot{\varepsilon}^{e'}_{ij} = \dot{\varepsilon}'_{ij} - \dot{\varepsilon}^{p'}_{ij} \tag{4-52}$$

for the case where $f \geq 0$, the stress rate may be expressed by the following equation.

$$\dot{\sigma}_{ij} = \begin{cases} \lambda \dot{\varepsilon}_{kk} \delta_{ij} + 2G \left[\dot{\varepsilon}_{ij} - \gamma \left(\dfrac{\sqrt{J_2'}}{\sum_{n=1}^{4} a_n J_1^{n-1}} - 1 \right) \dfrac{\sigma_{ij}'}{\sqrt{J_2'}} \right] & J_1 > b \\ \lambda \dot{\varepsilon}_{kk} \delta_{ij} + 2G \left[\dot{\varepsilon}_{ij} - \gamma \left(\dfrac{\sqrt{J_2'}}{a_5} - 1 \right) \dfrac{\sigma_{ij}'}{\sqrt{J_2'}} \right] & J_1 \leq b \end{cases} \tag{4-53}$$

If time is considered the integration parameter and the time step is Δt, the incremental stress is

$$d\sigma_{ij} = \lambda d\varepsilon_{kk} \delta_{ij} + 2G \left[d\varepsilon_{ij} - \gamma \left(\frac{\sqrt{J_2'}}{a_o + a_1 J_1} - 1 \right) \frac{\sigma_{ij}'}{\sqrt{J_2'}} \Delta t \right] \tag{4-54}$$

The absence of plastic volume strain is due to choosing a nonassociated flow rule in which J_1 does not appear in the plastic potential.

Some example calculations, which are summarized in Tables 4-3 and 4-4, are shown in Figures 4-11 through 4-13. Comparison with some data for a tonalite is shown in Figure 4-14. The comparison illustrates the ability of the model to represent increase ir strength with strain rate and its inability to represent nonlinear behavior prior to yielding. It can be shown that the effects of viscoplasticity can be accounted for entirely by a correction to the load vector (Reference 4-24). The technique is similar to that described above for rate-independent plasticity and to that described below for viscoelasticity. An important consequence of this is that time-consuming reformulation of the stiffness matrix is avoided.

TABLE 4-3. SUMMARY OF EXAMPLE CALCULATIONS

Case	Type of Loading	Stress Ratio, σ_3/σ_1	Strain Rate,* in./in.-sec
1	Proportional loading	0.293	200.00
2	Proportional loading	0.293	2.00
3	Proportional loading	0.293	0.20
4	Proportional loading	0.293	0.02
5	Proportional loading	0.200	0.20
6	Proportional loading	0.100	0.20
7	Uniaxial strain	0.293	0.02
8	Uniaxial strain	0.293	0.20
9	Uniaxial strain	0.293	2.00
10	Uniaxial strain	0.293	200.00

*For proportional loading, these are elastic strain rates.

TABLE 4-4. PROPERTIES USED IN PRESENT EXAMPLES

Properties		
Bulk modulus	B	$= 1.5 \times 10^6$ psi
Shear modulus	G	$= 10^6$ psi
Cohesion	a_o	$= 1450$
Angle of friction	a_1	$= -0.1$
Viscoplastic coefficient	γ	$= 1.0$

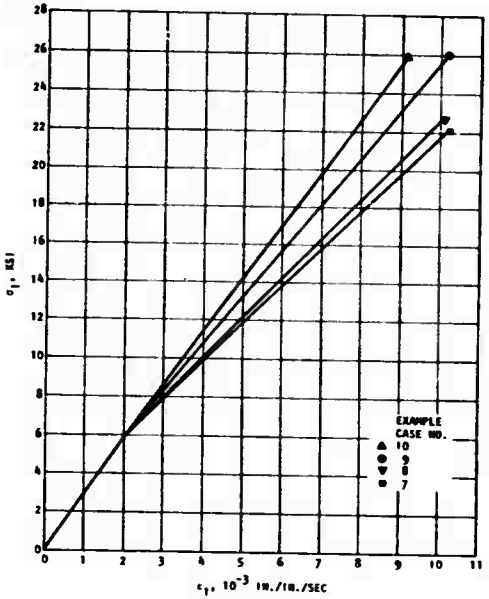

FIGURE 4-11. PRESENT MODEL SUBJECTED TO UNIAXIAL STRAIN AT VARIOUS STRAIN RATES

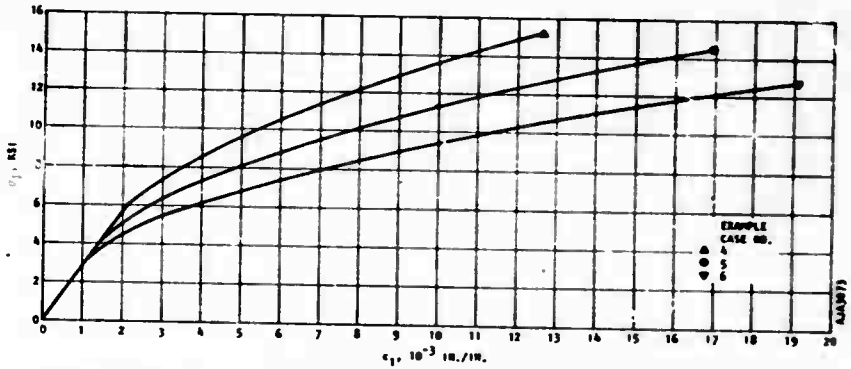

FIGURE 4-12. COMPRESSIVE STRESS/STRAIN RELATIONS FOR PRESENT MODEL SUBJECTED TO PROPORTIONAL LOADING AT DIFFERENT STRESS RATIOS

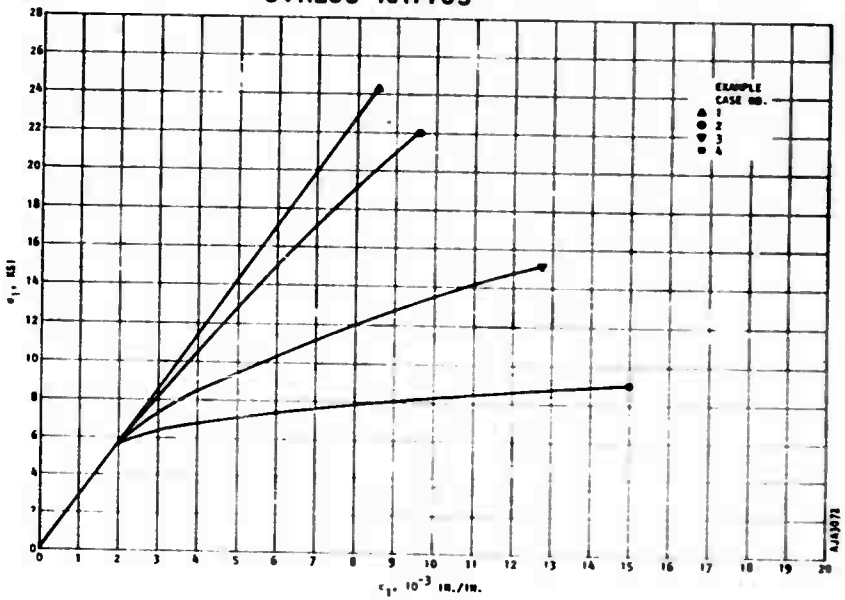

FIGURE 4-13. COMPRESSIVE STRESS/STRAIN RELATIONS FOR PRESENT MODEL SUBJECTED TO PROPORTIONAL LOADING

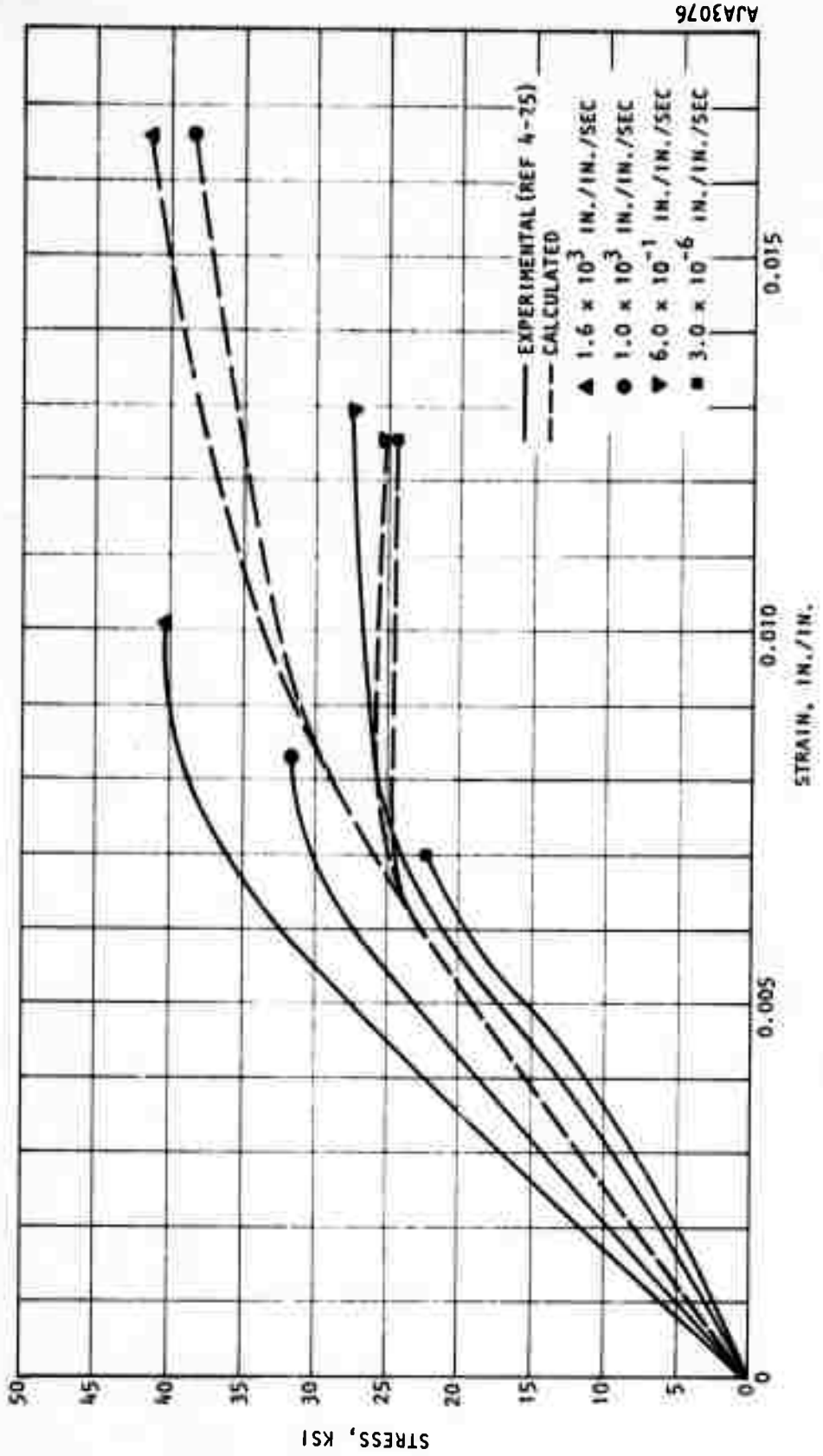

FIGURE 4-14. COMPRESSIVE STRESS/STRAIN RELATIONS FOR CEDAR CITY TONALITE AT VARIOUS STRAIN RATES

4.1.6 RATE EFFECTS--VISCOELASTICITY

The total strain is defined to be the sum of instantaneous elastic and viscoelastic parts. The strain is further divided into shear and volumetric components, which are treated separately as follows:

$$\varepsilon'_{ij} = \varepsilon_{ij} - \delta_{ij}\,\varepsilon_{kk} = (\varepsilon'_{ij})^e + (\varepsilon'_{ij})^c \qquad (4\text{-}55a)$$

$$\varepsilon_{kk} = (\varepsilon_{kk})^e + (\varepsilon_{kk})^c \qquad (4\text{-}55b)$$

In the computer program the user may choose to have either elastic or viscoelastic shear deformation and to have either elastic or viscoelastic volumetric deformation.

Kelvin, Maxwell and three-parameter fluid models are available as shown in Figure 4-15. To simplify the following discussion, no distinction is made between volumetric and shear components. The creep rate and creep strain at $t + \Delta t$ may be expressed as follows:

KELVIN

$$\dot{\varepsilon}^c + a_1\,\varepsilon^c = a_2\sigma \qquad (4\text{-}56a)$$

$$\varepsilon^c_{t+\Delta t} = \varepsilon^c_t \exp(-a_1\Delta t) + \sigma_t \frac{a_2}{a_1}(1 - \exp(-a_1\Delta t)) \qquad (4\text{-}56b)$$

where $a_1 = \frac{E}{\eta}$ and $a_2 = \frac{1}{\eta}$, E and η are the spring and dashpot constants respectively.

MAXWELL

$$\dot{\varepsilon}^c = a_1\dot{\sigma} + a_2\sigma \qquad (4\text{-}57a)$$

$$\varepsilon^c_{t+\Delta t} = \varepsilon^c_t + \left[(a_2\Delta t + a_1)\,\sigma_{t+\Delta t} - a_1\sigma_t\right] \qquad (4\text{-}57b)$$

where $a_1 = \frac{1}{E}$ and $a_2 = \frac{1}{\eta}$

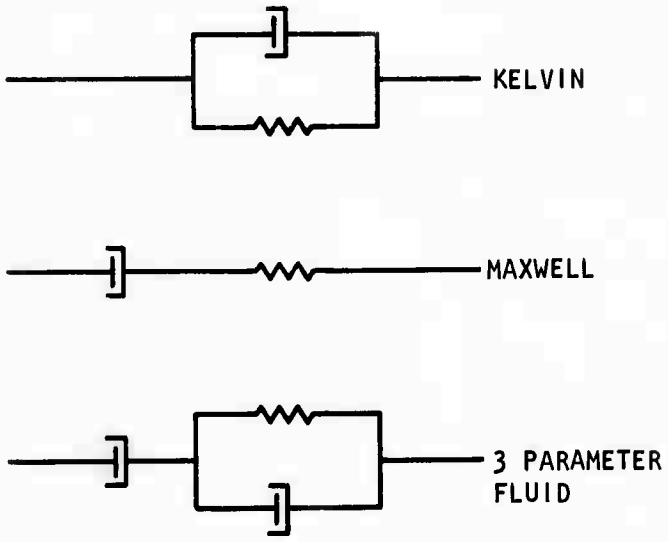

FIGURE 4-15. VISCOUS MODELS AVAILABLE IN THE PRESENT COMPUTER PROGRAM

THREE-PARAMETER FLUID

The creep strain of the three-parameter fluid is divided into two components ${}^1\varepsilon^c$ and ${}^2\varepsilon^c$ which represent the creep strain in a Kelvin model and dashpot

$$\varepsilon^c = {}^1\varepsilon^c + {}^2\varepsilon^c \tag{4-58a}$$

$${}^1\varepsilon^c_{t+\Delta t} = {}^1\varepsilon^c_t \exp(-a_1\Delta t) + \sigma_t \frac{a_2}{a_1}(1 - \exp(-a_1\,\Delta t)) \tag{4-58b}$$

$${}^2\varepsilon^c_{t+\Delta t} = {}^2\varepsilon^c_{t+\Delta t} + \frac{\Delta t}{a_2}\sigma t \tag{4-58c}$$

These models are illustrated in Figure 4-15. Various aspects of their properties are discussed in Reference 4-35. Equations 4-56a, -57a, and -58a are in suitable form for application to a time-marching integration procedure.

Typical creep and creep recovery data for several rocks are shown in Figure 4-16. Application of a Kelvin model to one of the rocks is shown in Figure 4-17. By suitably varying the parameters a_1 and a_2, a range of behavior can be reproduced. To assist the inexperienced user in selective coefficients for these models, the following guidelines are offered.

The finite element adaptation of these models uses the initial strain approach to writing the equilibrium equations based on the change in internal energy.

$$U = \int_{vol} \sigma^T\varepsilon \, dV - \int_S P^T u \, dS \tag{4-59}$$

The stress/strain relations are in terms of a matrix C of elastic stress/strain coefficients

$$\{\sigma_t\} = [C]\left|\varepsilon_o + d\varepsilon - \varepsilon^c_o\right| \tag{4-60}$$

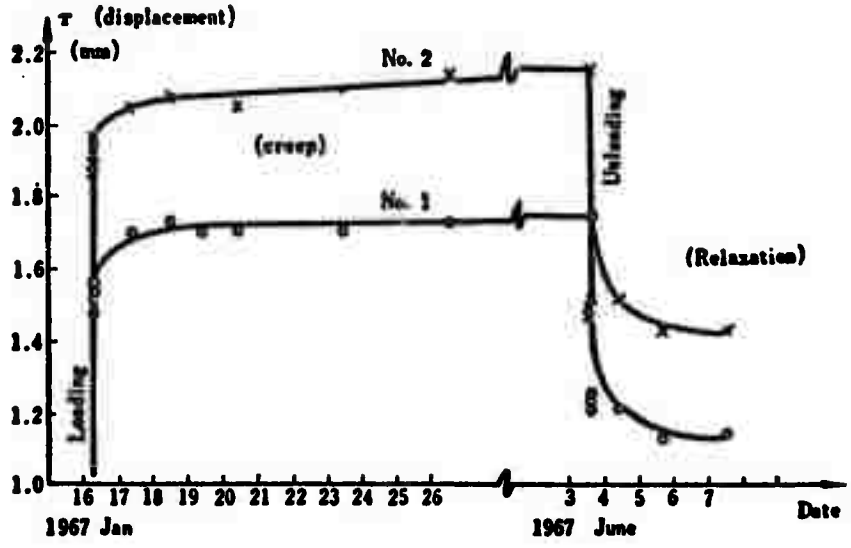

(a) CREEP AND CREEP RECOVERY (SLATE)--REFERENCE 4-28

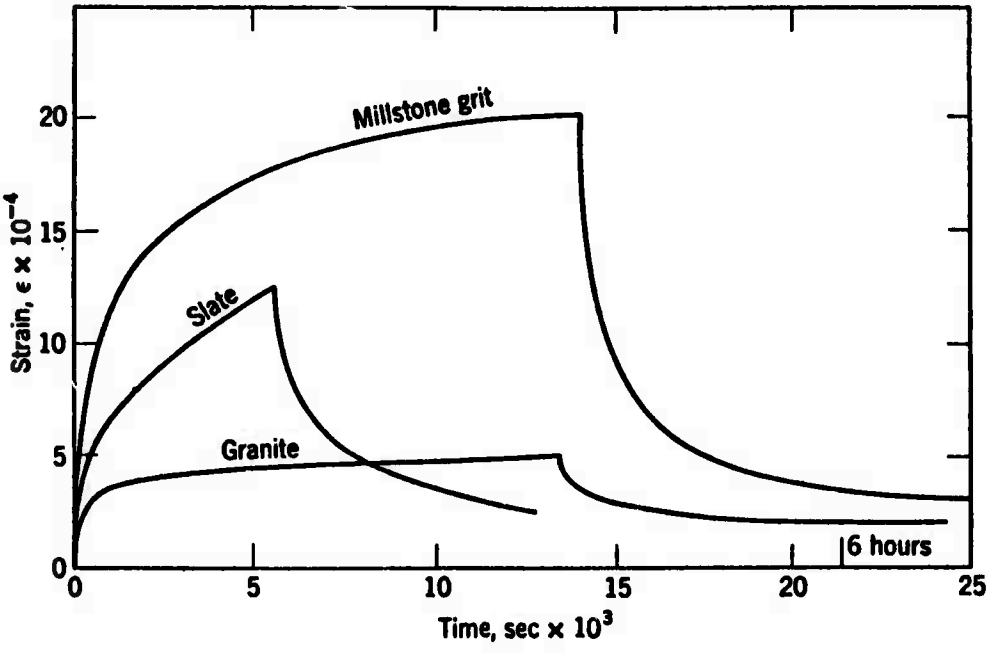

(b) CREEP UNDER CONSTANT STRESS AND RECOVERY CURVES--REFERENCE 4-30 (AFTER REFERENCE 4-31)

FIGURE 4-16. EXPERIMENTAL DATA ON VISCOELASTIC PROPERTIES OF SEVERAL ROCKS

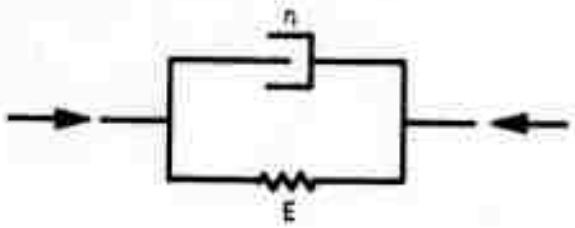

(a) $\begin{cases} E_1 = 476.2 \\ \eta_1 = 3.950 \end{cases}$ (b) $\begin{cases} E = E_1 \\ \eta = 1/2\eta_1 \end{cases}$ (c) $\begin{cases} E = E_1 \\ \eta = 1/4\eta_1 \end{cases}$

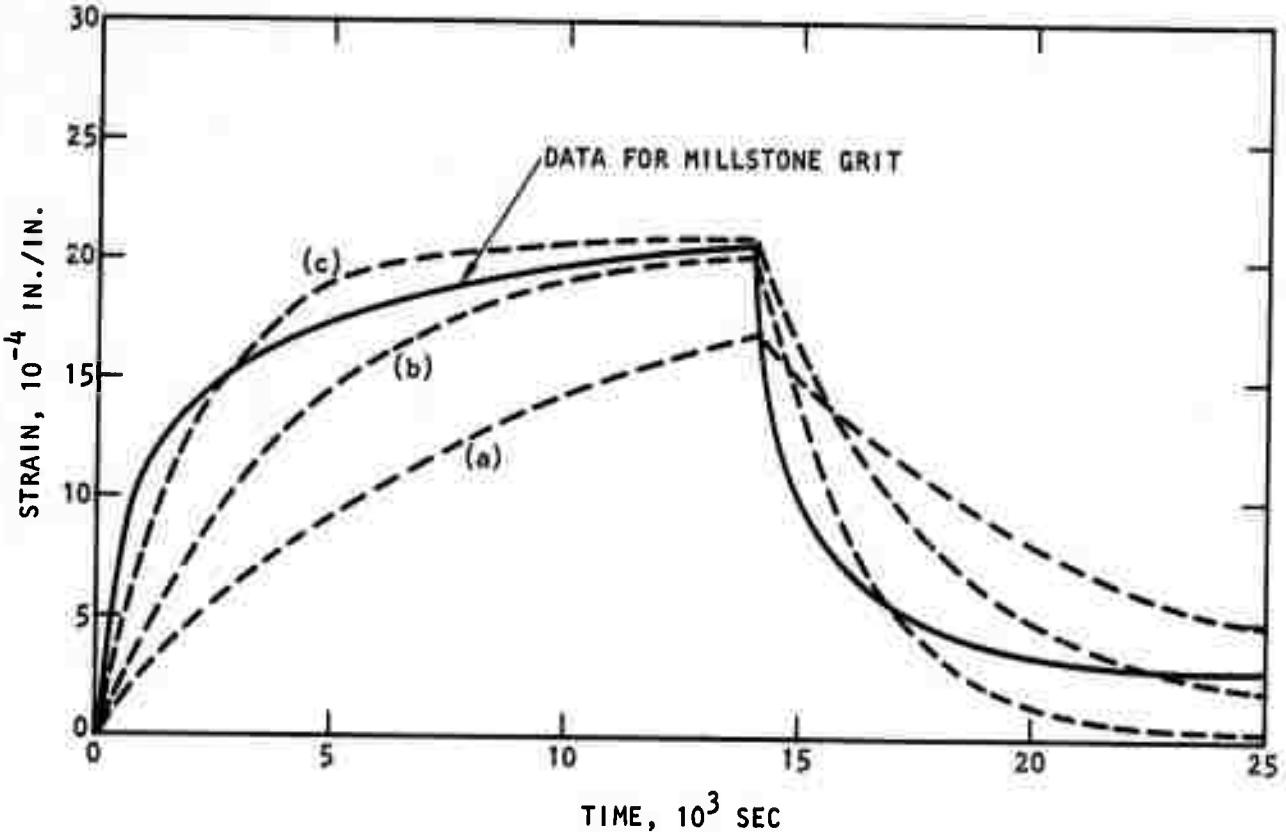

FIGURE 4-17. COMPARISON BETWEEN PRESENT CREEP MODEL AND EXPERIMENTAL DATA (REFERENCES 4-30, 4-31)

where

$\{\sigma_t\}$ = Stress at t

$\{\varepsilon_o\}$ = Total strain (including creep) at $t = t_o$

$\{d\varepsilon\}$ = Strain increment (including creep) during $\Delta t = t - t_o$

$\begin{Bmatrix} \varepsilon^c \\ \varepsilon_o \end{Bmatrix}$ = Accumulated creep to $t = t_o$

An error is committed in Equation 4-60 in that $d\varepsilon$ contains both elastic and viscous components, whereas it is treated as if it were entirely elastic. Defining the strain/displacement transformation matrix B as

$$\{\varepsilon\} = [B]\{u\} \tag{4-61}$$

The strain energy for an element is

$$U = du^T \int_{vol} B^T CB dV\, u + \int_{vol} \left(\varepsilon_o - \varepsilon_c\right)^T CB dV\, u \tag{4-62}$$

Defining

$$\int_{vol} B^T CB dV = k \tag{4-63}$$

where K is the element stiffness matrix and performing a variation with respect to the generalized displacements u results in

$$kdu = P - F_e \tag{4-64}$$

where

$$P = \int_s P^T dS$$

$$F_e = \int_{vol} \left(\varepsilon_o - \varepsilon_c\right)^T CB dV$$

It is significant that the element stiffness matrix consists entirely of linear elastic terms. Thus, the assemblage stiffness matrix needs to be formulated only once, resulting in great economy of computing. It is necessary to store the components of the creep strain at t_o for use in the next step.

This approach has been adapted to finite element for rock and concrete (Reference 4-26). Some experimental work which has been performed on rock is compared in Reference 4-27 with a series of Kelvin models. Reference 4-28 discusses methods of accounting separately for volumetric and deviatoric creep strains.

4.2 MATERIAL PROPERTIES OF JOINTS

This section describes the properties which may be assigned to joints. These properties consist of the shearing and normal stiffnesses of the joints. They correspond physically to the stiffness and strength of fault gouge, to the roughness of the joints and to the angles of slip surfaces relative to the principal plane of the joint. They are classed as dilatant if shearing produces joint expansion or contraction or nondilatant if shearing and normal displacement are uncoupled. The properties are specified by the user in natural coordinates which may be directions parallel and perpendicular either to slip surfaces or to the principal plane of the joint. In either case, transformation to global directions is automatically performed by the program.

As in the case of homogeneous material properties, the joint properties are controlled by subroutines CONECT and ELPL through modular subroutines. Presently, these contain built-in joint properties. As more data become available on properties of joints and the present joint material properties become obsolete, the present model may easily be modified without disturbing the main program or any of the other material properties.

4.2.1 NONDILATANT JOINTS

This class of joints is the simplest to model mathematically since there is no volume change due to shearing strains, and therefore the shear and the normal components of deformation are uncoupled and the stress-strain relations are as follows:

$$\begin{Bmatrix} \sigma_n \\ \sigma_s \end{Bmatrix} = \begin{bmatrix} C_{nn} & 0 \\ 0 & C_{ss} \end{bmatrix} \begin{Bmatrix} \varepsilon_n \\ \varepsilon_s \end{Bmatrix} \tag{4-65}$$

However, C_{nn} and C_{ss} are nonlinear functions.

In stress-deformation relationship in normal direction, three distinct stages can be recognized (see Figure 4-18);

a. Separation, $C_{nn} = C_{ss} = 0$ when $\varepsilon_n \geq 0$

b. Crushing of the surface irregularities or the compression of the material in the fault or joint, if any $C_{nn} = E_c$ $(\varepsilon_n^c < \varepsilon_n < 0)$. For smooth surfaces this case does not exist, therefore $\varepsilon_n^c = 0$.

c. Contact, $C_{nn} = E_f$. $(\varepsilon_n < \varepsilon_n^c)$

It is important to note that very high values can be assigned to E_f without any numerical problems with the special joint element described in Section 3.

The tangential stress-strain relationship is assumed to be elastic-perfectly plastic using a Mohr-Coulomb yield criterion:

$$\begin{aligned} C_{ss} &= G \qquad \sigma_s < c + \sigma_n \tan \phi \\ C_{ss} &= 0 \qquad \sigma_s = c + \sigma_n \tan \phi \end{aligned} \tag{4-66}$$

where c and ϕ are the cohesion or the angle of friction.

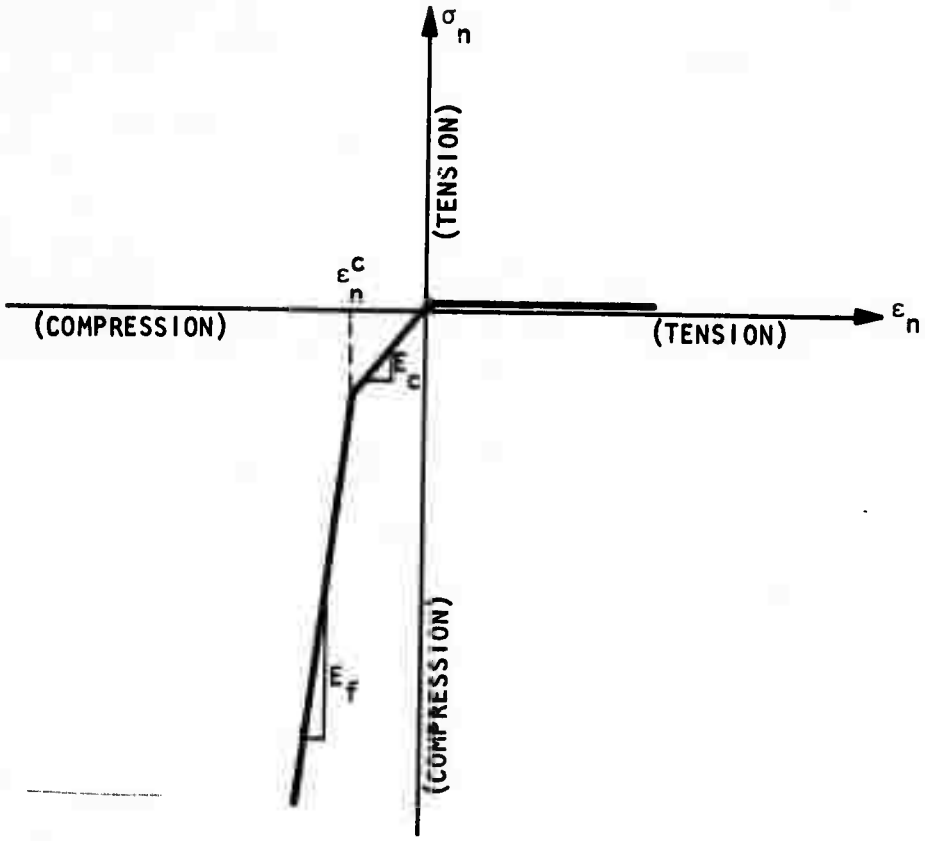

FIGURE 4-18. NORMAL STRESS-STRAIN RELATION FOR JOINTS

4.2.2 DILATANT JOINTS

Dilatancy of rock joints and faults are very complex to model mathematically; however, to include a measure of dilatancy, the procedure developed by Goodman, Dubois, and Brekke (Reference 4-36) is used here. Further data are available from Reference 4-37.

It is assumed that the deformation in p-q coordinate system shown in Figure 4-19 is nondilatant. The angle γ between the p direction and the joint surface is, therefore, defined to be a material property of the joint. The stress-strain relation in n-s coordinate is:

$$\begin{Bmatrix}\sigma_n\\ \sigma_s\end{Bmatrix} \begin{bmatrix}(C_{qq}\, C^2 + C_{pp}\, S^2) & (C_{qq} - C_{pp})\, SC\\ (C_{qq} - C_{pp})\, SC & (C_{qq}\, S^2 + C_{pp} C^2)\end{bmatrix} \begin{Bmatrix}\varepsilon_n\\ \varepsilon_s\end{Bmatrix} \qquad (4\text{-}67)$$

where

$C = \cos \gamma$

$S = \mathrm{Sin}\ \gamma$

4.2.3 DEMONSTRATION OF JOINT ELEMENT

The example problem in Figure 4-20 demonstrates the behavior of the present joint element. The problem consists of a plane system of three solid blocks and three joint planes. The system is restrained at the bottom and is subjected to lateral pressure P and vertical pressure 2P. The joints are assumed to be filled with nondilatent material having the properties shown in Figure 4-20. The blocks are assumed to have the isotropic elastic properties shown in Figure 4-20. The material in the joints is represented by joint elements which are shown as their shaded strips. Ambiguity with respect to nodal displacements would arise at the point of the wedge-shaped block if the joint elements were to extend to the point. Ambiguity is avoided by stopping the elements short of the point. This is a good approximation to a physical

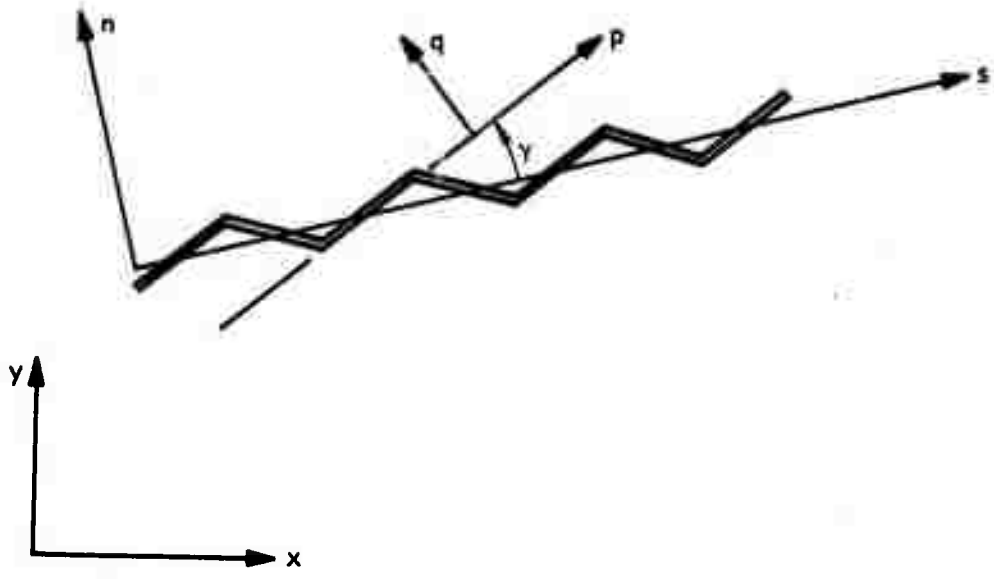

FIGURE 4-19. DILATANT JOINT

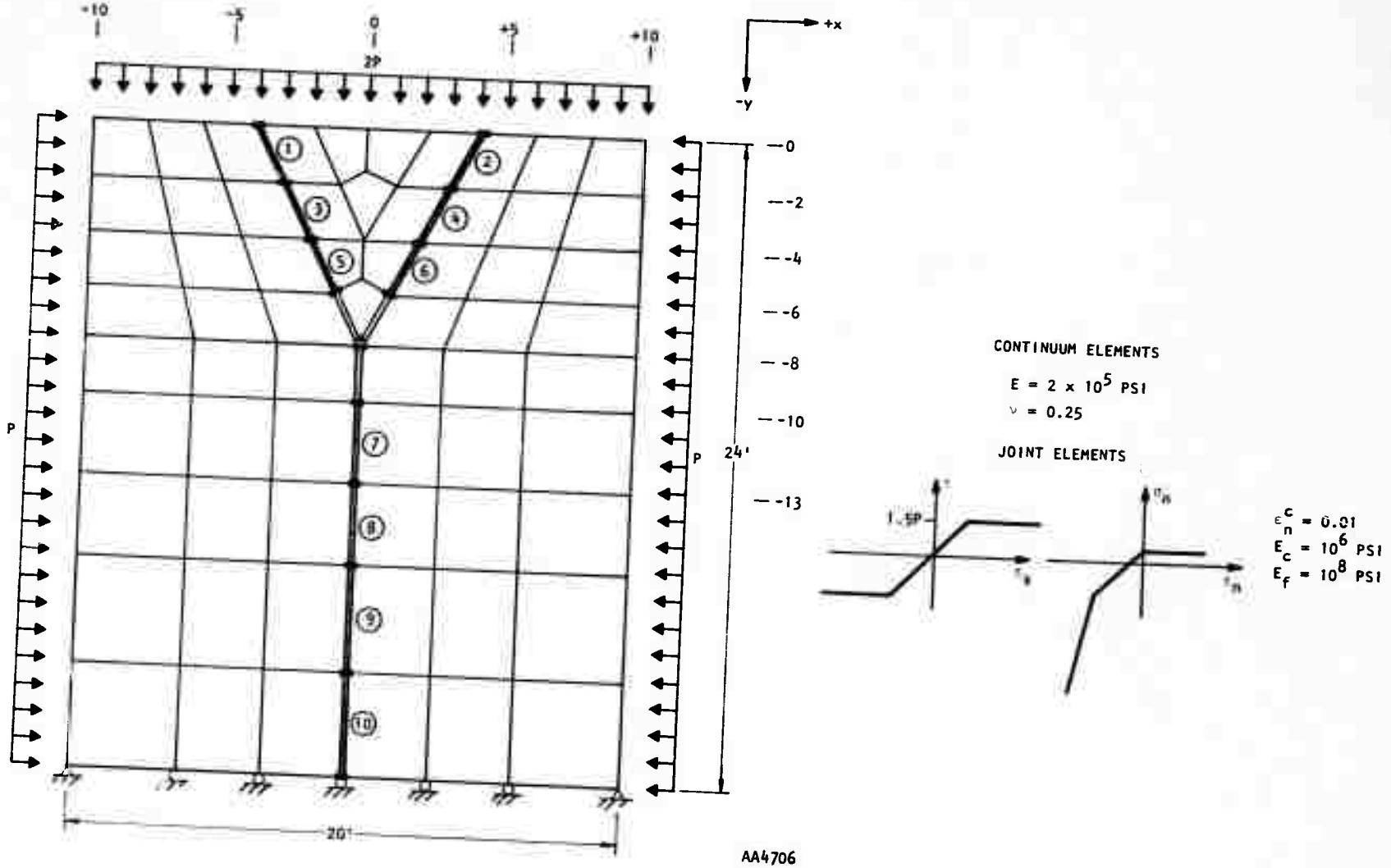

FIGURE 4-20. GEOMETRY OF EXAMPLE PROBLEM USING PLANE SLIP ELEMENT

system if the joint elements extend infinitesimally close to the point. In the present example, the gap is made large to illustrate how the difficulty is avoided. The blocks are represented by plane strain elements.

Results of the present example are shown in Figures 4-21 and 4-22. Figure 4-21 shows how the vertical displacement varies as a function of horizontal distance from the centerline. Each curve in Figure 4-21 corresponds to a different distance below the top surface. Figure 4-22 shows the wedge in its final position.

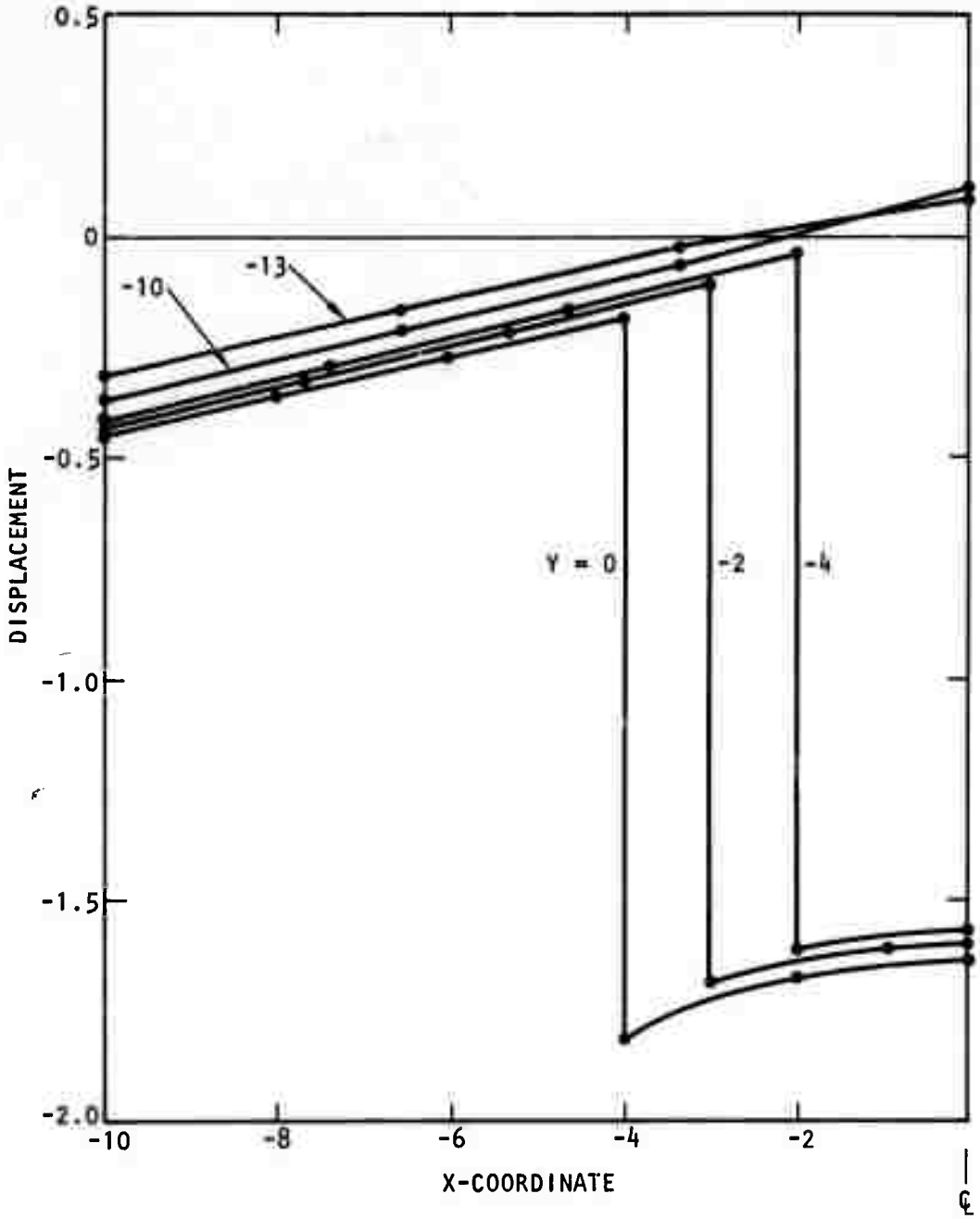

FIGURE 4-21. VERTICAL DISPLACEMENTS FOR EXAMPLE WEDGE PROBLEM

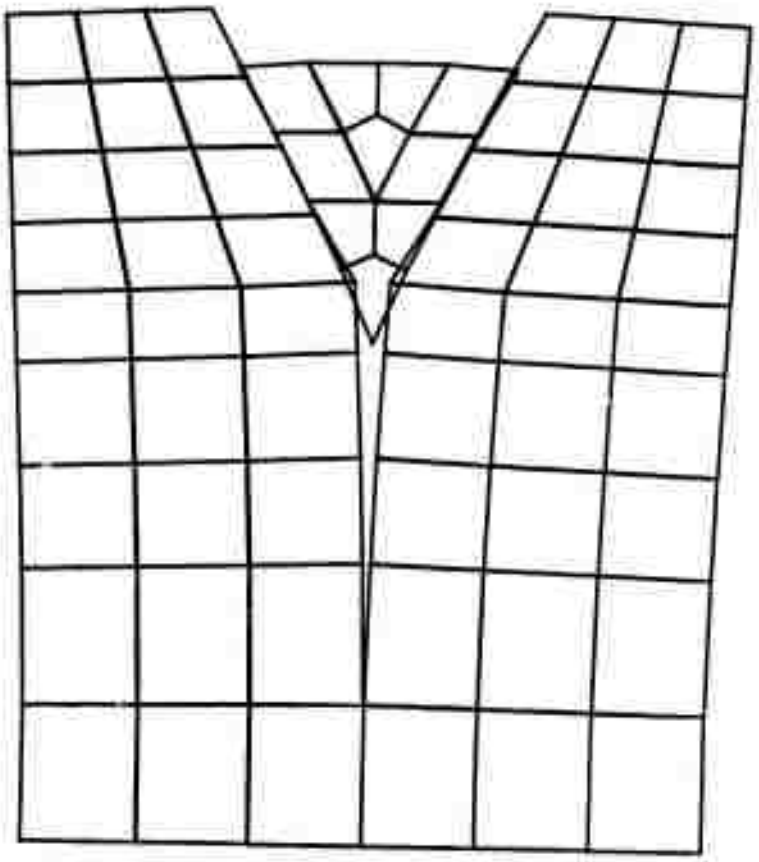

FIGURE 4-22. FINITE ELEMENT MESH IN THE DISPLACED CONFIGURATION FOR WEDGE PROBLEM IN FINAL EQUILIBRIUM STATE

REFERENCES

4-1. Saucier, K. L., *Properties of Cedar City Tonalite*, MPC-69-9, U.S. Army Corps of Engineers, Waterways Experiment Station, June 1969.

4-2. LaMori, P. N., *Compressibility of Three Rocks, (A) Westerly Granite and Solenhofen Limestone to 40 Kbar and 300°C, (B) Cedar City Tonalite to 40 Kbar at Room Temperature*, DASA 2151, Battelle Memorial Institute, August 1968.

4-3. Jones, A. H., and N. H. Froula, *Uniaxial Strain Behavior of Four Geological Materials to 50 Kilobars*, DASA 2209, General Motors Materials and Structures Laboratory, March 1969.

4-4. Petersen, C. F., *Shock Wave Studies of Selected Rocks*, Stanford Research Institute, May 1969.

4-5. Simmons, G., "Velocity of Shear Waves in Rocks to 10 Kilobars, Part 1," *J. Geophys. Res.*, Vol. 69, No. 6, 1964, p. 1123.

4-6. Stephens, D. R., *Elastic Constants of Fractured Granodiorite*, UCID-15369, Lawrence Radiation Laboratory, (to be published).

4-7. Walsh, J. B., "The Effect of Cracks on Poisson's Ratio," *J. Geophys. Res.*, Vol. 70, No. 2, January 15, 1965.

4-8. Walsh, J. B., "The Effect of Cracks on Poisson's Ratio," *J. Geophys. Res.*, Vol. 70, No. 20, October 15, 1965.

4-9. Hill, R., *The Mathematical Theory of Plasticity*, Oxford, 1950.

4-10. Drucker, D. C., "A More Fundamental Approach to Stress/Strain Relations," *Proc., 1st U.S. Cong. Appl. Mech.*, ASME, 1950.

4-11. Drucker, D. C., "Some Implications of Work Hardening and Ideal Plasticity," *Quart. Appl. Math.*, Vol. 7, 1950, pp. 411-418.

4-12. Drucker, D. C., and W. Prager, "Soil Mechanics and Plastic Analysis or Limit Design," *Quart. Appl. Math.*, Vol. 10, 1952, pp. 157-175.

4-13. Sandler, I., and F. L. Dimaggio, *Material Model for Rocks*, DASA 2595, Paul Weidlinger Consulting Engineering, October 1970.

4-14. Walsh, J. B., and W. F. Brace, "A Fracture Criterion for Brittle Anisotropic Rocks," *J. Geophys. Res.*, Vol. 69, No. 16, 1964, p. 3449.

4-15. Griffith, A. A., "Theory of Rupture," *Proc. 1st Int. Cong. Appl. Mech.*, 1924, p. 55.

4-16. McClintock, F. A., and J. B. Walsh, "Friction on Griffith Cracks Under Pressure," *Proc. 4th U.S. Natl. Cong. Appl. Mech.*, 1963, pp. 1015-1021.

4-17. Jaeger, J. C., "Shear Failure of Anisotropic Rocks," *Geologic Magazine*, Vol. 97, 1960, pp. 65-72.

4-18 McLamore, R., and K. E. Grey, "The Mechanical Behavior of Anisotropic Sedimentary Rocks," *Trans.*, ASME, February 1967.

4-19. Mogi, K., "Effect of the Intermediate Principal Stress on Rock Failure," *J. Geophy. Res.*, Vol. 72, No. 20, October 1967, p. 5117.

4-20. Pariseau, W. G., "Plasticity Theory for Anisotropic Rocks and Soils," *10th Symposium on Rock Mechanics*, University of Texas, Austin, May 1968.

4-21. Perzyna, R., "The Constitutive Equations for Work-Hardening and Rate Sensitive Plastic Materials," *Proc. Vib. Prob.*, 3, 4, 1963. pp. 281-290.

4-22. Hohenemser, K., and W. Prager, *Über die Ansätze der Mechanik Isotroper Kontinua*, ZAMM, 12, 1932, pp. 216-226.

4-23. Dimaggio, F. L., and I. Sandler, *The Effect of Strain Rate on the Constitutive Equations of Rock*, DNA 2801T, Paul Weidlinger Consulting Engineering, October 1971.

4-24. Isenberg, J., and F. S. Wong, *A Viscoplastic Model with a Discussion of its Stress/Strain and Wave Propagation Properties*, R-7110-1886, Agbabian-Jacobsen Associates, April 1971.

4-25. Perkins, R. D., and S. J. Green, *Uniaxial Stress Behavior of Porphyritic Tonalite at Strain Rates to 10^3/Second*, DASA 2200, General Motors Manufacturing Development, February 1969.

4-26. Zienkiewicz, O. C., "A Numerical Method of Viscoelastic Stress Analysis," *Intl. J. Mech. Sci.*, Vol. 10, 1968, pp. 807-827.

4-27. Hayashi, M., and S. Hibino, "Progressive Relaxation of Rock Masses During Excavation of Underground Cavity," *Proc. Intl. Symp. on Rock Mech.*, Madrid, October 1968.

4-28. Soydemu, C., and W. E. Schmid, "Deformation and Stability of Visco-elastic Soil Media," *J. Soil Mech. and Found. Div.*, Proc. ASCE, Vol. 96, No. SM6, November 1970.

4-29. Yaghmai, S., *Incremental Analysis of Large Deformations in Mechanics of Solids with Applications to Axisymmetric Shells of Revolution*, NASACR-1350, University of California, Berkeley, June 1969.

4-30. Obert, L., and W. I. Duvall, *Rock Mechanics and the Design of Structures in Rock*, John Wiley and Sons, Inc., New York, 1967.

4-31. Evans, R. H., "The Elasticity and Plasticity of Rocks and Artificial Stone," *Leeds Philosophical and Literary Soc.*, Proc., 3, Part 3, 1966.

4-32. Brace, W. F., et al., "Dilatency in the Fracture of Crystalline Rocks," *J. Geophys. Res.*, Vol. 71, No. 16, August 15, 1966.

4-33. Giardini, A. A., et al., "Triaxial Compression Data on Nuclear Explosion Shocked, Mechanically Shocked and Normal Granodiorite from the Nevada Test Site," *J. Geophys. Res.*, Vol. 73, No. 4, February 15, 1968.

4-34. Army Corps of Engineers, Missouri River Division Laboratory, *Tests for Strength Characteristics of Rock, Pile Driver Project*, MRDL-64190, 1964.

4-35. Flugge, W., *Viscoleasticity*, Blaisdell Publishing Co., Waltham, Mass., 1967.

4-36. Goodman, R. E., and J. Dubois, "Duplication of Dilatency in Analysis of Jointed Rocks," *J. of the Soil Mechanics*, Proc. ASCE, Vol. 98, No. SM4, April 1972.

4-37. Goodman, R. E., et al., *Research on Strength-Deformability--Water Pressure Relationships for Faults in Direct Shear*, Final Report on ARPA Contract H0210020, University of California, April 1972.

SECTION 5

DESCRIPTION OF THE COMPUTER PROGRAM

This section describes the computer program in terms of features which are apparent to the user, such as automatic mesh generation, and in terms of its logical structure. The first part of the section describes the steps which the user takes in order to prepare the input data. The mesh generator, bandwidth reducer and plotting capability are described. The motive and logic diagrams for element renumbering are also described.

The second part of this section describes the execution part of the computer program in terms of logic diagrams. Subroutines are described which control the computation, form the global stiffness matrix and compute the load vector, form element stiffnesses and other operations. Also described is the technique of multibuffering whereby data is transferred between core and peripheral storage units at the same time that computations are being performed in core. This technique greatly improves the efficiency of the program for problems where large blocks of data are stored on peripheral memory units.

5.1 PROCESSING OF INPUT DATA

The sequence in which input data are processed is shown in Figure 5-1. There are three basic phases. The first consists of generating continuum (two- or three-dimensional) and joint elements and plotting the results. The second phase consists of adding other elements (beam, thick shell, bar, etc.) manually, reducing the bandwidth, shuffling the element numbers so that they appear in the order of contribution to the global stiffness matrix, and plotting the final mesh. The third phase consists of reading additional data such as material properties and loads.

MESH GENERATOR

The automatic mesh generation scheme incorporated in the program requires the user to provide a coarse mesh which the program refines by subdivision under the control of the user. The main goal is to minimize the

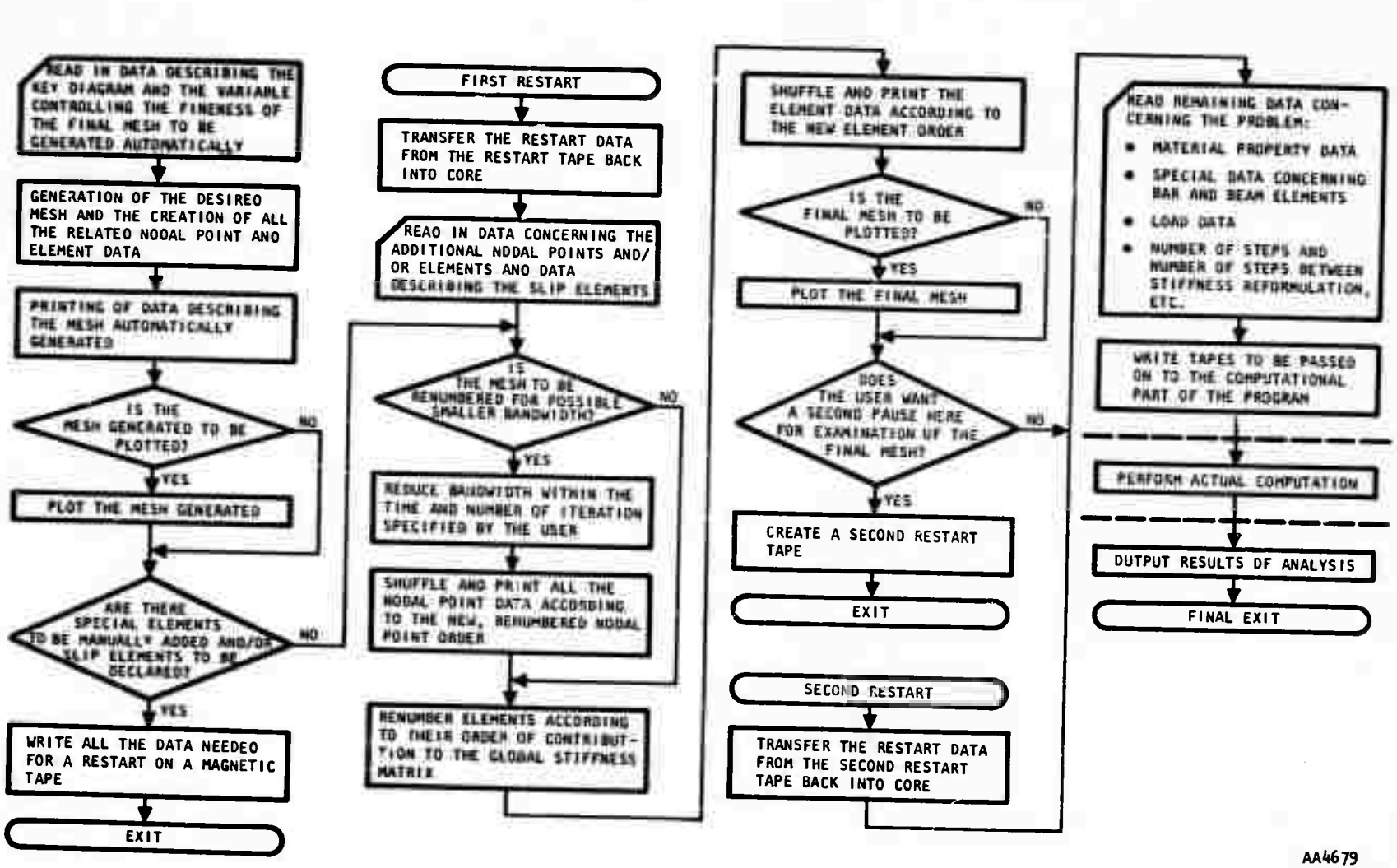

FIGURE 5-1. OPERATIONS OF THE INPUT PORTION OF THE PRESENT COMPUTER PROGRAM

the input preparation on the part of the user. The method uses the key diagram concept described in Reference 5-1; the remainder of the present mesh generation scheme is new and original work.

The subdivision of the given, coarse mesh to obtain the final, fine mesh is carried out by subdividing each one of the mesh units, as "zones," within the coarse mesh in the following manner. Consider the simple case of a general, two-dimensional mesh, in which the basic mesh unit or zone is a parabolic quadrilateral as shown in Figure 5-2. Assume that the x and y coordinates of the four corner mesh points, 1, 2, 3, and 4, as well as those of the four midpoints, 5, 6, 7, and 8, are known. The x and y coordinates of an arbitrary point P within this zone can then be expressed conveniently in terms of the coordinates of the eight points through the use of the local, curvilinear coordinates, ξ and η, whose values range from -1 to +1 on opposite sides as indicated in Figure 5-2. Thus, one can write

$$x = \sum_{i=1}^{8} N_i x_i$$
$$y = \sum_{i=1}^{8} N_i y_i \qquad (5\text{-}1)$$

in which N_i's are the so-called "isoparametric shape functions" expressible in terms of the curvilinear coordinates as follows:

$$\begin{aligned}
N_1 &= -\frac{1}{4}(1-\xi)(1-\eta)(\xi+\eta+1) \\
N_2 &= -\frac{1}{4}(1-\xi)(1+\eta)(\xi-\eta+1) \\
N_3 &= \frac{1}{4}(1+\xi)(1+\eta)(\xi+\eta-1) \\
N_4 &= \frac{1}{4}(1+\xi)(1-\eta)(\xi-\eta-1) \\
N_5 &= \frac{1}{2}(1-\xi)(1-\eta^2) \\
N_6 &= \frac{1}{2}(1-\xi)(1-\eta^2) \\
N_7 &= \frac{1}{2}(1-\xi^2)(1+\eta) \\
N_8 &= \frac{1}{2}(1-\xi^2)(1+\eta)
\end{aligned} \qquad (5\text{-}2)$$

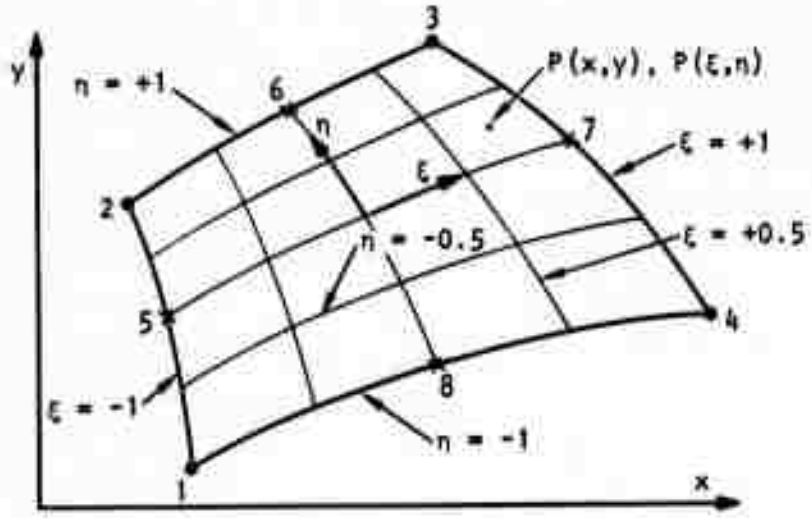

FIGURE 5-2. QUADRILATERAL ZONE, WHOSE SHAPE AND COORDINATES ARE EXPRESSED BY PARABOLIC SHAPE FUNCTIONS

Thus, for a certain set of values of the curvilinear coordinates, or "natural coordinates," the corresponding Cartesian coordinates can be easily found from Equations 5-2. Consequently, to subdivide the zone into a 4 x 4 mesh, for example, and establish the Cartesian coordinates of the twenty-one new mesh points, one merely substitutes into Equations 5-1 twenty-one times, each time with a different combination of values of ε and η which are incremented successively by 0.5.

This technique can be used to treat each one of the zones in a given, coarse mesh of any configuration. The only restriction that has to be observed is that the number of subdivisions between any two adjoining zones must match. This is to satisfy the fundamental connectivity requirement of the finite element method. To satisfy this continuity requirement and to facilitate the preparation of the input that defines the basic coarse mesh, it is convenient to introduce the so-called "key diagram."

A key diagram, in general, is a rectangular grid resembling a checker-board. It has no physical dimensions. Its purpose is to present, or define, the connectivity of the zones in the coarse mesh and to facilitate defining the position of a mesh point in the form of row and column numbers in the coarse mesh. Another purpose of the key diagram is to help define the extent of subdivision of a zone, for, to satisfy the aforementioned connectivity, a newly introduced mesh line has to extend across all the zones located in the same row or column in the key diagram.

Figure 5-3 illustrates the generation of a simple finite element mesh representing a dam and part of its foundation. The domain has been blocked into three zones which are connected as shown in the accompanying key diagram. The final mesh is the result of subdividing the first and the last zone into two subdivisions and the second into three subdivisions in the vertical direction, and all three zones into three subdivisions in the horizontal direction.

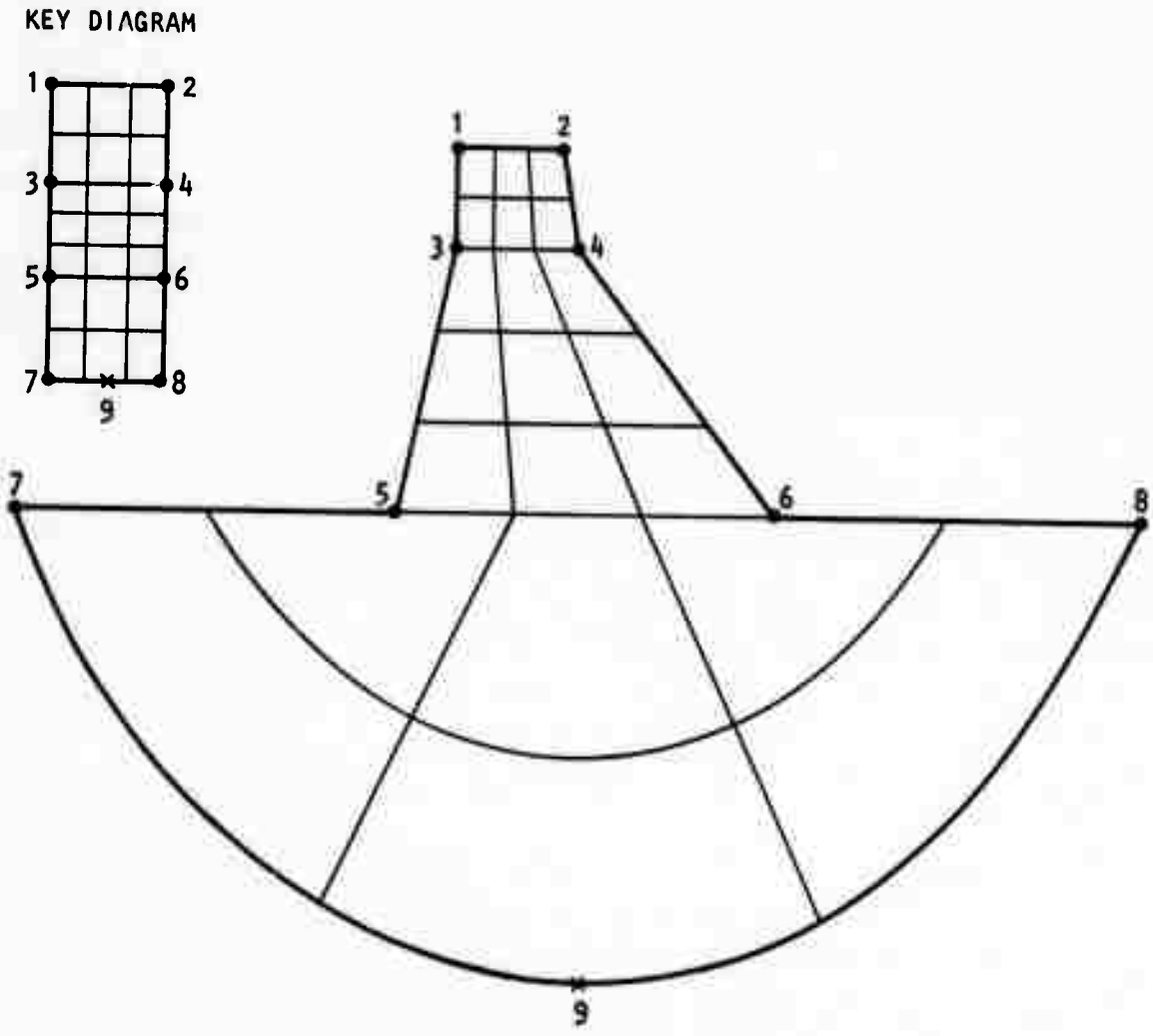

FIGURE 5-3. KEY DIAGRAM AND RESULTING FINITE ELEMENT MESH FOR A DAM AND FOUNDATION

The Input to the program for this particular example would consist of the following:

a. A statement that the key diagram, or the original coarse mesh, is 3 by 1.

b. The rectangular coordinates of the given, eight mesh points and those of the single midpoint that define the lower boundary on a curve.

c. Three material numbers to associate the first two zones with concrete and the third with the soil medium.

d. The three numbers, 2, 3 and 2, that specify the number of subdivisions in the vertical direction, and the number 2 for the horizontal direction.

The computer program would assign the material number for a zone to all of the elements that are created in the zone, and number the nodal points and elements in the final mesh column-wise, from the top to the bottom, from the left toward the right by referring to the key diagram. The curved mesh lines in the third zone are meant only to emphasize the fact that nodal points are generated on a second degree curve because of the nature of the shape function; the actual mesh line is always a straight line between two neighboring mesh points.

In the previous example, if the user is not satisfied with the refinement of the final mesh or with that in any one of the zones, he can quickly rerun the problem by modifying the four integers mentioned in Item *d* without having to change any of the data mentioned in the first three items which define the given, coarse mesh. This is perhaps the most important feature of this particular mesh generation scheme.

Aside from being used to define an edge of a zone on a curve, a midpoint can also be used to imply a mesh grading. The mesh shown in Figure 5-4 is the result of specifying the three midpoints, M_1, M_2 and M_3, purposely off-centered and toward the edge of the circular hole. Midpoints M_1 and M_2 are there merely to form the edge of the hole on a curve. In this particular example, number of subdivisions of 5 and 5 in the vertical direction (in the key diagram) and of 16 in the horizontal direction were specified.

Another feature that makes the scheme versatile and powerful is the provision for the user to prescribe a zone as void merely by assigning zero for the material number of that zone. With this provision, one can easily generate a mesh around a notch or a cutout. The mesh around a tunnel shown in Figure 5-5 is such an example.

The final feature to be mentioned here is the program's ability to join any two edges in the key diagram. This makes it possible to produce the meshes shown in Figures 5-6 and 5-7. The user may prefer the type of mesh shown in Figure 5-7 over that shown in Figure 5-5 for the radiating pattern of the mesh lines which makes it easier to make a finer mesh around the edge of the tunnel.

The same scheme can be used to generate a three-dimensional mesh. The necessary changes are to replace the two-dimensional shape function and key diagram by their three-dimensional counterparts, and to introduce the third Cartesian coordinate. The basic "zone" or "block" in this case is a general, six-sided body with parabolic edges. It has eight corner nodes and twelve midpoints as shown in Figure 5-8, and the Cartesian coordinates at an arbitrary point P within the block having the natural coordinates ξ, η and ζ are expressible in terms of the Cartesian coordinates of the twenty controlling points as follows:

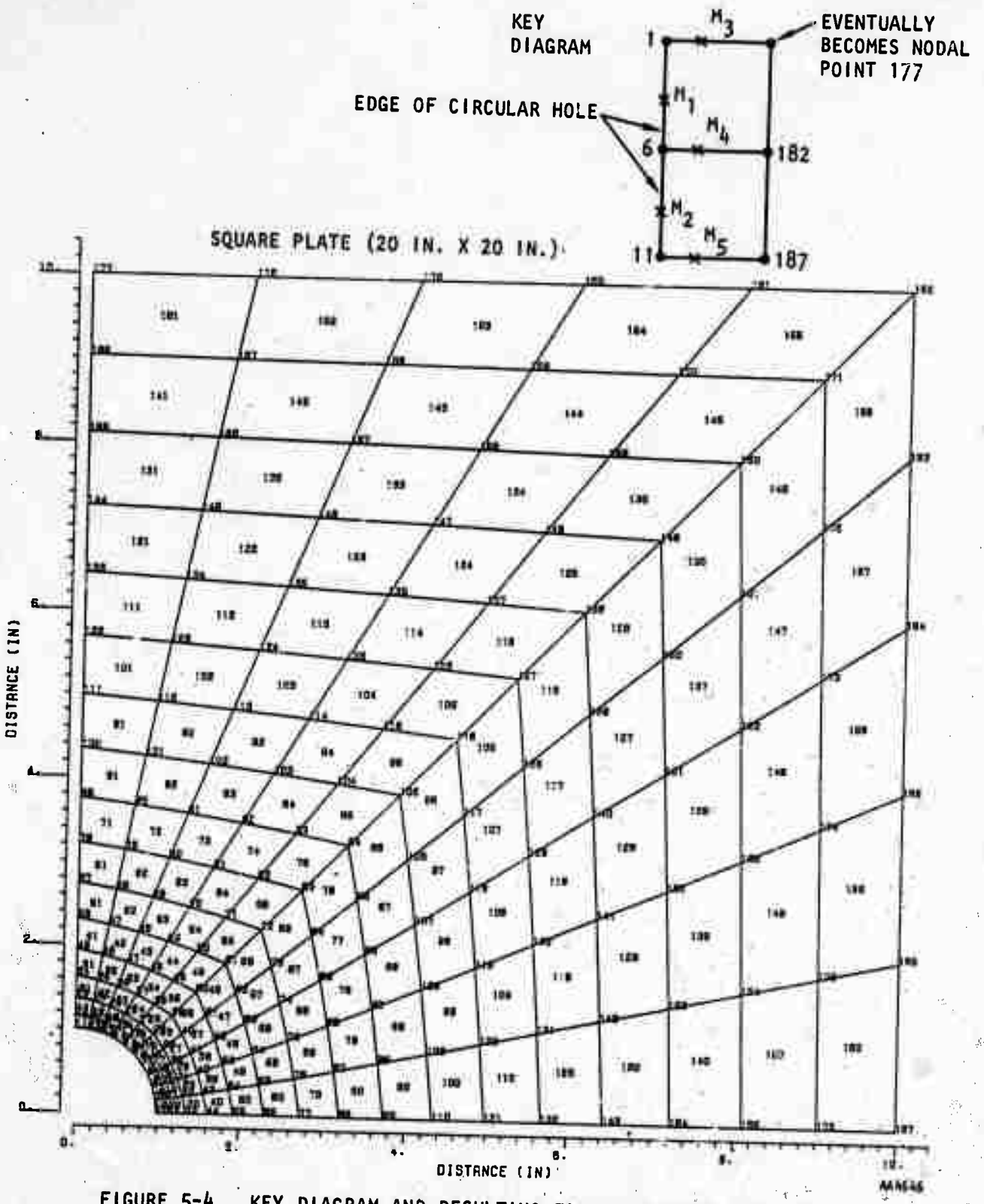

FIGURE 5-4. KEY DIAGRAM AND RESULTING FINITE ELEMENT MESH FOR A QUADRANT OF A SQUARE PLATE WITH A CIRCULAR HOLE

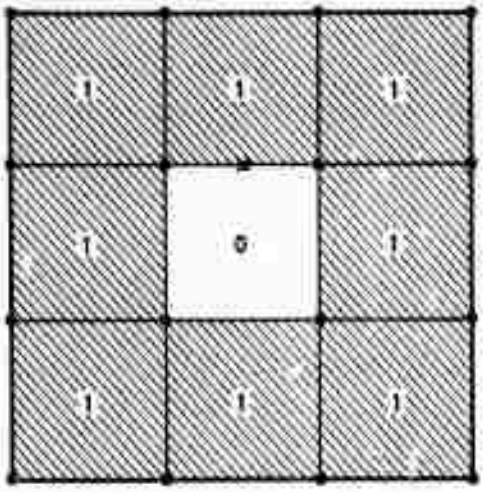

KEY DIAGRAM

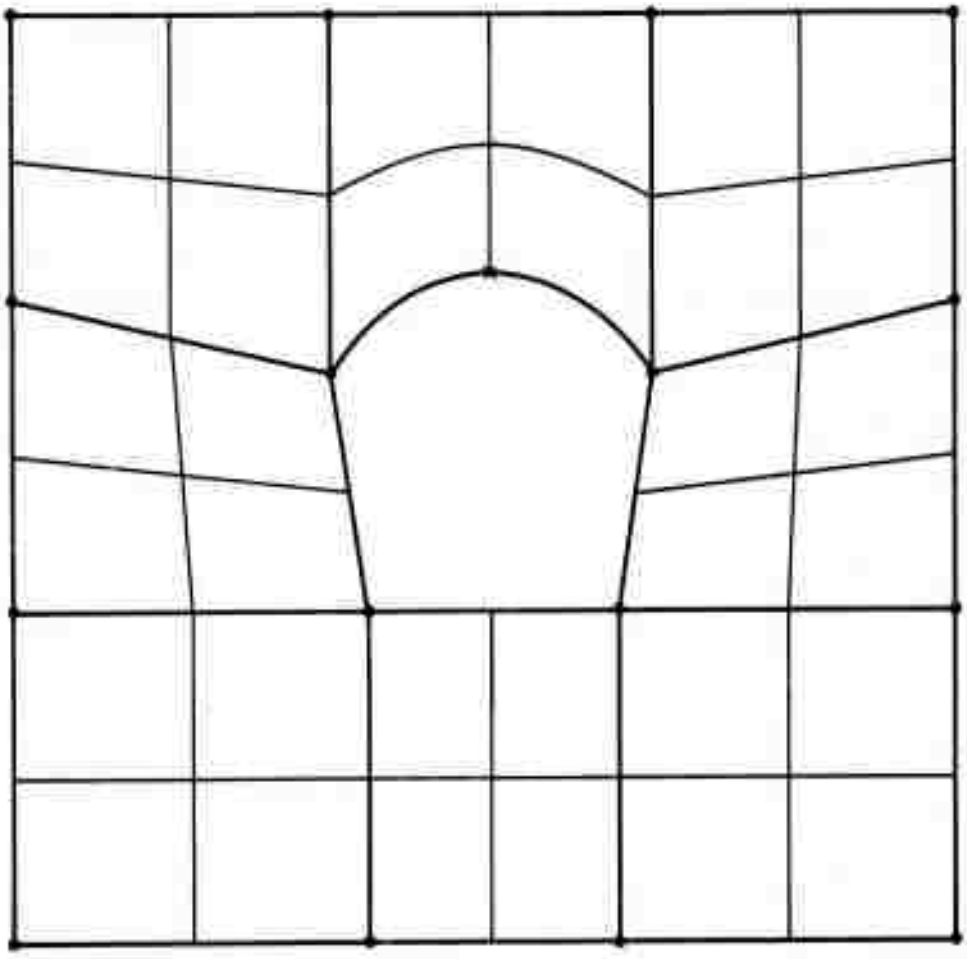

AA4680

FIGURE 5-5. KEY DIAGRAM AND RESULTING FINITE ELEMENT MESH FOR A TUNNEL

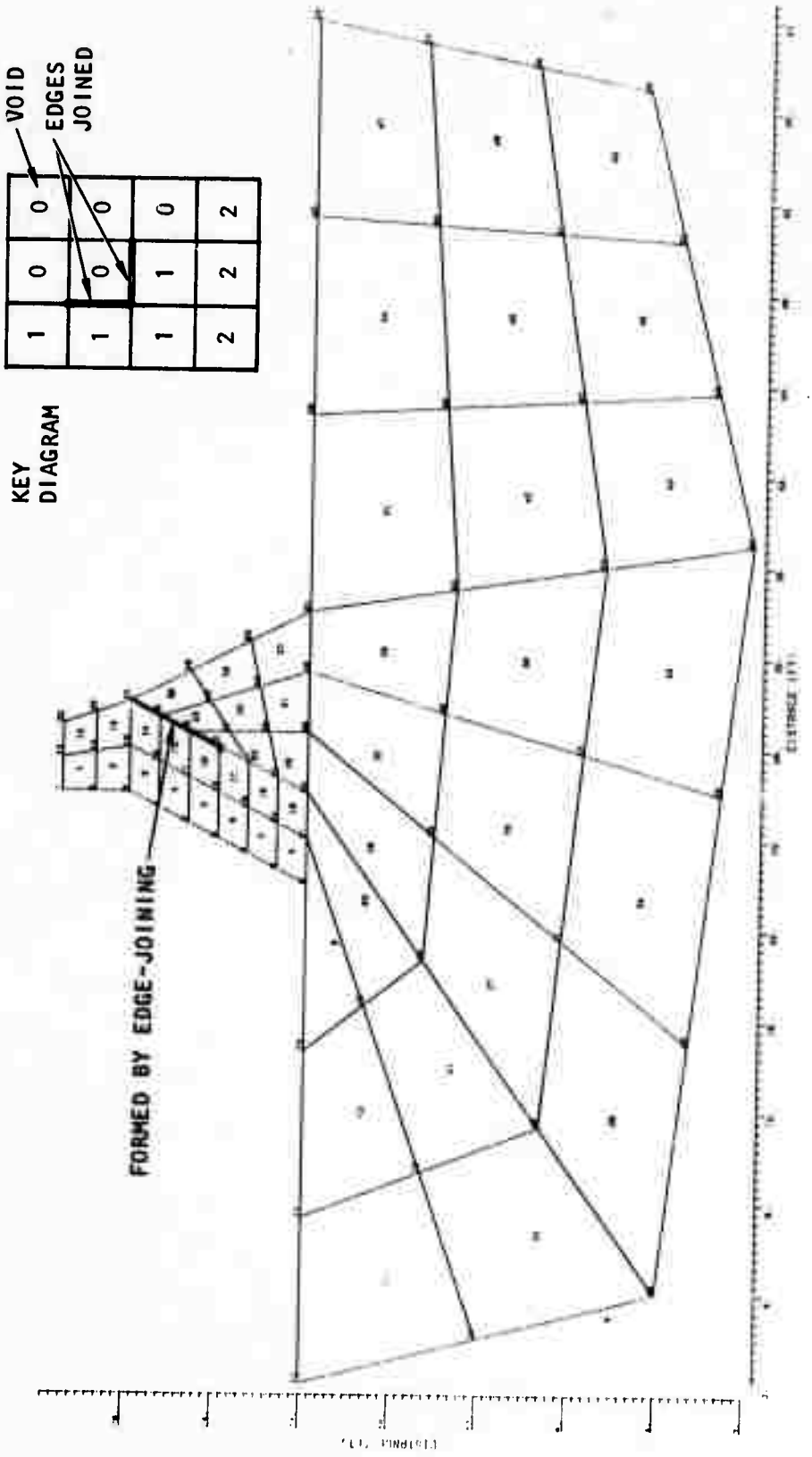

FIGURE 5-6. KEY DIAGRAM AND RESULTING FINITE ELEMENT MESH FOR A DAM ON FOUNDATION, ILLUSTRATING CAPABILITY TO JOIN ANY TWO EDGES IN THE KEY DIAGRAM

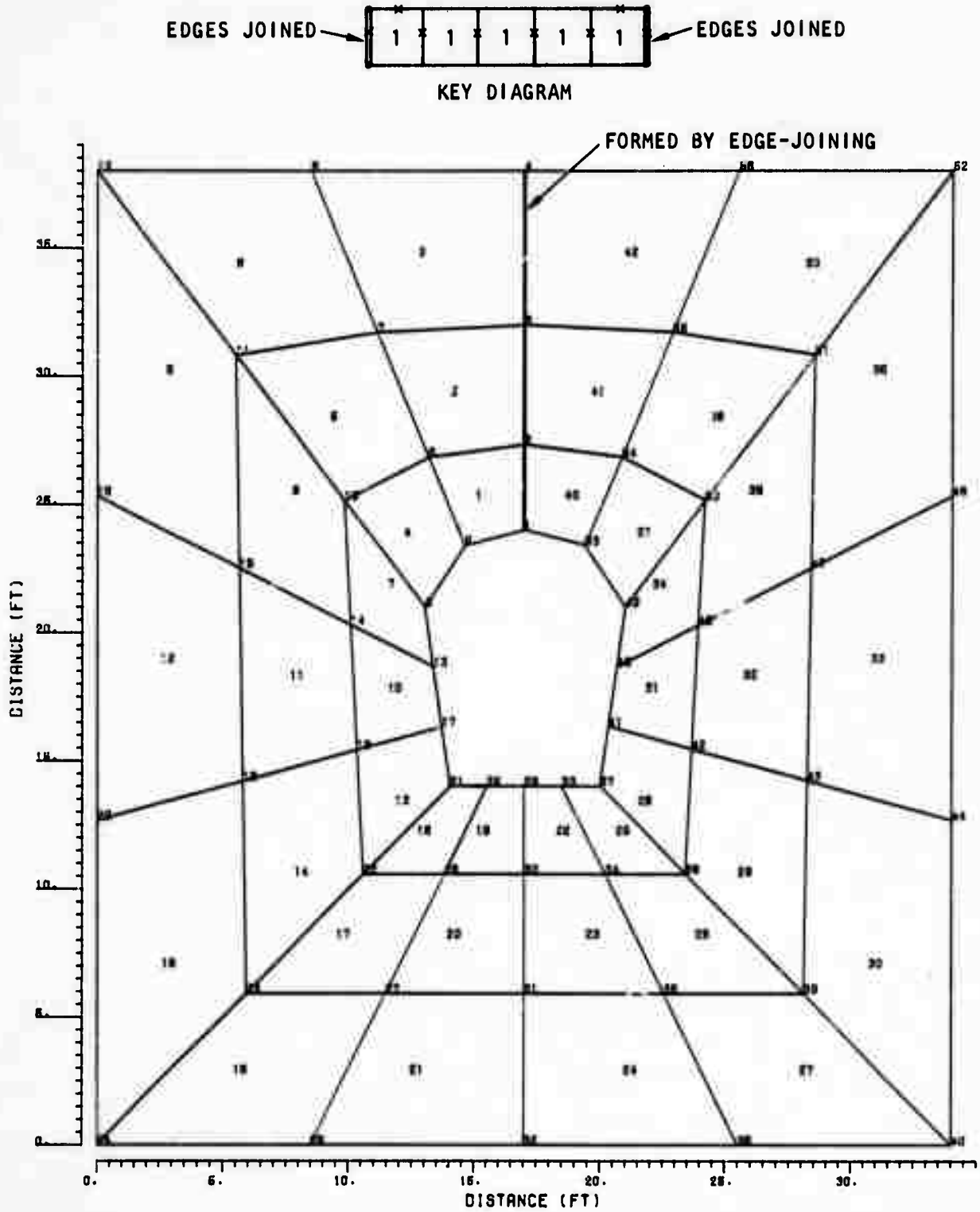

FIGURE 5-7. KEY DIAGRAM AND RESULTING FINITE ELEMENT MESH FOR A TUNNEL, ILLUSTRATING CAPABILITY TO JOIN ANY TWO EDGES IN THE KEY DIAGRAM

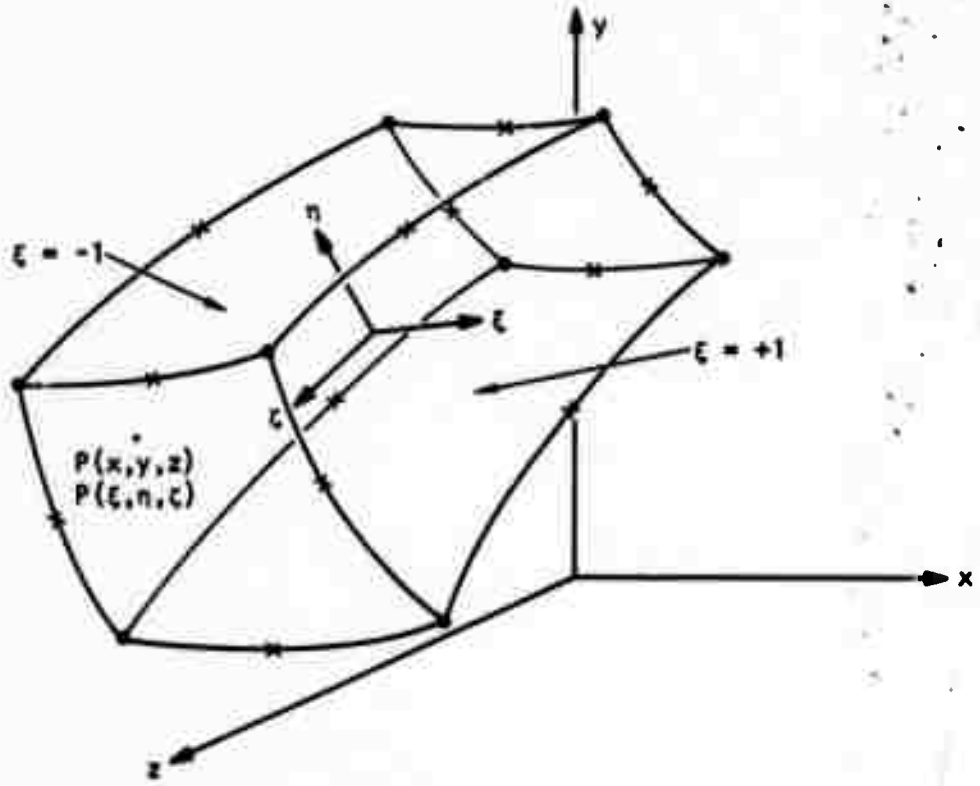

FIGURE 5-8. THREE-DIMENSIONAL ZONE WHOSE SHAPE AND COORDINATES ARE EXPRESSED BY PARABOLIC SHAPE FUNCTIONS

$$x = \sum_{i=1}^{20} N_i x_i$$

$$y = \sum_{i=1}^{20} N_i y_i \qquad (5\text{-}3)$$

$$z = \sum_{i=1}^{20} N_i z_i$$

where, for corner points,

$$N_i = \frac{1}{8}(1 + \xi_i\xi)(1 + \eta_i\eta)(1 + \zeta_i\zeta)(\xi_i\xi + \eta_i\eta + \zeta_i\zeta - 2) \qquad (5\text{-}4)$$

and for midpoints,

$$N_i = \frac{1}{4}(1 - \xi^2)(1 + \eta_i\eta)(1 + \zeta_i\zeta) \quad \text{for points with } \xi_i = 0$$

$$N_i = \frac{1}{4}(1 + \xi_i\xi)(1 - \eta^2)(1 + \zeta_i\zeta) \quad \text{for points with } \eta_i = 0$$

$$N_i = \frac{1}{4}(1 + \xi_i\xi)(1 + \eta_i\eta)(1 - \zeta^2) \quad \text{for points with } \zeta_i = 0$$

As before, zero can be used as material number to imply void or cavity, and a midpoint can be so specified as to imply a curved edge as well as a mesh grading along the edge. Instead of joining two edges, one can now join any two interfaces as long as the meshes on them are compatible. Some three-dimensional meshes automatically generated in this manner are illustrated in Figures 5-9 and 5-10.

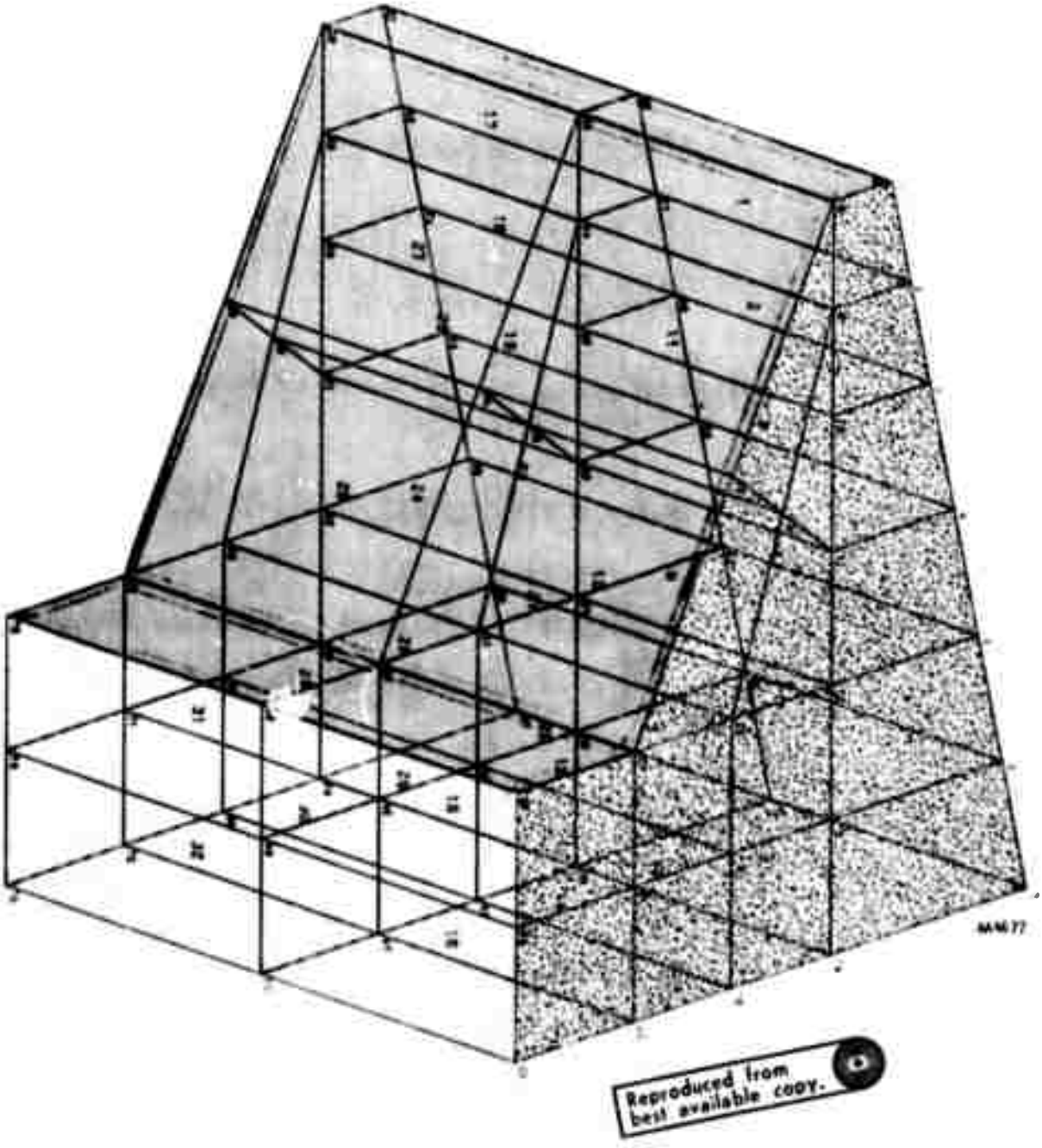

FIGURE 5-9. AUTOMATICALLY GENERATED THREE-DIMENSIONAL MESH

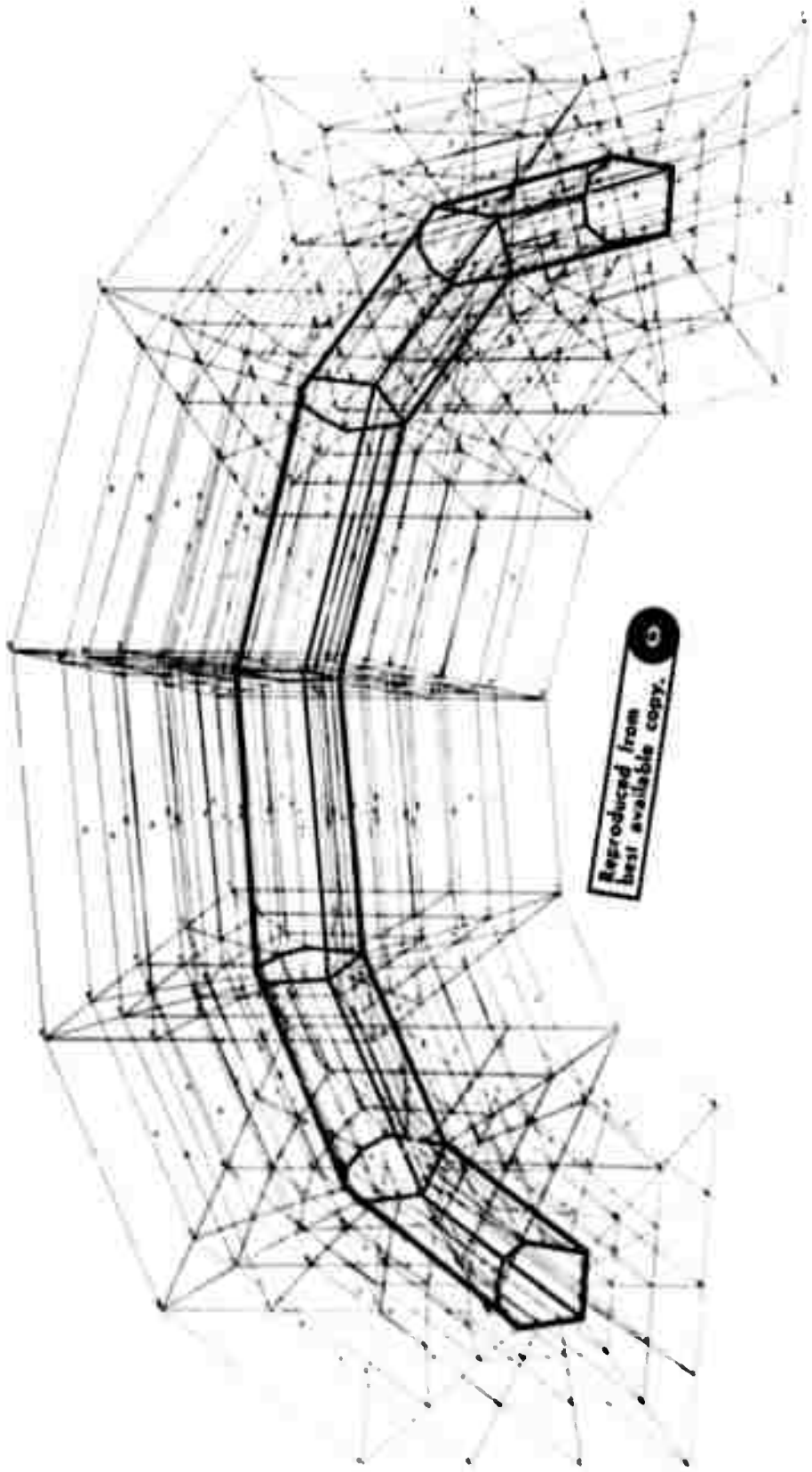

FIGURE 5-10. THREE-DIMENSIONAL FINITE ELEMENT MESH REPRESENTING A TUNNEL (PREPARATION TIME, INCLUDING FURTHER REFINEMENT OF ANY SECTION--ABOUT 1 HOUR)

BANDWIDTH REDUCER

The computer time required to perform a computation is approximately proportional to the square of the bandwidth. Thus it is important to aim for a minimum bandwidth when numbering nodal points. However, when the finite element mesh is generated automatically by the technique described above, no attention whatever is paid to minimizing bandwidth. The user can influence the bandwidth to some extent by judicious choice of key diagram. Nevertheless, it is very likely that the bandwidth so generated will not be optimum. The situation will often be made worse when elements are added manually. To help alleviate this difficulty and thus encourage the user to use the automatic mesh generator, a bandwidth reducer is included in the present computer program.

The function of the bandwidth reducer is shown in Figure 5-11. The INPUT NODAL POINT configuration is typical of the mesh which would be generated automatically for which the maximum difference in nodal point numbers for any element is 31. This configuration was submitted to the bandwidth reducer. The result, after 2 sec of computation time by the bandwidth reducer is the REDUCED NODAL POINT configuration, for which the maximum difference in node numbers is 6. That this configuration is not optimum is shown by the IDEAL configuration for which the maximum difference is 5. Thus, the technique is not optimum because it does not always converge to the minimum bandwidth in the computer time which the user has selected. Also, the technique operates on nodal point numbers rather than on degree of freedom numbers. Thus, when several types of elements are mixed, the configuration corresponding to minimum difference in node numbers does not necessarily correspond to minimum bandwidth.

Logic diagrams for the bandwidth reducer are shown in Figures 5-12 and 5-13.

ELEMENT NUMBERING

In addition to renumbering nodal points to reduce the bandwidth of the global stiffness matrix, the elements are numbered in the order of their contribution to the global stiffness matrix. In this way, the strain/

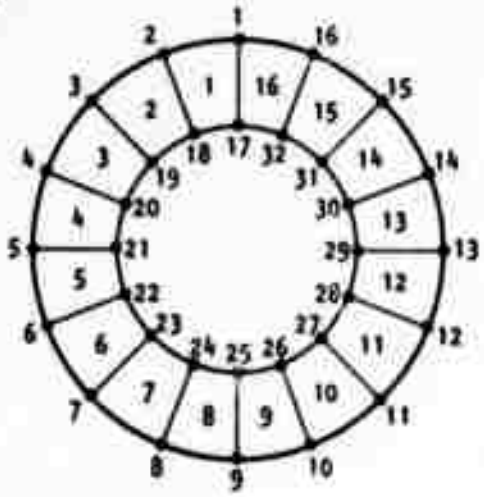

INPUT NODAL POINT CONFIGURATION

MAXIMUM NODAL POINT DIFFERENCE = 31

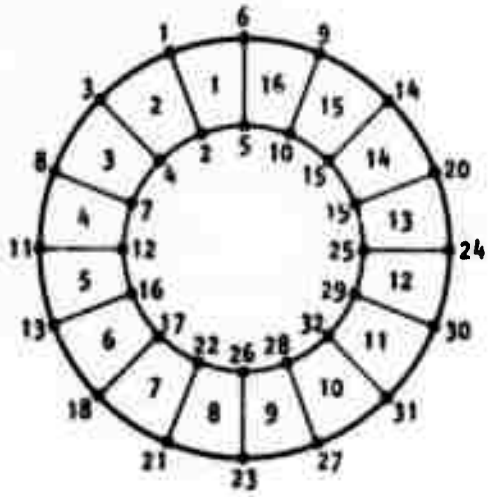

REDUCED NODAL POINT CONFIGURATION

MAXIMUM NODAL POINT DIFFERENCE = 6

SOLUTION TIME = 2 SECONDS

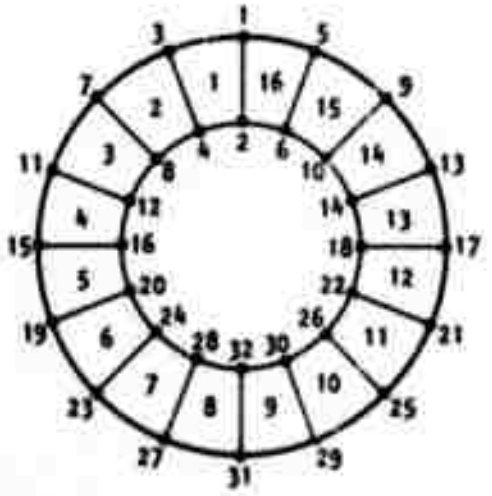

IDEAL CONFIGURATION

MAXIMUM NODAL POINT DIFFERENCE = 5

AA4681

FIGURE 5-11. EXAMPLE OF BANDWIDTH REDUCER

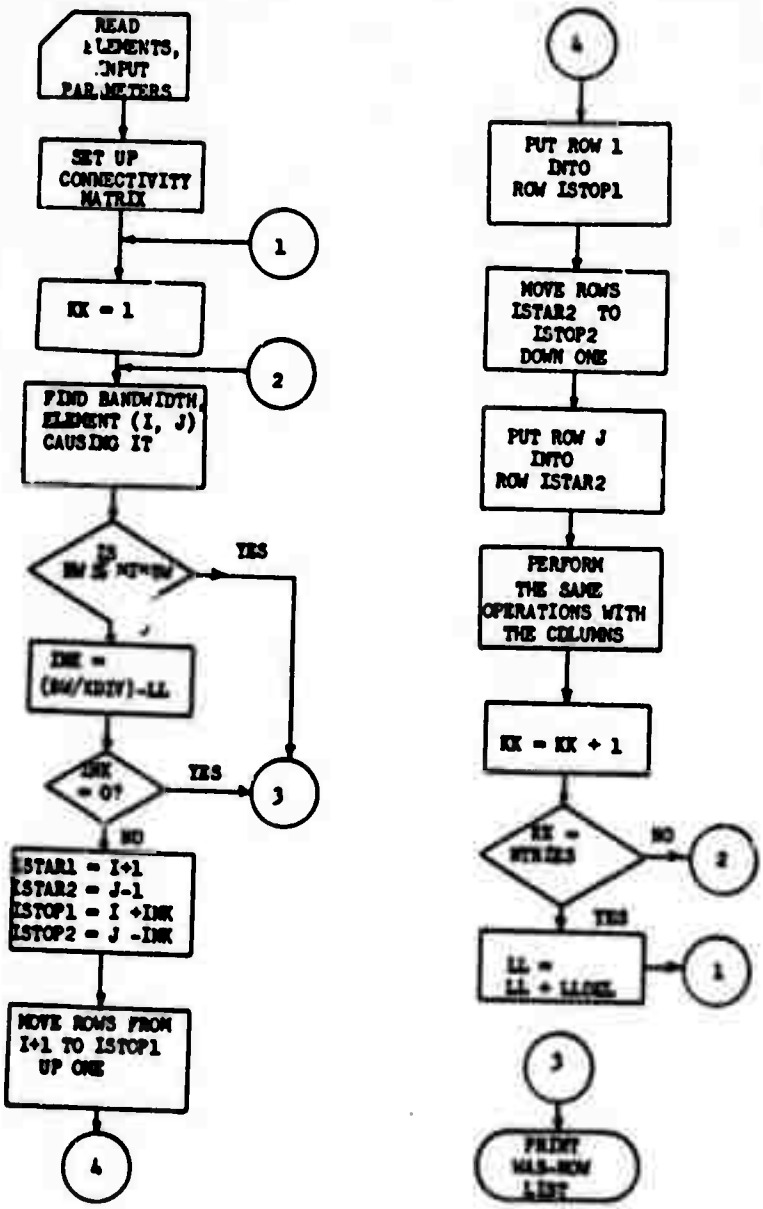

FIGURE 5-12. PROCEDURE USED IN BANDWIDTH REDUCER (REFERENCE 5-2)

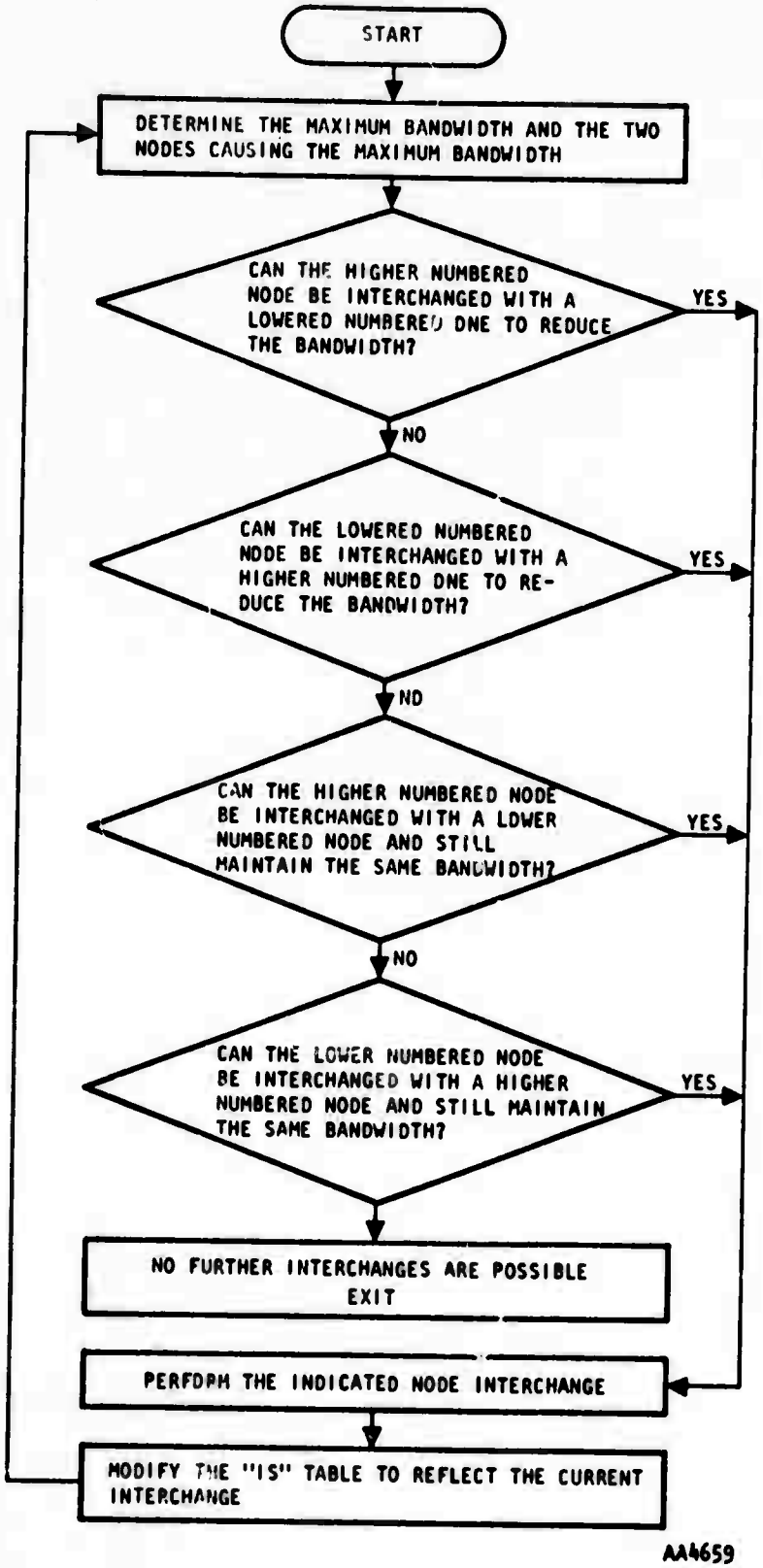

FIGURE 5-13. PROCEDURE USED IN BANDWIDTH REDUCER (REFERENCE 5-3)

stiffness matrixes can be retrieved from peripheral storage in the least time. Since the element data are used in the basic operations of forming the global stiffness matrix and effective load vector, the efficiency gained by performing these complicated operations is essential.

The element numbers assigned by the mesh generator and the user are revised such that

$$\min(LM(I)) \text{ for the } n^{th} \text{ element} \leq \min(LM(I)) \text{ for the } n+1^{th} \text{ element}$$

where

LM(I) = Array of degree of freedom members for the element

Element data are stored sequentially on peripheral storage units such that the data for Element 1 is at the head of the unit, and then in sequence

$$\text{Element Number} = 1 \leq \ldots n, n+1 \ldots \leq \text{NUMEL}$$

where

NUMEL = Total number of elements

In order to modify the effective load vector F, to obtain the matrix C of stress/strain coefficients and to obtain element stresses and strains, an array containing the previous loads F, the displacements u and the incremental displacements du is brought into core as shown in Figure 5-15. Also required are data stored on the element data tape such as the strain/displacement transformation matrixes and LM arrays for the elements of interest. As shown in Figure 5-14, all degrees of freedom to which Element n contributes are found in a sequence of F, u, du array one bandwidth (MBAND) long. Thus it is possible to process to F, u, du array by reading the element data tape only once.

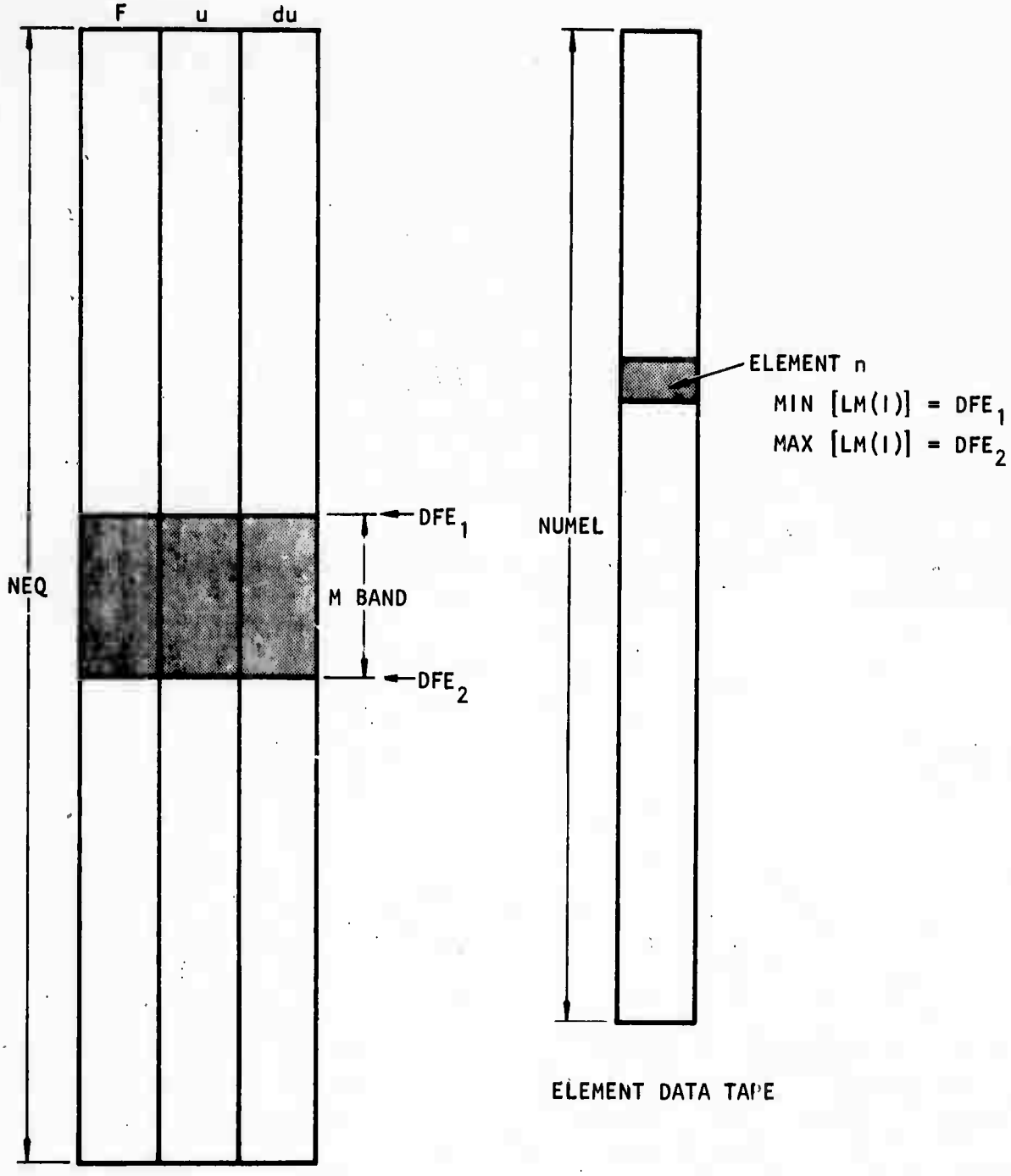

FIGURE 5-14. OPERATION ON FORCE, DISPLACEMENT AND INCREMENTAL DISPLACEMENT ARRAYS

In order to assemble the global stiffness matrix, which is stored in blocks, Block nn is brought into core as shown in Figure 5-15. At the same time, data from Element n is made available from the element data tape. Element n fits entirely into Block nn. Elements n, nn + 1, etc. are processed so long as

$$DFE_1 \geq DFK_2$$

and

$$DFE_2 \leq DFK_2$$

In this event, element stiffness is directly added to the appropriate rows and columns of Block nn. If

$$DFE_1 \geq DFK_2$$

and

$$DFE_2 > DFK_2$$

it signifies that Element n contributes to Block nn and to Block nn + 1. In this event, those contributions which can be made to Block nn are made, and the stiffnesses and LM arrays of those elements which contribute also to Block nn + 1 are written temporarily on storage unit T1 for subsequent insertion into Block nn + 1. Elements are processed and their stiffnesses are added to Block nn and or accumulated on T1 until

$$DFE_1 > DFK_2$$

This signifies that Block nn of the global stiffness matrix is prepared except for data stored on unit T0, which contains element data overlapping Blocks nn - 1 and nn. This data is read into core and that part for which

$$DFE_1 < DFK_1 \quad .$$

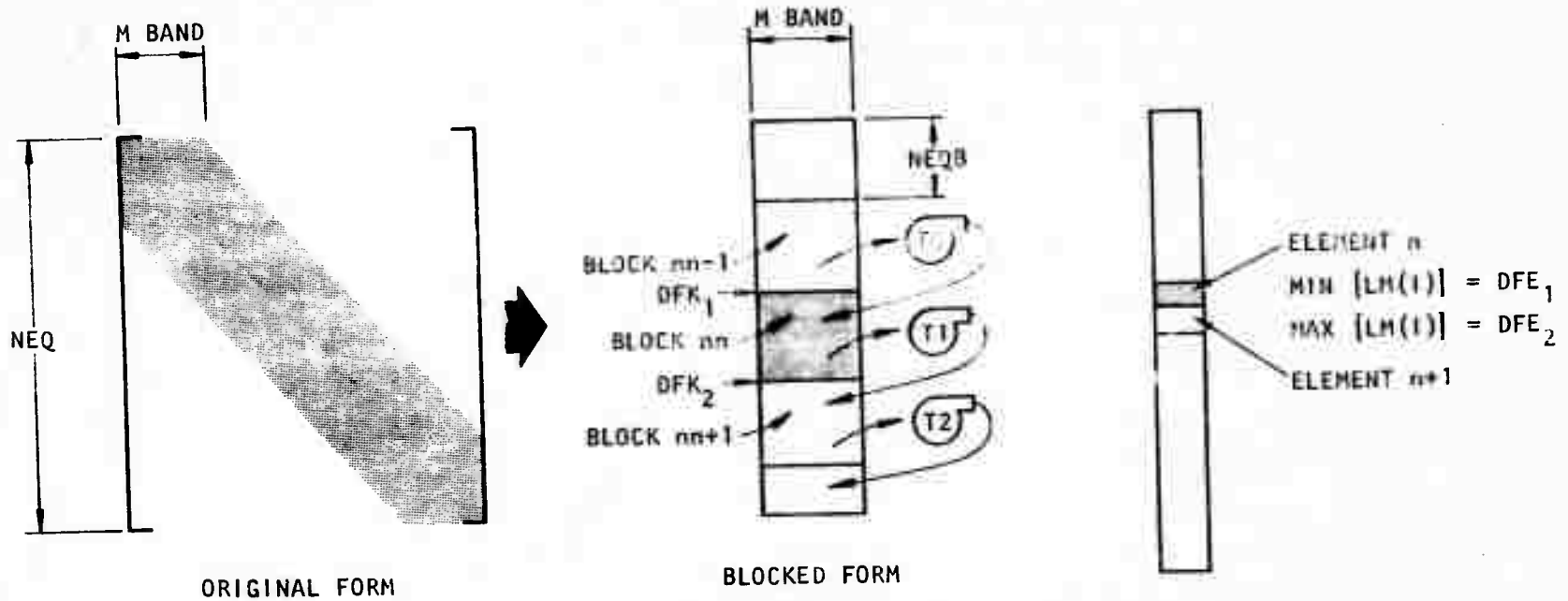

FIGURE 5-15. GENERATION OF GLOBAL STIFFNESS MATRIX FROM ELEMENT DATA

is added to Block nn. Now Block nn is completely prepared and is moved out of core while Block nn + 1 is brought into core. Block nn + 1 is filled in the same way as Blocks nn - 1 and nn, which is by passing sequentially through the element data array. When all direct contributions to Block nn + 1 have been made and all data which contributes to Block nn + 2 has been stored on unit T2, the data stored on unit T1 is read into core and added to Block nn + 1. This block is now completely prepared and is transferred to peripheral storage.

SIMULATION OF THE CONSTRUCTION AND EXCAVATION SEQUENCE

The construction and excavation sequence will be represented by modification of the material properties of the elements involved. Initially elements will be assigned to the regions to be constructed or excavated later. A flag will indicate the time of the addition or subtraction of each element. In case of excavation, the elements of that region will have the appropriate material properties and will contribute to the global stiffness of the system up to the indicated time, beyond which the contribution of these elements to the global stiffness of the system will be zero. The reverse of this procedure will be applied to the elements of the regions to be constructed later. All these operations will be performed in the element package.

SELF-LOADING

The initial state of the system will be assumed to be stress free. Then the dead load, if any, will be applied in a specified number of increments prior to the application of the external load. It is necessary to apply the self-loading incrementally due to the fact that the system is, in general, nonlinear.

5.2 EXECUTION PHASE OF PROGRAM

The execution phase of the program is summarized in Figures 5-16 through 5-21. The controlling program is BMCALC, Figure 5-16. The first main operation is to form the effective load vector and global stiffness matrix, which is performed by Subroutine KFORM, Figure 5-17. The assembly of the global stiffness from the element stiffnesses is performed by Subroutine BSTIF, Figure 5-18. Subroutines FWRT, TDRUM and FILLFU transfer data from peripheral storage to core.

5.2.1 MULTIBUFFERING TECHNIQUE

Multibuffering is a technique whereby central processor wait time for all binary Read/Write operations involving the peripheral storage of data is minimized. (Formatted I/O operations such as card reading, punching, and printing are not included in this discussion.) The reason for using multibuffering techniques is that data moves faster between core locations than between peripheral storage and core.

The problem which multibuffering overcomes is the standard I/O feature of higher level programming languages, such as FORTRAN, which requires that when an I/O operation (READ or WRITE) is initiated, computation ceases until the I/O operation is completed. This feature assures the user that data he may wish to use is in core before he tries to use it. The amount of time the program must wait for completion of I/O operations depends on (1) the access time and (2) the data transfer time. These times depend on the type of peripheral device being used and the amount of data to be transferred. Thus, as the amount of peripheral storage increases, the time spent waiting for completion of I/O operations increases and for large volumes of data the I/O time may control overall run times. Multibuffering minimizes the wait time of these I/O operations by allowing computations to proceed *at the same time data transfer from peripheral storage is occurring*. This requires standard FORTRAN I/O operations to be replaced. This is possible on most large scale scientific computers by the use of special machine-dependent

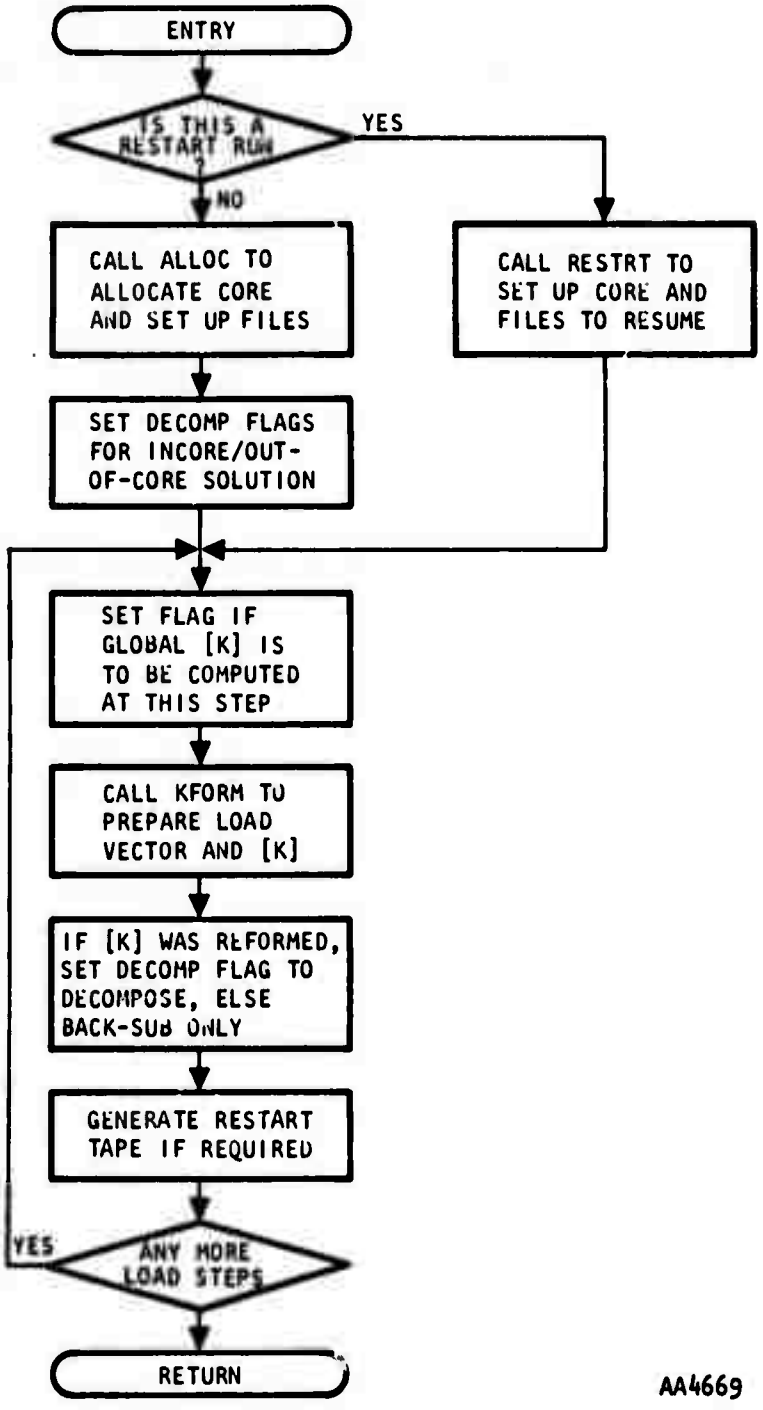

FIGURE 5-16. PROGRAM BMCALC--CONTROLS MAIN OPERATIONS OF THE COMPUTATION SECTION

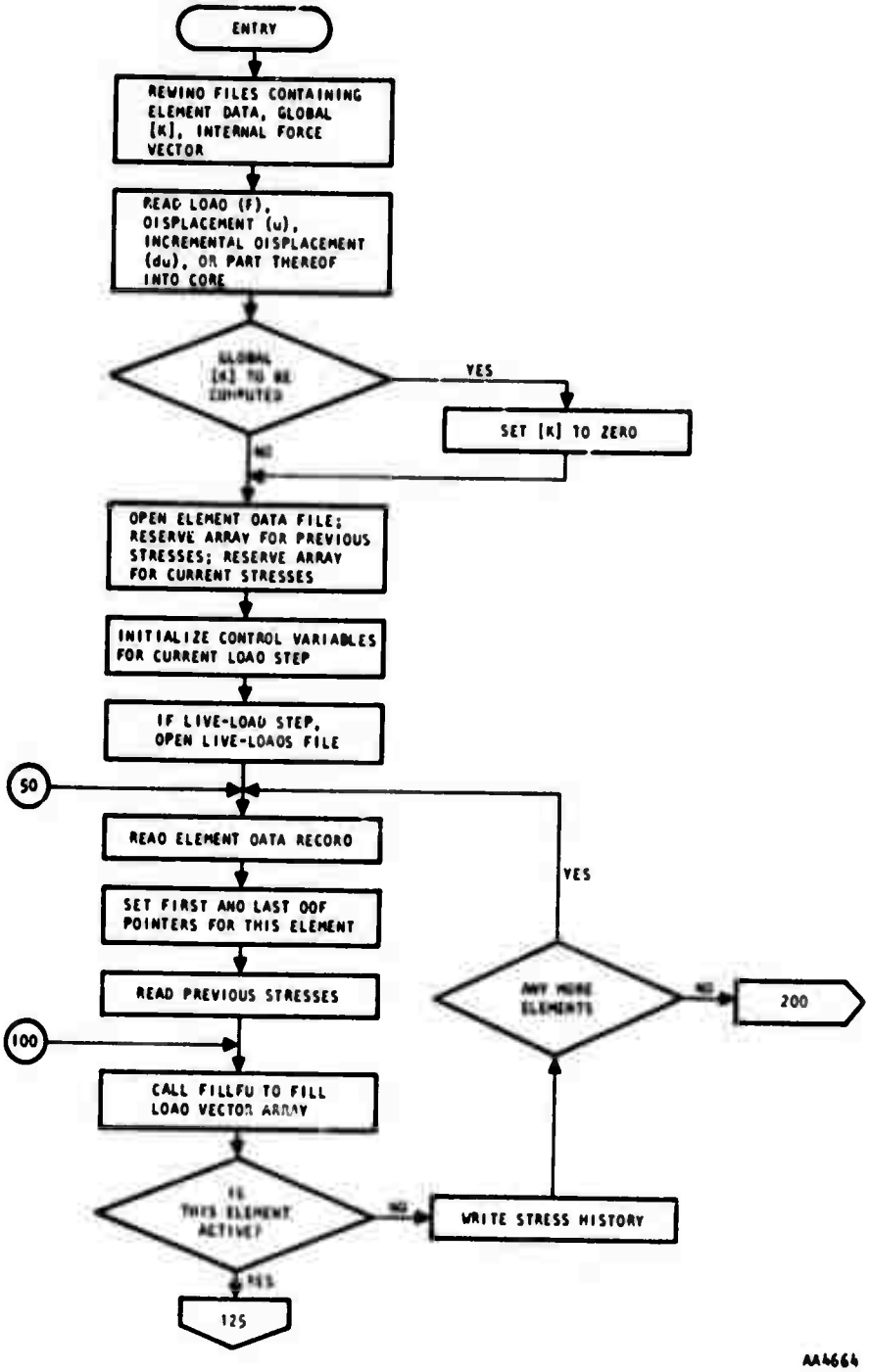

FIGURE 5-17. SUBROUTINE KFORM--CALLS SUBROUTINES TO COMPUTE THE LOAD VECTOR AND GLOBAL STIFFNESS

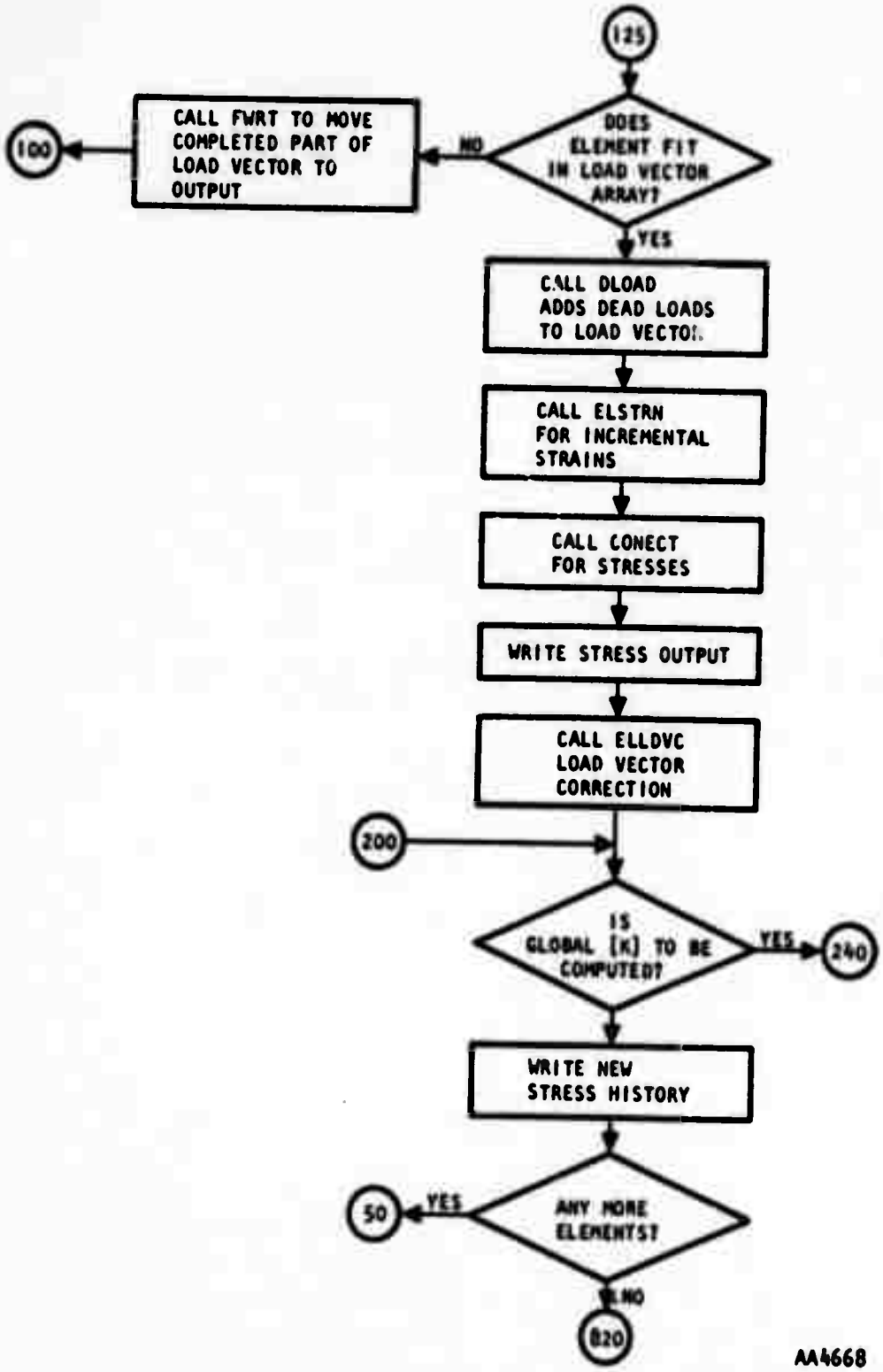

FIGURE 5-17. (CONTINUED)

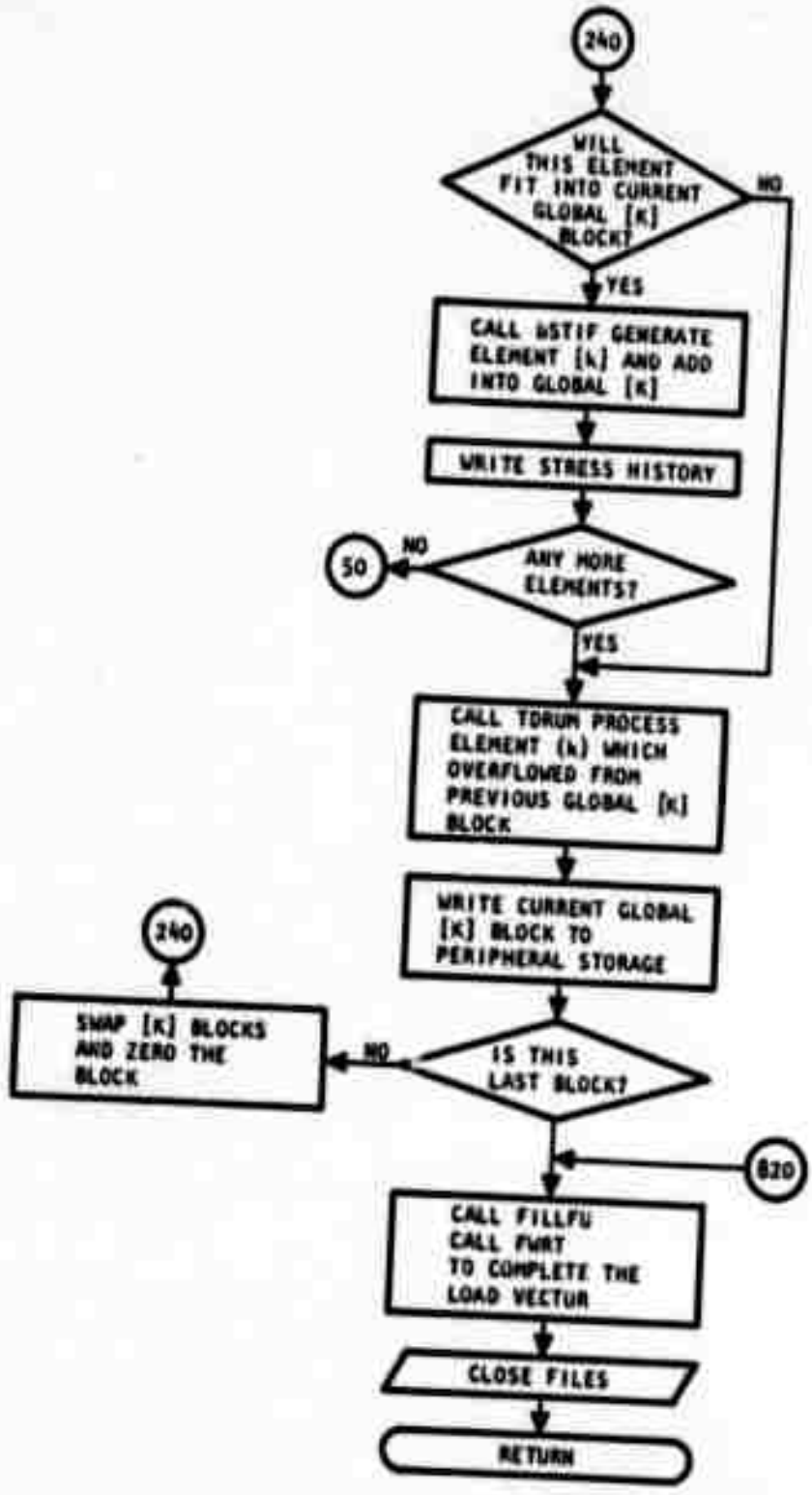

AA4671

FIGURE 5-17. (CONTINUED)

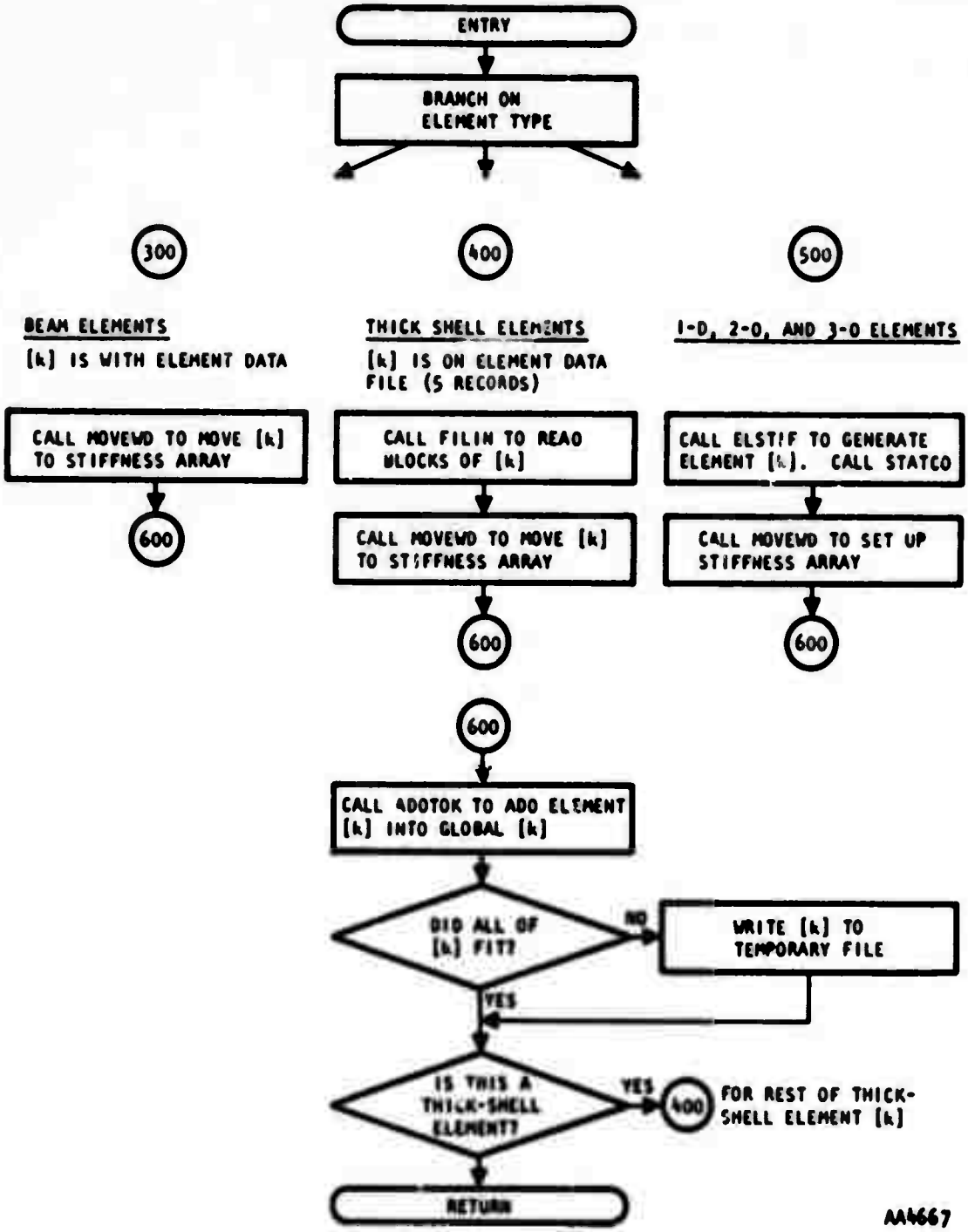

FIGURE 5-18. SUBROUTINE BSTIF--COMPUTER ELEMENT STIFFNESS [k] AND ADDS TO GLOBAL [k]

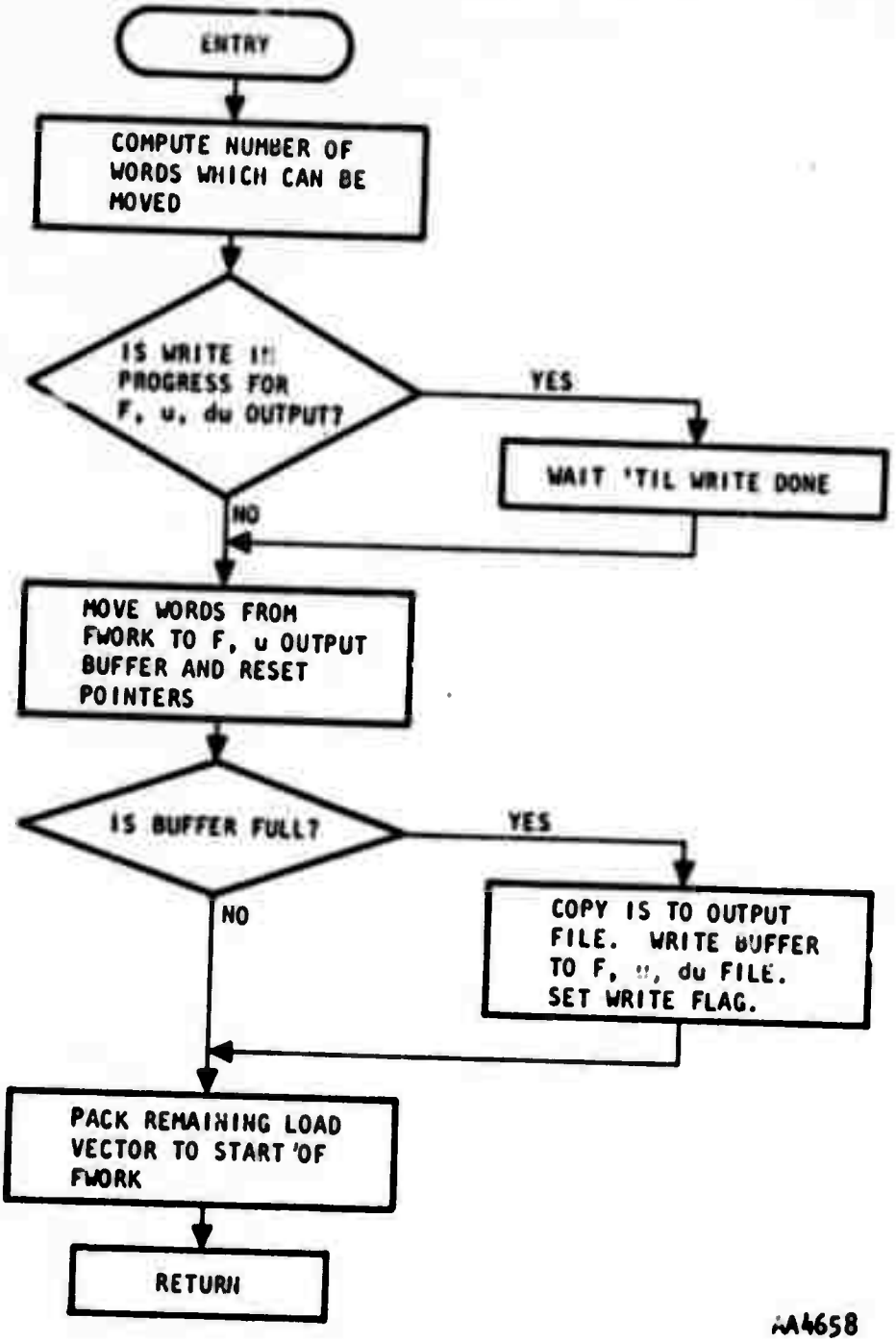

FIGURE 5-19. SUBROUTINE FWRT--MOVES DATA FROM LIVE LOAD VECTOR (FWORK) TO F, u, du OUTPUT BUFFER AND TO u OUTPUT FILE

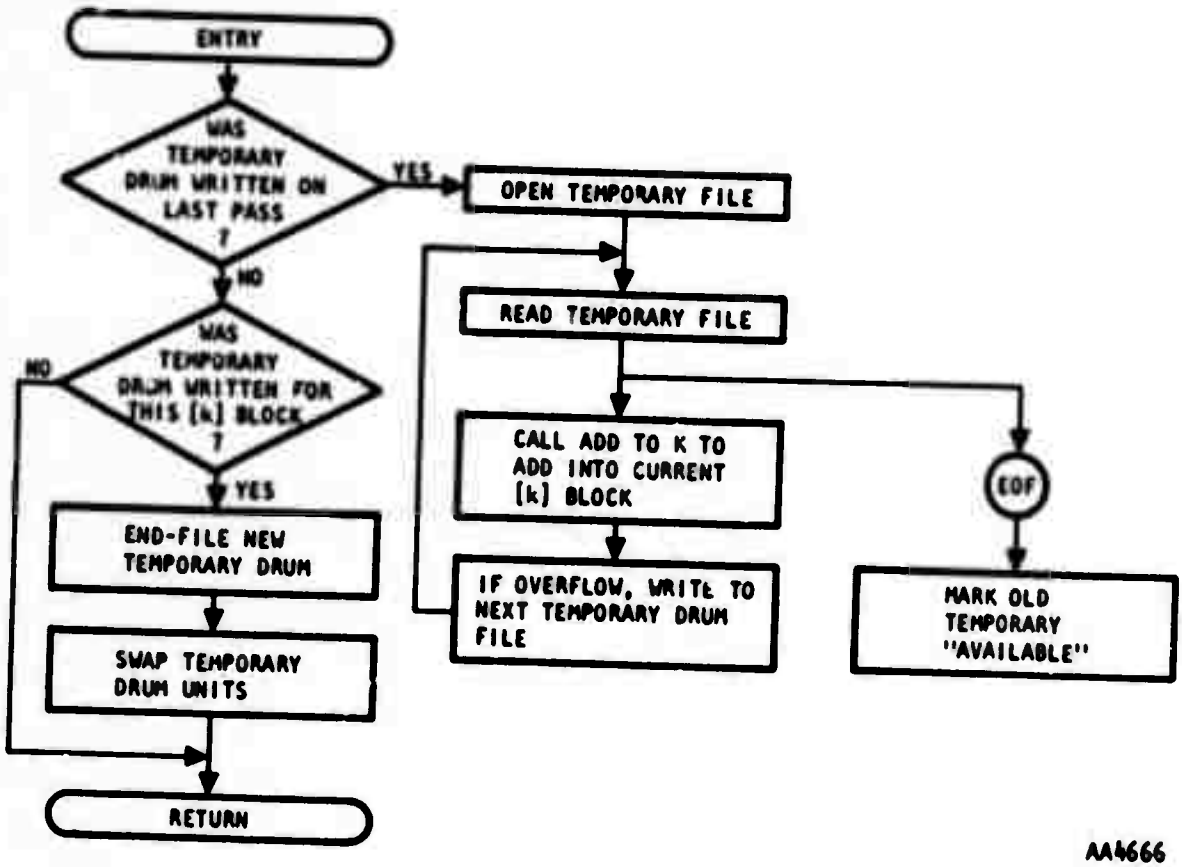

FIGURE 5-20. SUBROUTINE TDRUM--ADDS IN ELEMENT [k] WHICH OVERFLOWED FROM PREVIOUS BLOCK OF [k]

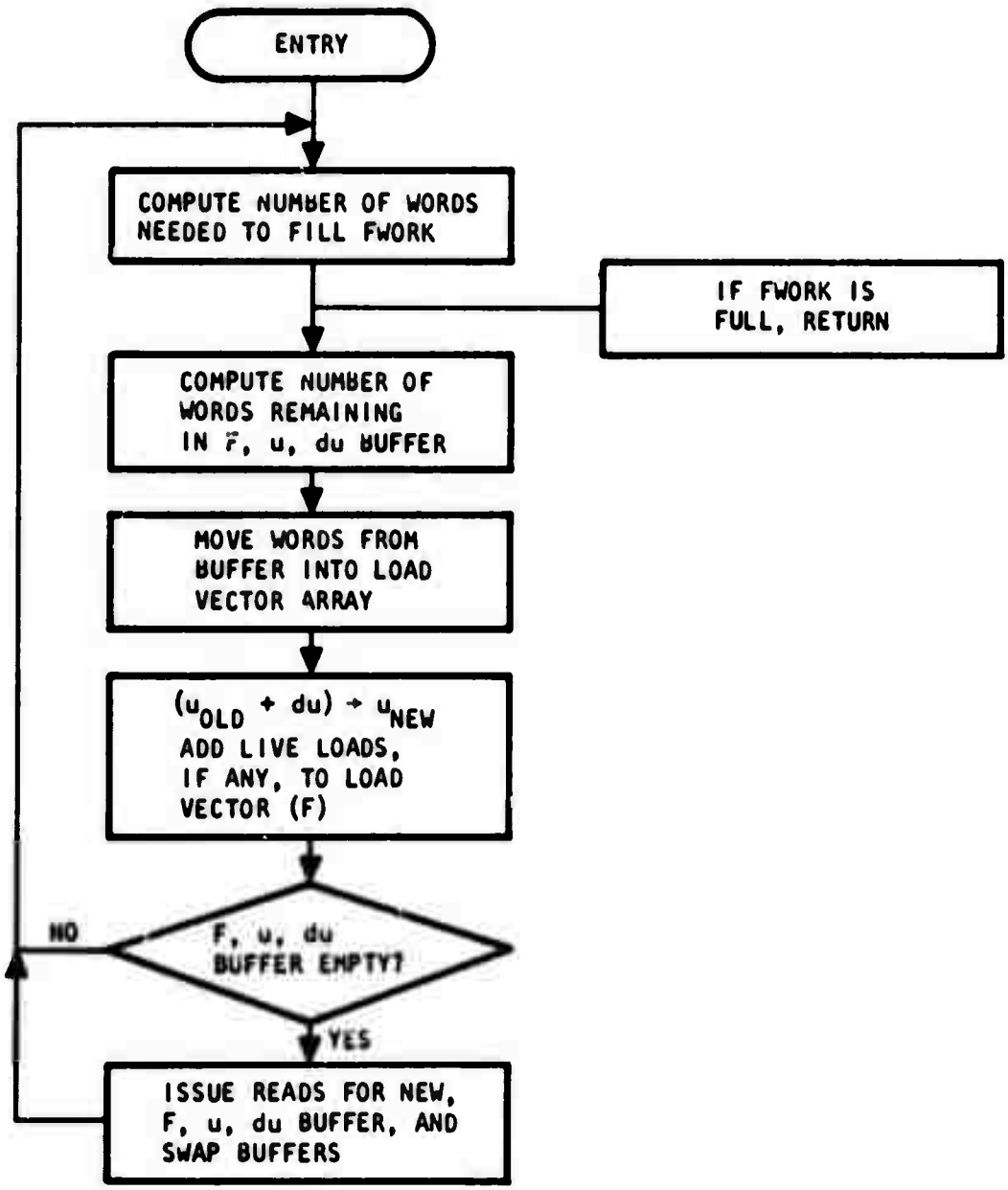

FIGURE 5-21. SUBROUTINE FILLFU--ADDS LIVE LOADS TO LOAD VECTOR, UPDATES DISPLACEMENTS, FILLS BUFFER AREA WITH F, u, du ARRAY

statements or subroutines. These interface routines are generally different on each machine and, unless care is exercised, a program may become machine dependent. This danger is avoided in the present application of multibuffering by isolating all I/O statements in one subroutine which may easily be modified when moving the program to a different machine.

A general multibuffering scheme to perform computations on a set of data stored on peripheral devices is shown in Figure 5-22. This scheme, which is incorporated in the present computer program, requires either the amount of main storage used for buffers to be increased or the size of each buffer to be decreased relative to the buffer size that might be used with standard FORTRAN I/O procedures. Since most of the main storage is already used in determining buffer sizes, the latter alternative is employed. Extensive testing and previous experience have shown that, although the number of I/O operations increases, multibuffering results in substantial overall reduction in computer run time for a given problem. Savings increase with the problem size and thus the volume of data on peripheral storage increases.

5.2.2 BAND SOLVER

The solution of large structural systems requires the solution of a set of linear simultaneous equations of the form

$$\{F\} = [K]\{u\} \qquad (5\text{-}5)$$

where

- $\{F\}$ is a vector of applied loads
- $\{u\}$ is a vector of unknown displacements or, as in the present case, displacement increments
- $[K]$ is the global stiffness matrix. In the present case it is banded and positive definite

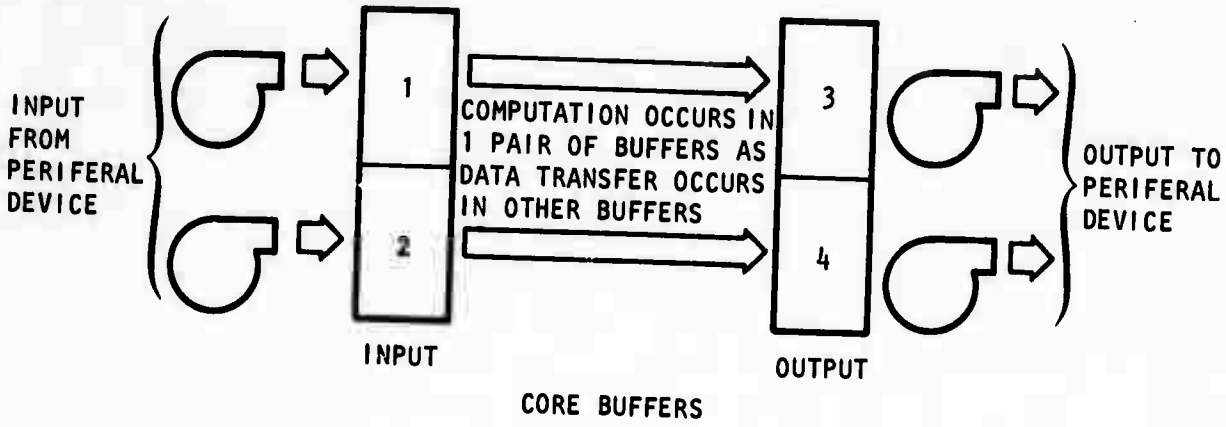

a. Initiate read of data into (1)

b. Test for completion of Step *a* data transfer

c. Initiate read of data into (2)

d. Perform computation on data in (1) storing results of computation in (3)

e. Initiate write of data in (3)

f. Test for completion of Step *c* data transfer; if incomplete, stop computation until completed.

g. Initiate read of data into (1)

h. Perform computation on data in (2) storing results in (4)

i. Test for completion of Step *e* data transfer

j. Initiate write of data in (4)

k. Test for completion of Step *g* data transfer

l. Loop to Step *c* until all data has been processed

m. Test for completion of final buffer operation

FIGURE 5-22. TYPICAL OPERATION OF MULTIBUFFERING TECHNIQUE

Many methods of obtaining a solution to Equation 5-5 are available. A frequently used method is the Choleski Decomposition Method. Defining

$$[K] = [L]\,[D]\,[L]^T \tag{5-6}$$

where

[L] is a lower triangular matrix with ones on the diagonal terms

[D] is a diagonal matrix

then substituting Equation 5-6 into Equation 5-5

$$\{F\} = [L]\,[D]\,[L]^T\,\{u\} \tag{5-7}$$

and defining

$$\{Z\} = [D]\,[L]^T\,\{u\} \tag{5-8}$$

Equation 5-7 becomes

$$\{F\} = [L]\,\{Z\} \tag{5-9}$$

There are many algorithms for solving Equations 5-8 and 5-9. The algorithms used in this code are (Reference 5-4).

$$L_{ij} = \frac{1}{D_j}\left[K_{ij} - \sum_{m=1}^{j-1} L_{im}\,D_m\,L_{J_jm}\right] \qquad i > j \tag{5-10}$$

$$D_j = K_{jj} - \sum_{m=1}^{j-1} D_m\,L_{jm}^2 \tag{5-11}$$

$$Z_i = F_i - \sum_{m=1}^{i=1} L_{im}\,Z_m \tag{5-12}$$

$$U_j = \frac{Z_j}{D_j} - \sum_{m=j+1}^{n} L_{mj}\,U_m \tag{5-13}$$

where

n = Total number of equations

i,j = Row and column indices

The use of Equations 5-10 and 5-11 to obtain the [L] and [D] matrices in the most general case of a block-by-block solution is illustrated in Figures 5-23 through 5-25. Figure 5-23 shows a typical banded stiffness matrix with the arrangement of the terms in each core block. Although shown as a two-dimensional array, the actual locations of storage may be consecutive. Figure 5-24 shows a method of assigning core storage to allow the double buffering scheme of Section 5.2.1 to be used. The indicated Scratch Core area may be of any size (it must be at least four words in length) and is used as a buffer area to save columns of the reduced stiffness matrix needed for for reduction, i.e., decomposition of future stiffness blocks. All I/O operations between the scratch area of core and peripheral devices use the technique of Section 5.2.1. Thus storage and retrieval of intermediate data required for the computation of [L] and [D] may in the optimum case be performed at core speed. Only a single output buffer is shown in Figure 5-24. This presents no contradiction to the double buffering scheme. Figure 5-25 shows that between initiation of the write and storage of new data in the output buffer many calculations are performed. Tests have shown that this calculation time is greater than the data transfer time thus allowing a single output buffer to be used. Figure 5-25 shows the sequence of operations in decomposing the stiffness matrix. The generation of {Z} (from Equation 5-12) may be performed at the same time [L] and [D] are generated.

After completing decomposition of the stiffness matrix and generating the {Z} matrix, the displacements {u} are computed by Equation 5-13. Figure 5-26 shows the sequence of operations in computing the {u} matrix.

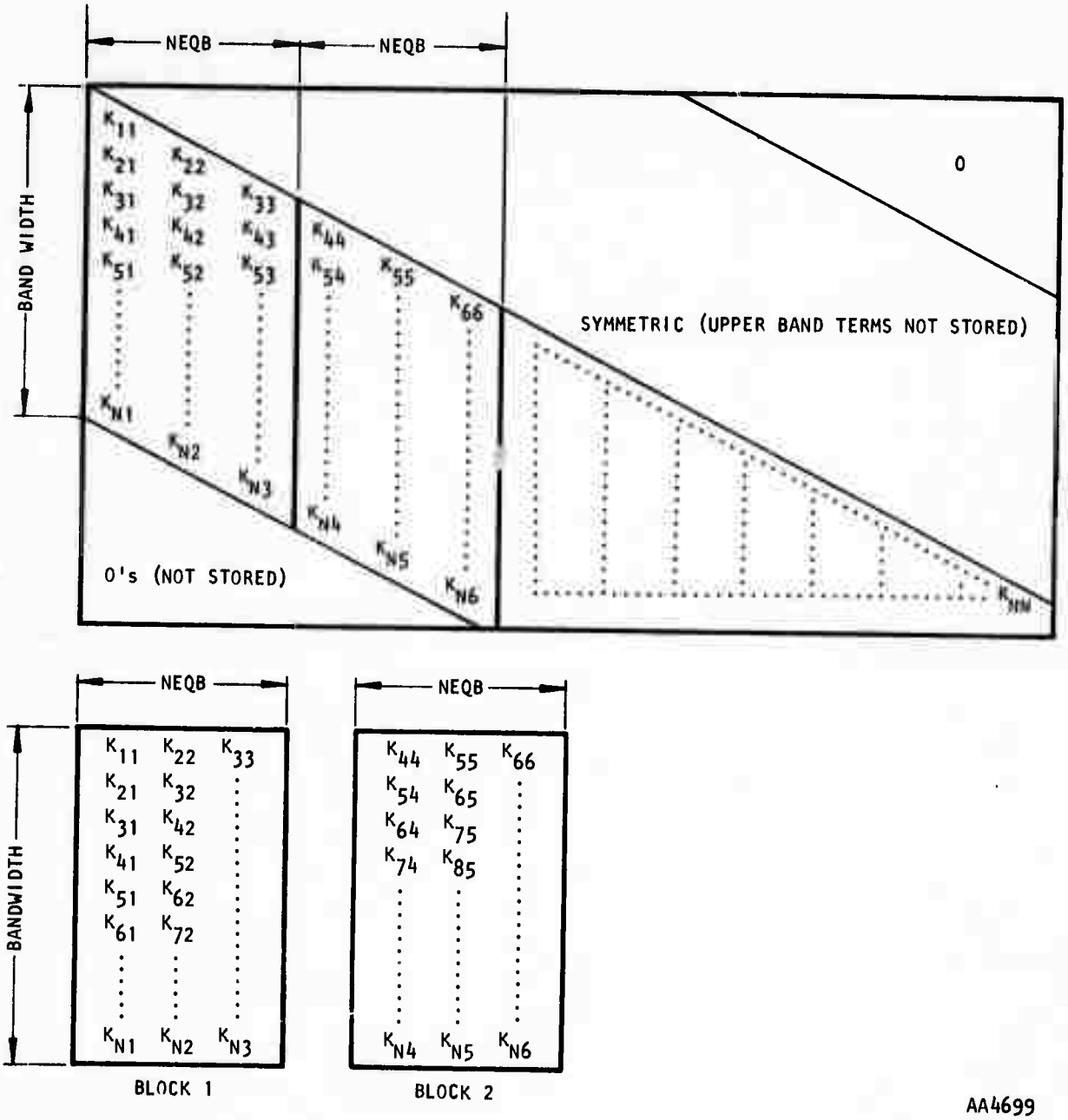

FIGURE 5-23. METHOD OF STORING STIFFNESS MATRIX USED IN PRESENT PROGRAM

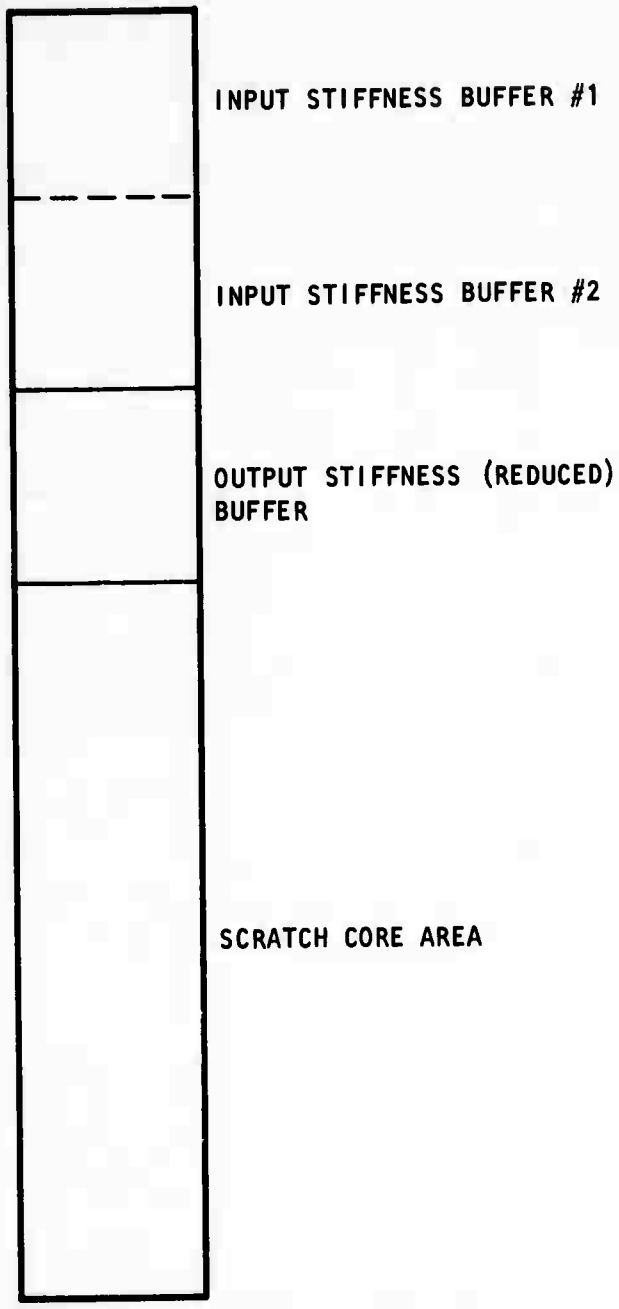

FIGURE 5-24. CORE BUFFERS FOR STIFFNESS MATRIX DECOMPOSITION

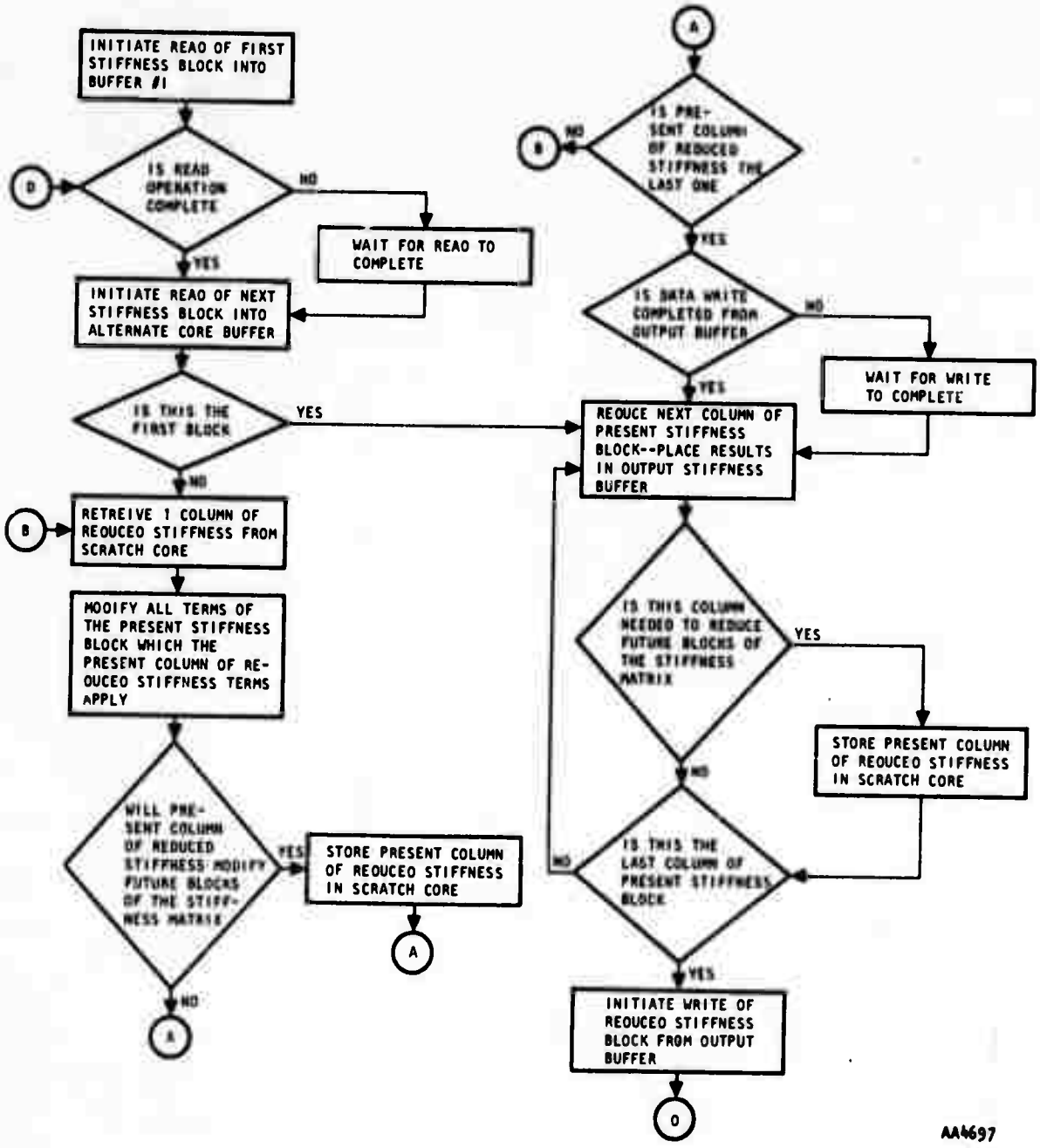

FIGURE 5-25. SCHEMATIC DIAGRAM OF STIFFNESS MATRIX DECOMPOSITION

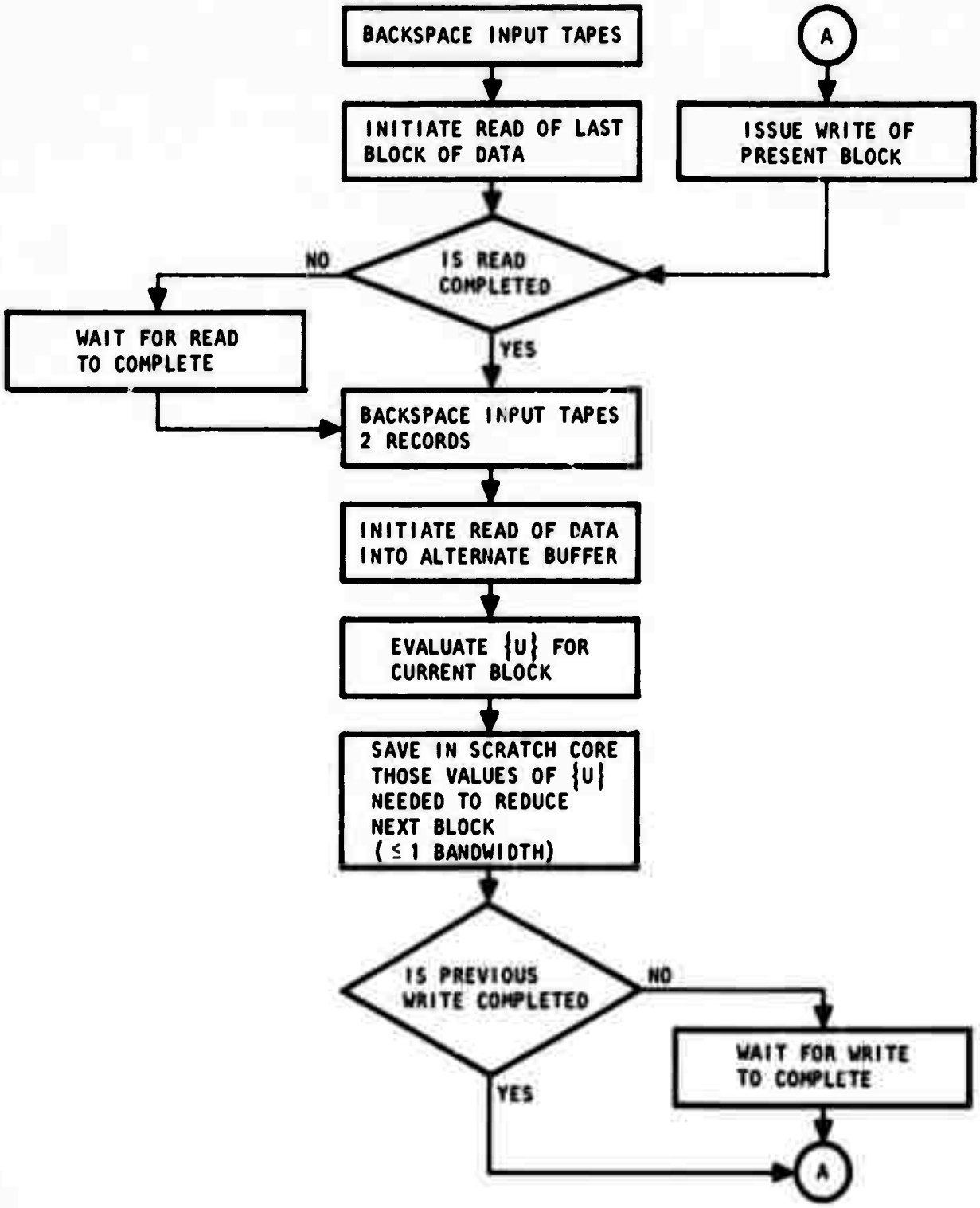

FIGURE 5-26. SCHEMATIC DIAGRAM OF SOLUTION VECTOR EVALUATION

REFERENCES

5-1. Zienkiewicz, O. C., and D. V. Phillips, "An Automatic Mesh Calculation Scheme for Paine and Curved Surfaces by Isoparametric Coordinates," *Numerical Methods in Engineering*, Vol. 4, No. 3, October-December 1971.

5-2. Grooms, H. R., "Algorithm for Matrix Bandwidth Reduction," *J. of the Structural Division*, Proc. ASCE, Vol. 98, No. ST1, January 1972.

5-3. Rosen, R., "Matrix Bandwidth Minimization," Proc. 1968 ACM National Conference.

5-4. Rubinstein, M. F., and R. Rosen, "Structural Analyses by Matrix Decomposition, *J. of Franklin Institute*, Vol. 286, No. 4, October 1968.

SECTION 6

COMPARISON WITH CLOSED-FORM ANALYTIC SOLUTIONS

6.1 SAMPLE PROBLEMS

To investigate the numerical accuracy of the present computer program and to determine the computer time required to solve problems of various size and complexity, several example problems have been formulated and their numerical solutions compared with closed-form, analytic solutions. One-, two-, and three-dimensional linear elastic solutions are considered as well as one- and two-dimensional elastic/plastic and two-dimensional visco-elastic solutions. These are listed in Table 6-1.

Problem 1--Stress Around a Circular Hole

The geometry of Problem No. 1 is illustrated in Figure 6-1. The finite element mesh is illustrated in Figure 6-2. The solution is shown in Figure 6-3 in terms of principal stresses at $\theta = 5.7$ and 42.1°. It does not depend on the material properties of the plate.

Problem 2--Stress and Displacement in an Elastic Thick-Walled Cylinder Under Internal Pressure

The geometry of Problem No. 2 is illustrated in Figure 6-4. The finite element mesh is also shown. The solution is shown in Figure 6-5 in terms of radial and tangential stresses.

Problem 3--Stress in an Elastic, Perfectly Plastic Thick-Walled Cylinder Under Internal Pressure

The geometry of Problem No. 3 is the same as that of Problem No. 2 and is shown in Figure 6-4. For this problem, an additional material property, the Mises yield criterion, is specified as follows:

$$f = \sqrt{J_2'} - a_1 \leq 0 \qquad (6\text{-}1)$$

The analytic solution is shown in Figure 6-6.

TABLE 6-1. PROBLEMS SOLVED BY FINITE ELEMENT AND CLOSED-FORM METHODS

Number	Description	Geometry	Material Property	Closed-Form Solution
1	Stress around a circular hole	Two-dimensional (plane)	Elastic	Reference 6-1
2	Stress in a thick walled cylinder under internal pressure	One-dimensional (axisymmetric)	Elastic	Reference 6-2
3	Stress in a thick walled cylinder under internal pressure	One-dimensional (axisymmetric)	Elastic, perfectly plastic	Reference 6-2
4	Stress in a reinforced thick walled cylinder	One-dimensional (axisymmetric)	Viscoelastic	Reference 6-3
5	Stress concentration around a cylindrical hole in a semiinfinite body	Three-dimensional	Elastic	Reference 6-4

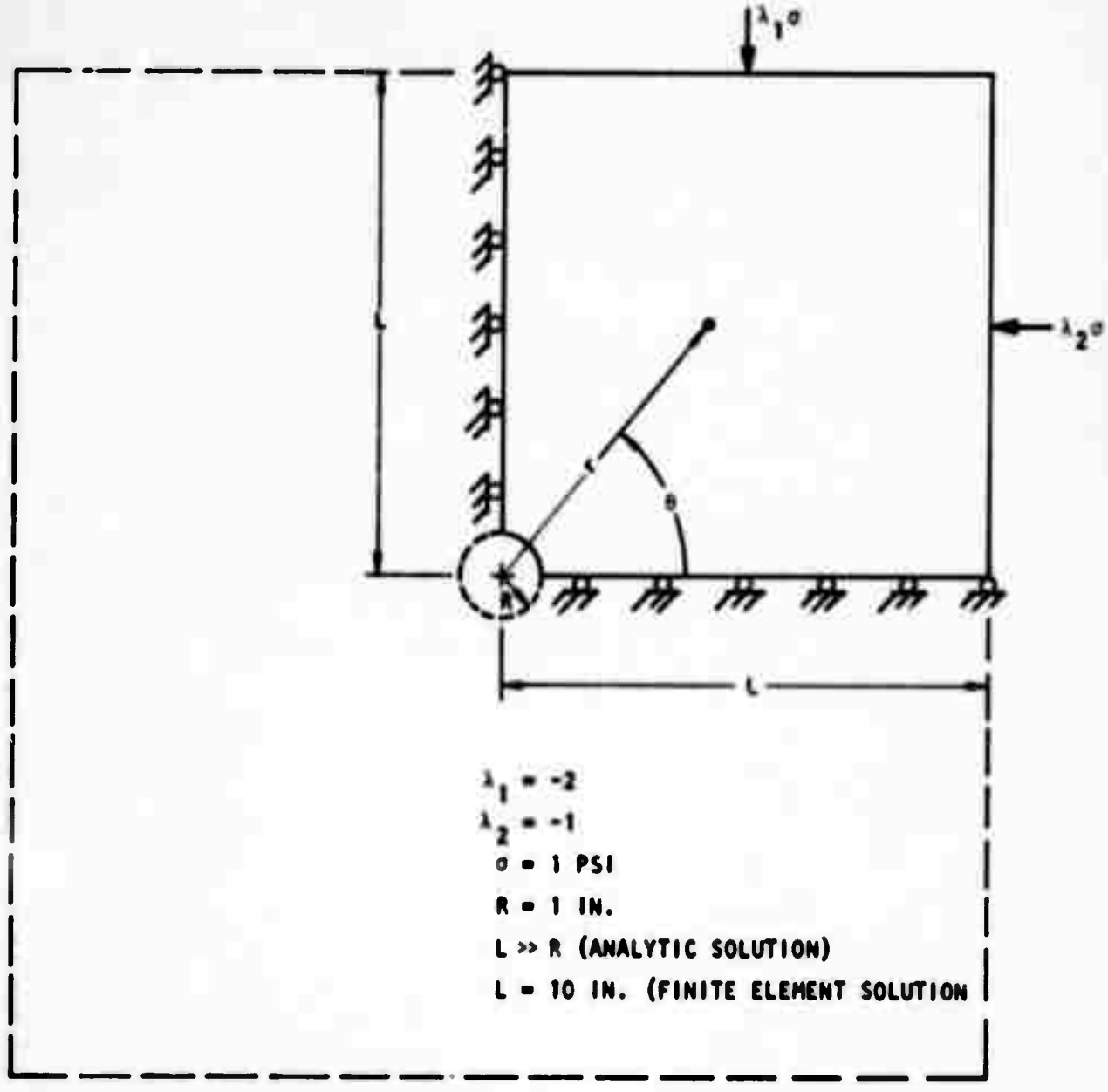

FIGURE 6-1. PROBLEM 1--STRESSES AROUND A CIRCULAR HOLE

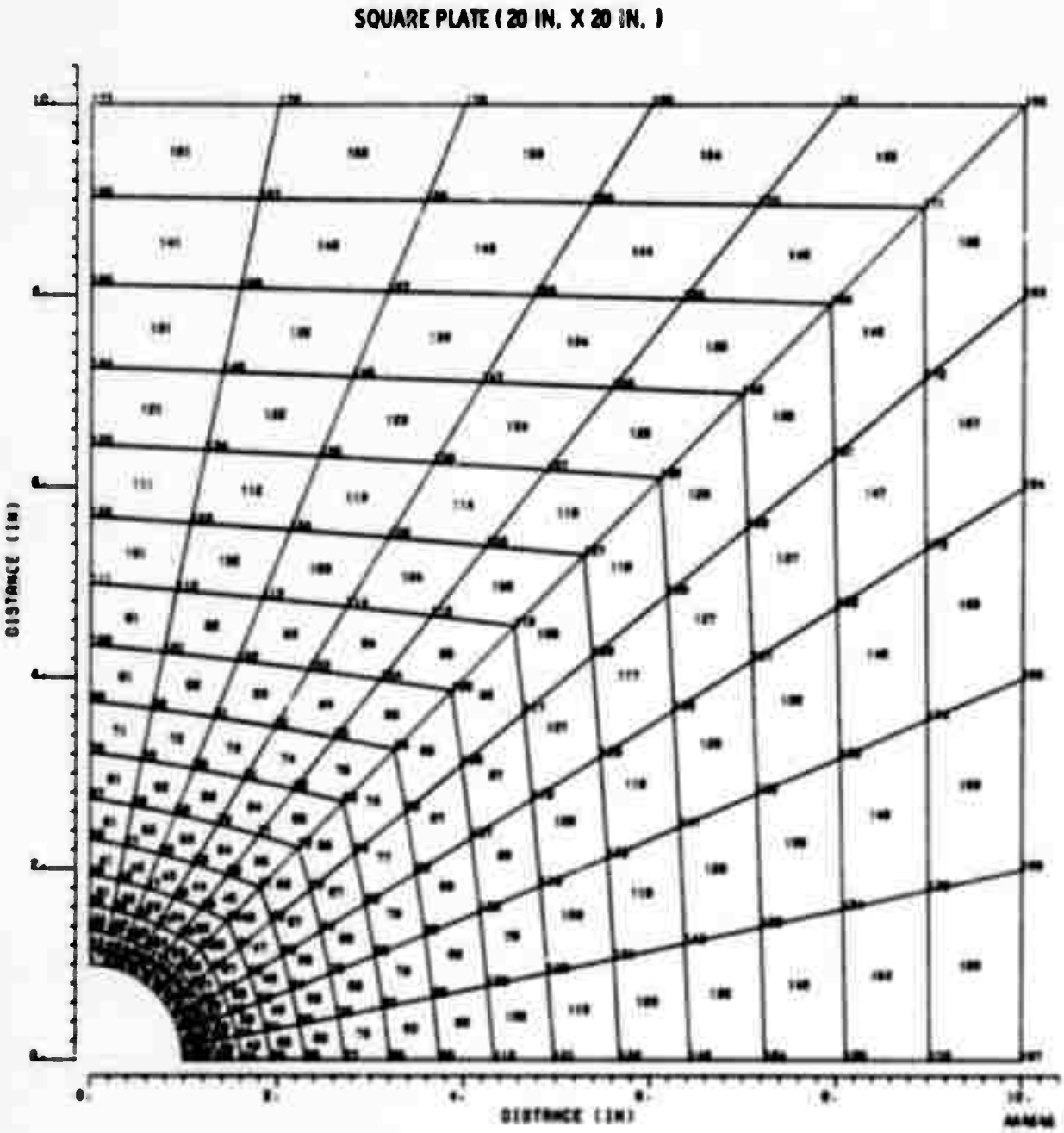

FIGURE 6-2. FINITE ELEMENT MESH FOR STRESS CONCENTRATION AROUND CIRCULAR HOLE

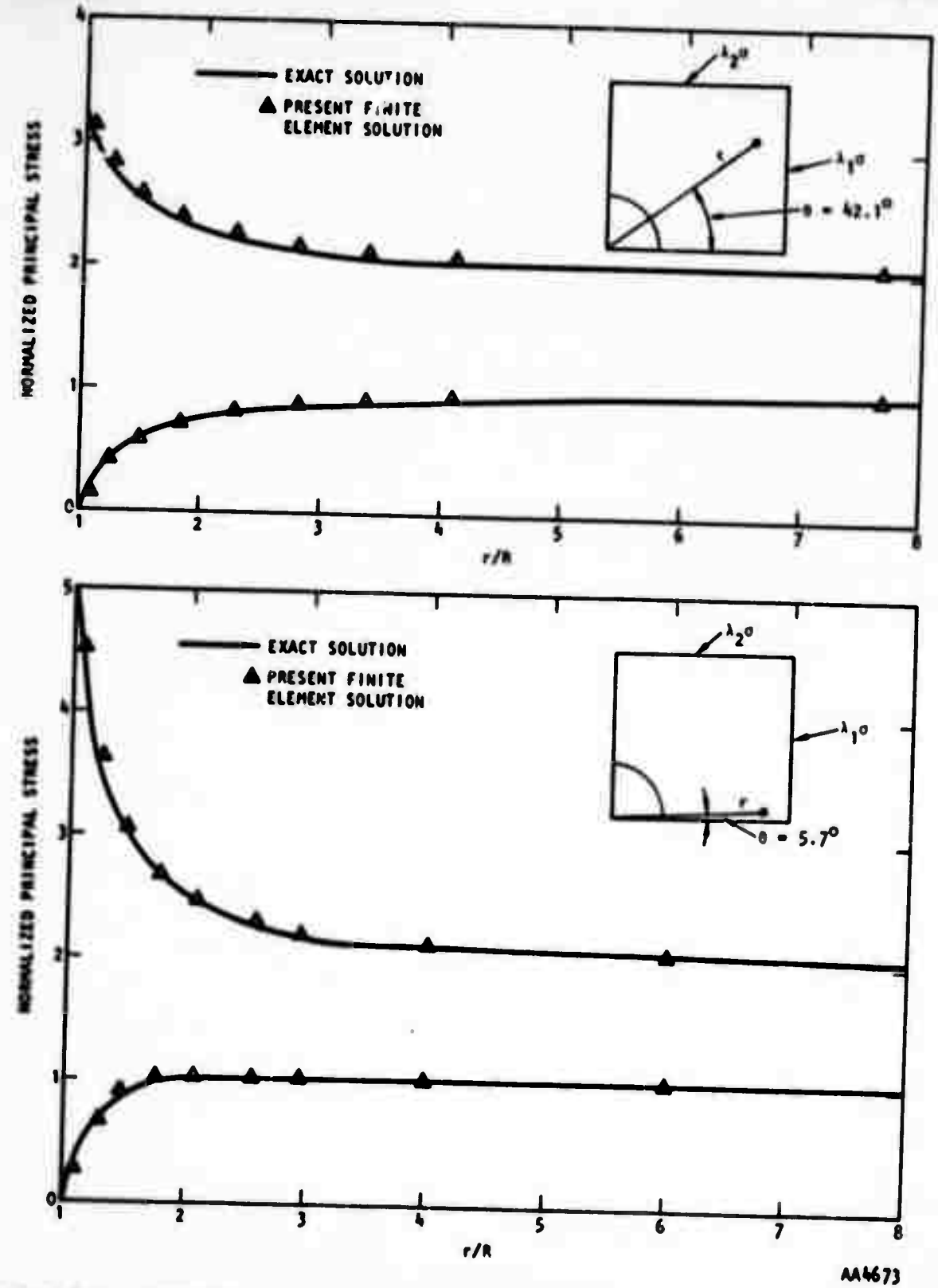

FIGURE 6-3. COMPARISON BETWEEN PRESENT FINITE ELEMENT SOLUTION AND ANALYTIC SOLUTION FOR PROBLEM 1, STRESSES AROUND A CIRCULAR HOLE

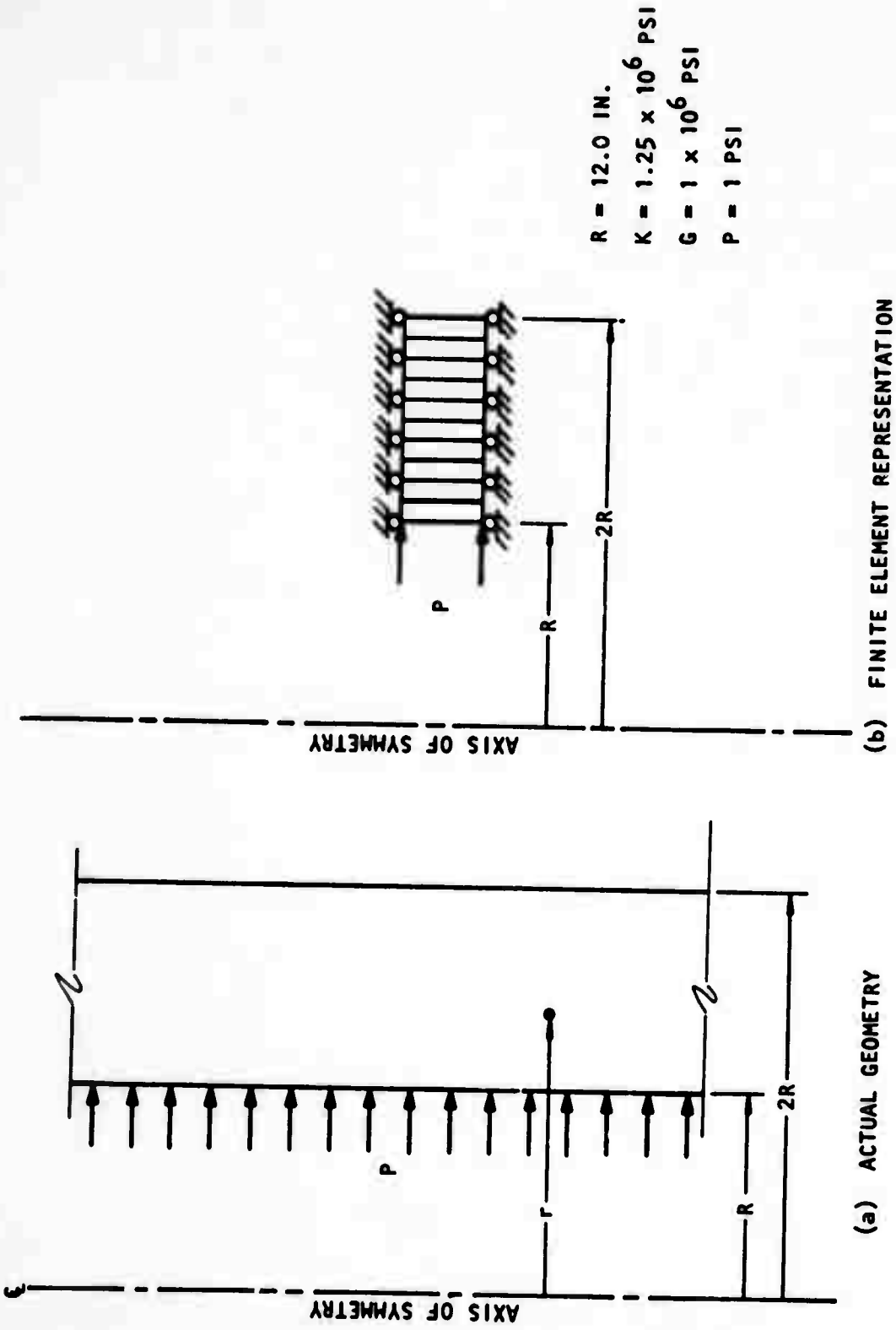

FIGURE 6-4. PROBLEM 2--INFINITELY LONG, THICK ELASTIC CYLINDER SUBJECT TO INTERNAL PRESSURE

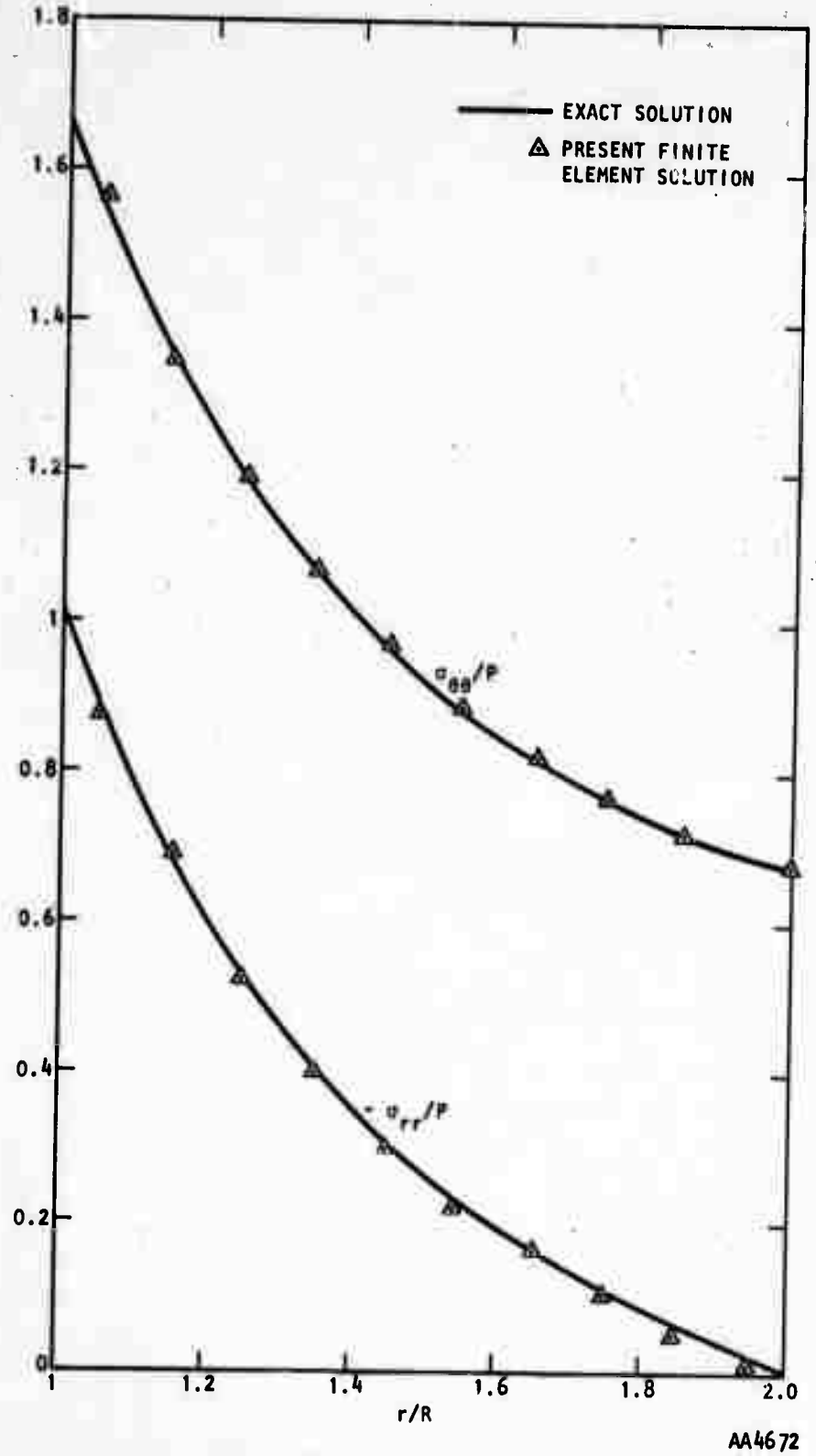

FIGURE 6-5. COMPARISON BETWEEN PRESENT FINITE ELEMENT SOLUTION AND ANALYTIC SOLUTION FOR PROBLEM 2, THICK ELASTIC CYLINDER SUBJECT TO INTERNAL PRESSURE

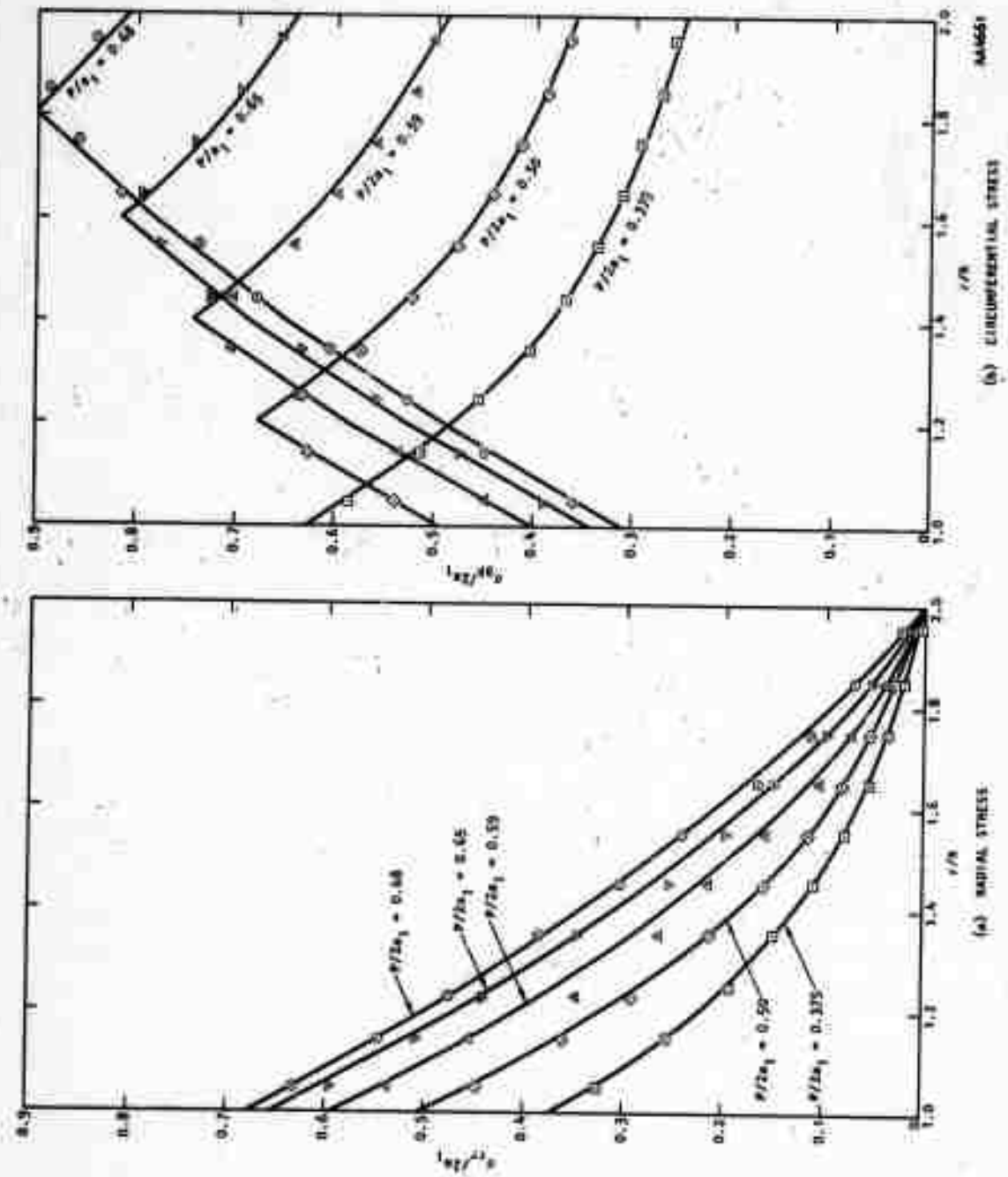

FIGURE 6-6. COMPARISON BETWEEN PRESENT FINITE ELEMENT SOLUTION AND ANALYTIC SOLUTION FOR PROBLEM 3, ELASTIC ELASTIC CYLINDER SUBJECT TO INTERNAL PRESSURE

Problem 4--Stress in a Visco-Elastic, Reinforced Cylinder Under Internal Pressure

The geometry of Problem No. 4, shown in Figure 6-7, is similar to that of Problems 2 and 3. The main difference is a steel reinforcing ring around the outer circumference. The material of the cylinder is assumed to be governed by a Maxwell-type law as follows:

$$\sigma_{ij} = 2G(\varepsilon'_{ij}) \exp(-t/B) \qquad (6\text{-}2)$$

where

ε'_{ij} = Component of deviatoric strain tensor

G = Elastic shear modulus

t = Time in units of $B = \eta/G$ where η = viscoelastic parameter)

Volumetric deformation of the cylinder and all deformations of the reinforcing ring are assumed to be linearly elastic inviscid. The variation of radial and circumferential stresses are shown as functions of radius and time in Figure 6-8.

Problem 5--Three-Dimensional Stress Concentration Around a Cylindrical Hole in a Semiinfinite Elastic Body

The geometry of Problem No. 5 is illustrated in Figure 6-9. The stress distribution around the hole near the stress free face (X_1 - X_2 plane) is appropriate to plane stress, while in the interior there is axial stress along the axis of the hole. The finite element mesh is shown in Figure 6-10. The loading condition selected for this example is uniaxial stress parallel to the X_2-axis. Thus the faces parallel to the X_2-ρ plane are stress free as is one face parallel to the X_2-X_1 plane. The finite element solution is compared with the anaiytic solution in Figure 6-11.

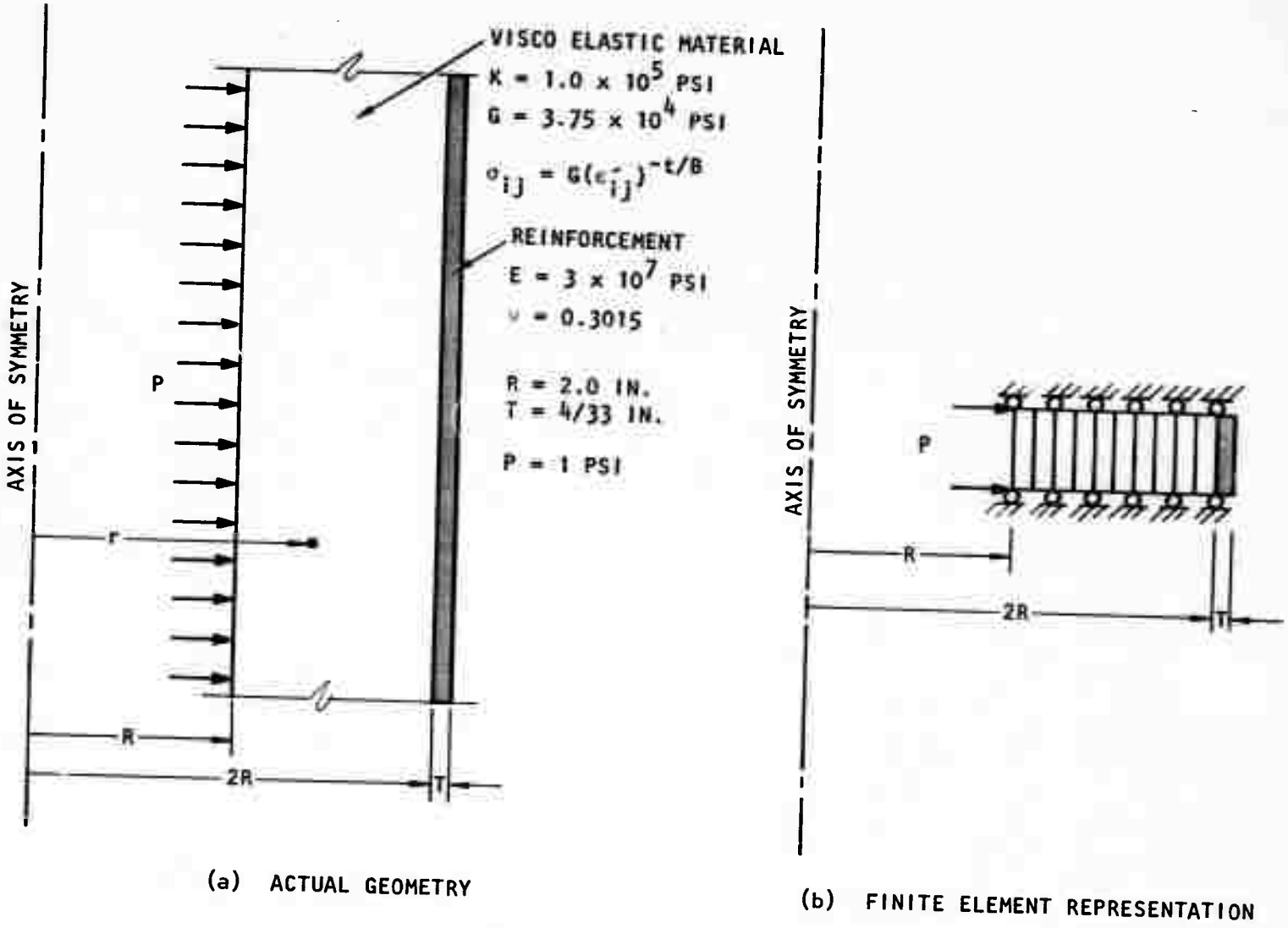

(a) ACTUAL GEOMETRY

(b) FINITE ELEMENT REPRESENTATION

FIGURE 6-7. PROBLEM 4--INFINITELY LONG REINFORCED THICK VISCOELASTIC CYLINDER SUBJECTED TO INTERNAL PRESSURE

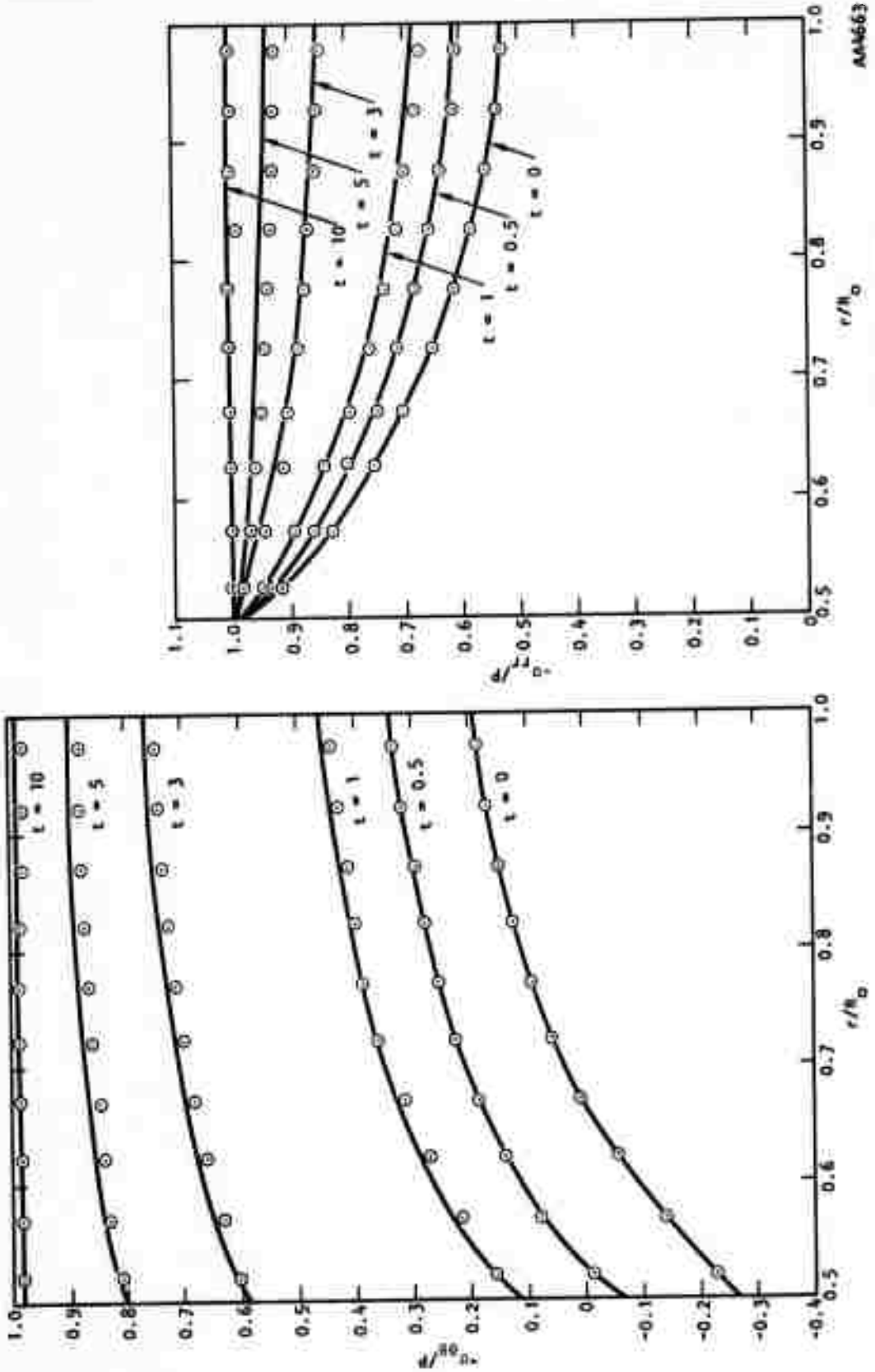

(a) CIRCUMFERENTIAL STRESS

(b) RADIAL STRESS

FIGURE 6-6. PROBLEM 4--REINFORCED VISCOELASTIC CYLINDER SUBJECTED TO INTERNAL PRESSURE (REFERENCE 6-4)

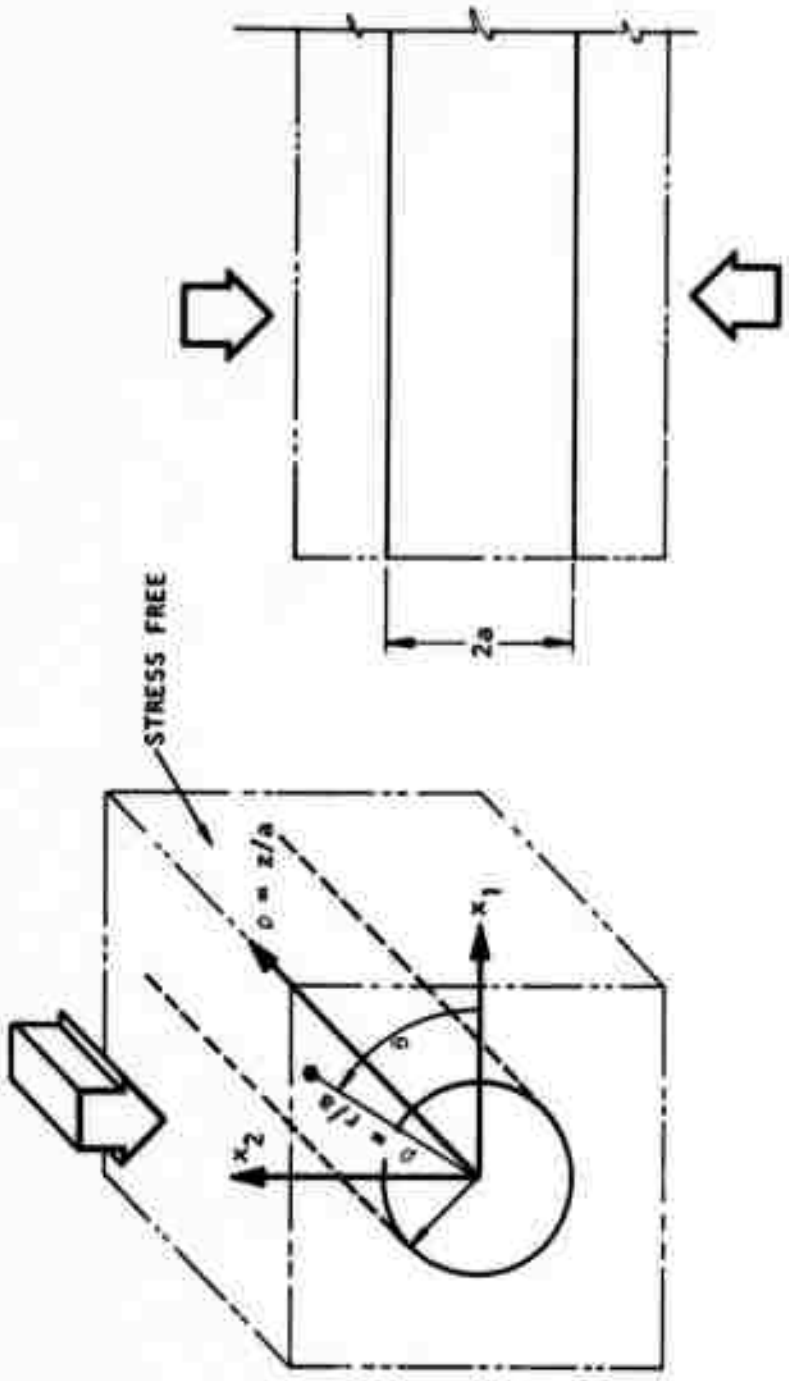

FIGURE 6-9. PROBLEM 5--THREE-DIMENSIONAL STRESS CONCENTRATION AROUND A CYLINDRICAL HOLE IN A SEMIINFINITE ELASTIC BODY

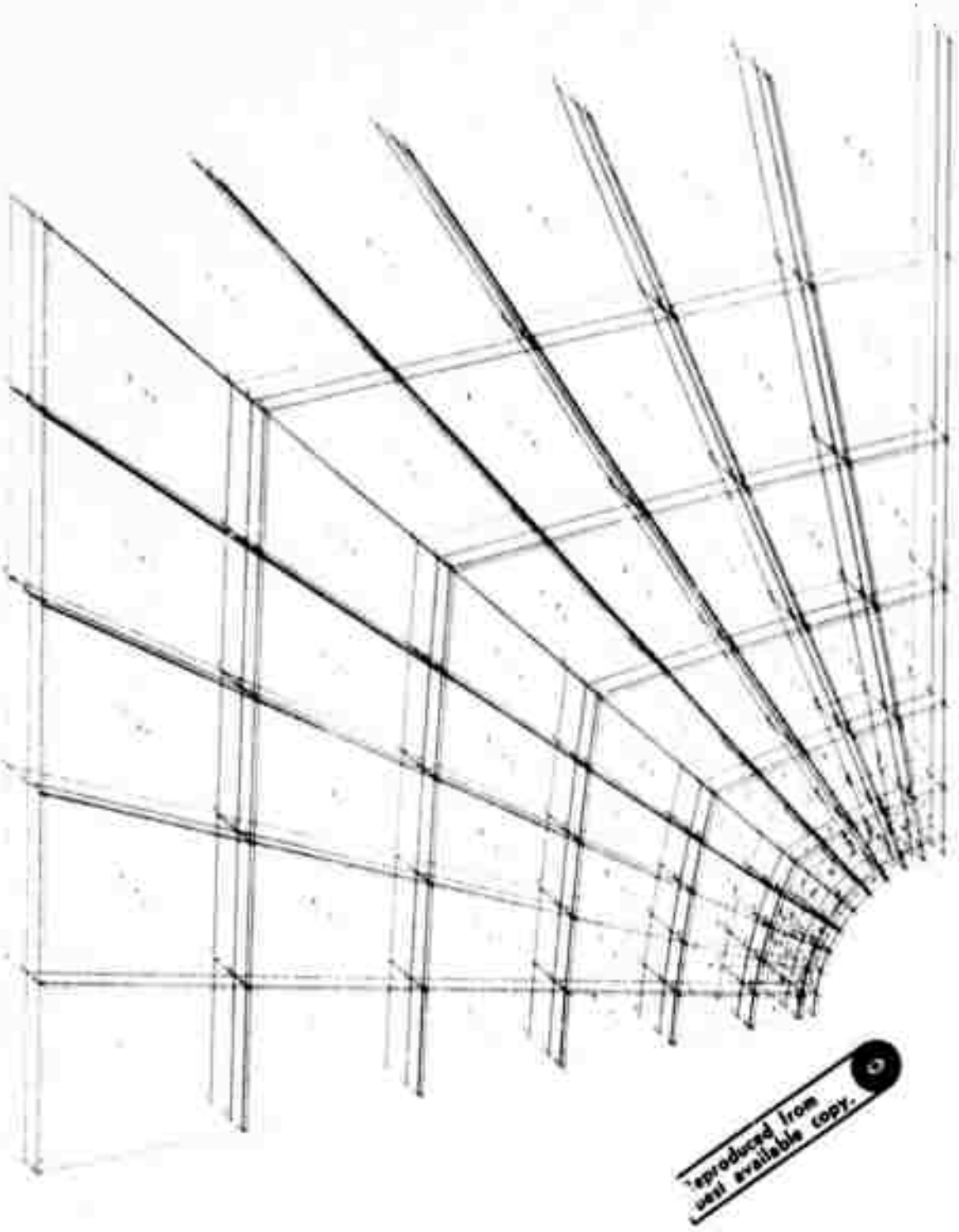

FIGURE 6-10. PROBLEM 5--FINITE ELEMENT MESH (ONLY FIRST THREE LAYERS ARE SHOWN FOR CLARITY. COMPLETE MESH CONTAINS EIGHT LAYERS.)

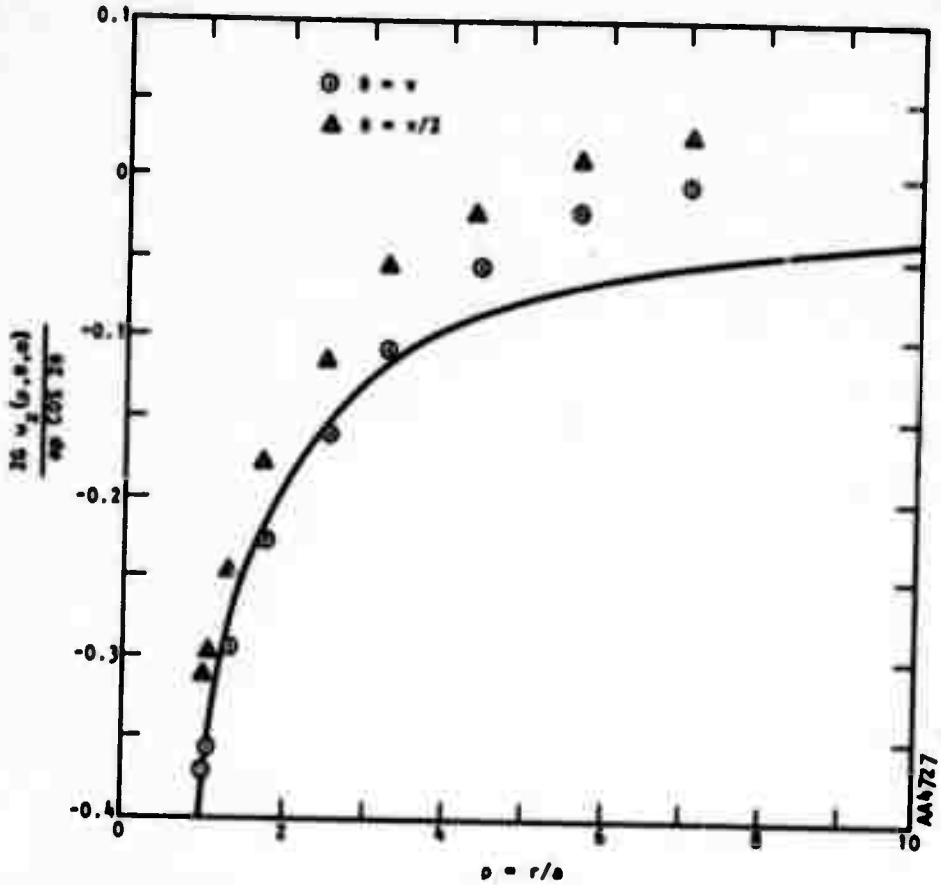

(a) AXIAL DISPLACEMENT ON THE STRESS FREE PLANE ρ = 0 (NOTICE THAT THE FINITE ELEMENT SOLUTION WHICH ENCOMPASSES A FINITE DOMAIN DIVERGES FROM THE ANALYTIC SOLUTION, WHICH CONSIDERS AN INFINITE DOMAIN, AS THE FINITE BOUNDARY IS APPROACHED)

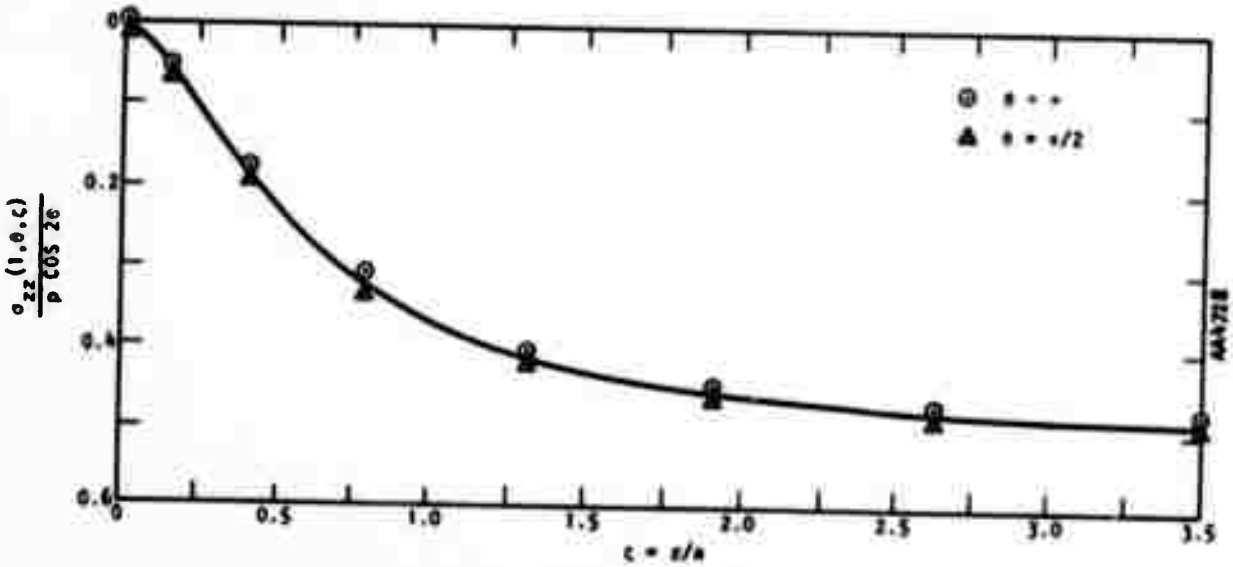

(b) AXIAL STRESS AT EDGE OF THE HOLE

FIGURE 6-11. PROBLEM 5--THREE-DIMENSIONAL STRESS CONCENTRATION (REFERENCE 6-4)

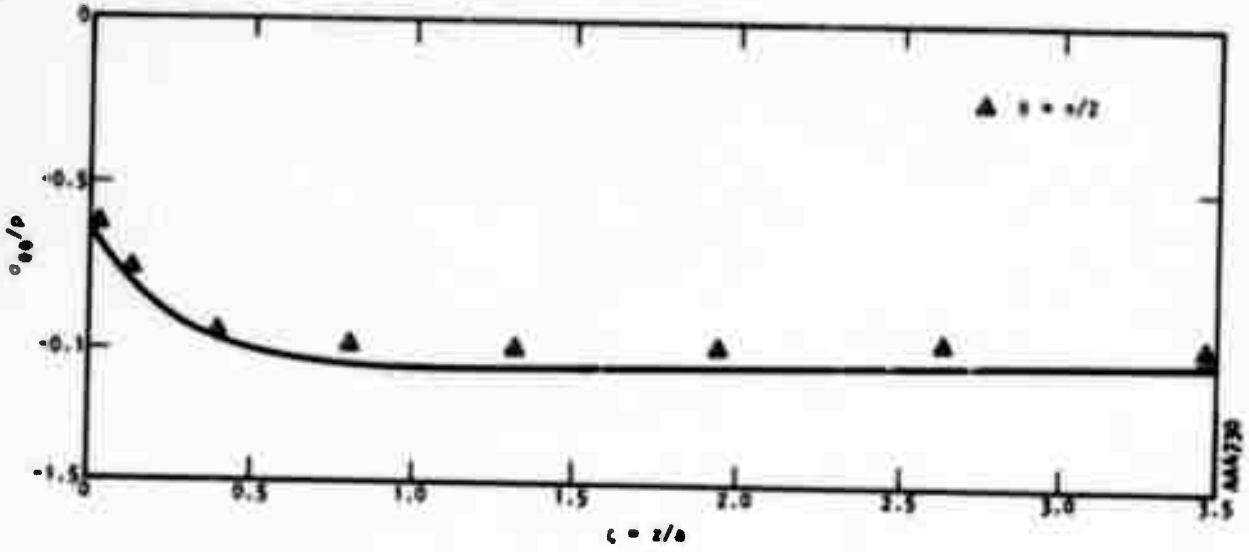

(c) TANGENTIAL STRESS AT EDGE OF HOLE (CROWN)

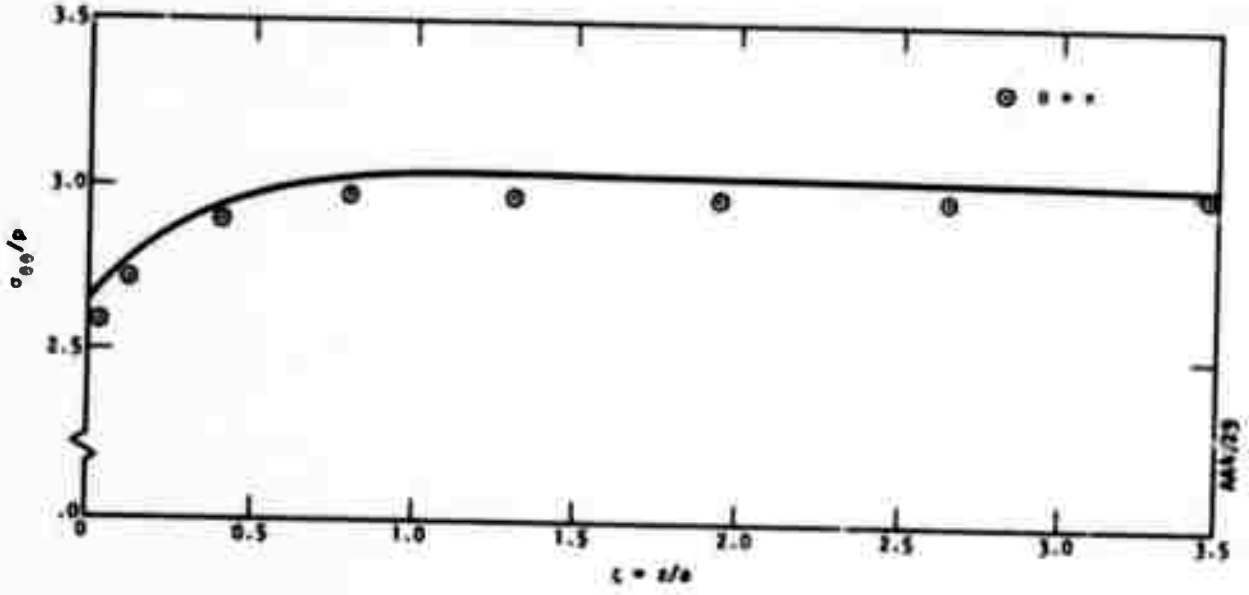

(d) TANGENTIAL STRESS AT EDGE OF HOLE (SPRING LINE)

FIGURE 6-11. (CONTINUED)

6.2 COMPUTING TIME REQUIRED FOR SOLUTION

The computing time required to solve Problem 5 and several small problems on a Univac 1108 with 65,000 words of core is shown in Table 6-2. More data on time to solve various sizes of problems will be gathered during the second phase of the contract.

TABLE 6-2. COMPUTING TIME REQUIRED FOR SOLUTIONS

	Number of Equations	Bandwidth	Number of Blocks for Global Stiffness	Number of Equations/ Block	Number of Elements	Time to Form Global Stiffness, sec	Triangularize, sec	Back-sub, sec	Compute Stress, sec
1	2412	312	87	28	640	540	2178	180	30
2*	2144	278	86	25	560	2400	--	60	30
3†	496	278	16	31	80	61	333	--	3
4†	558	312	20	28	80	72	464	--	4
5†	168	42	1	168	21	17	3.7	--	1.1
6	168	42	14	12	21	24	8	1	5.5
7	168	42	56	2	21	37	20	3	3.7

*Global stiffness matrix triangularized as formed; forward reduction of load vector included in backsubstitution.

†Triangularization includes backsubstitution time.

REFERENCES

6-1. Savin, G. N., "Stress Concentration Around Holes," *Pergamon Press*, New York, 1961.

6-2. Prager, W. and P. G. Hodge, Jr., *Theory of Perfectly Plastic Solids*, John Wiley & Sons, Inc., New York, 1951

6-3. Zienkiewicz, O. C., et al., "A Numerical Method of Viscoelastic Stress Analysis," *Int. J. Mech. Sci.*, Pergamon Press, 1968, pp. 807-827.

6-4. Youngdahl, C. K., and E. Sternbery, *Three-Dimensional Stress Concentration Around a Cylindrical Hole in a Semi Infinite Elastic Body*, Argonne National Laboratory, ANL-7097, September 1965.

APPENDIX A

LOGIC DIAGRAMS FOR MATERIAL PROPERTIES

Logic diagrams for subroutines in the material property package are shown below. Subroutine CONECT connects the package to the main program. Subroutine ELPL controls all the other subroutines.

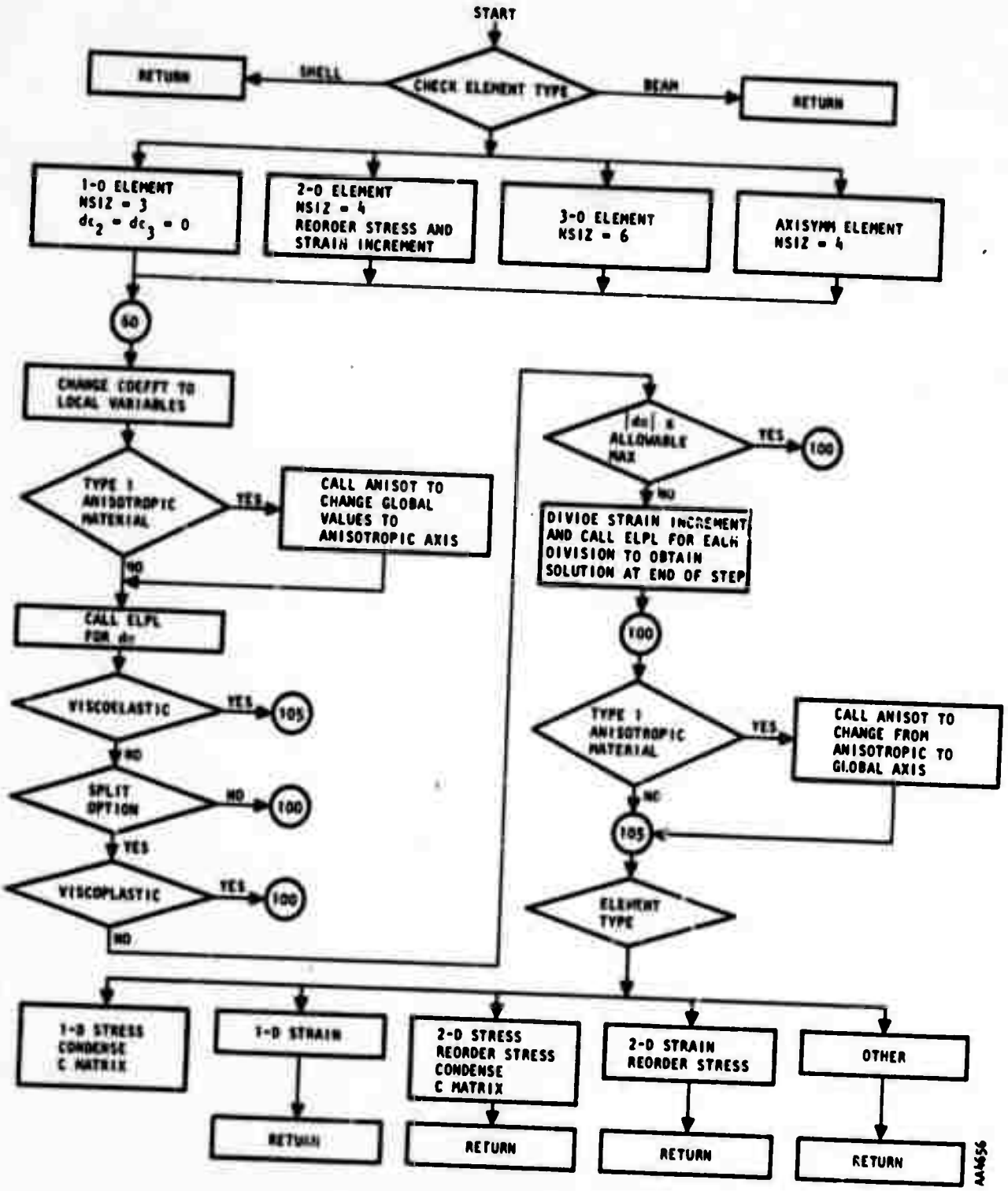

FIGURE A-1. CONECT--SUBROUTINE CONECT LINKS MAIN LINE PROGRAM TO MATERIAL PACKAGE ELPL

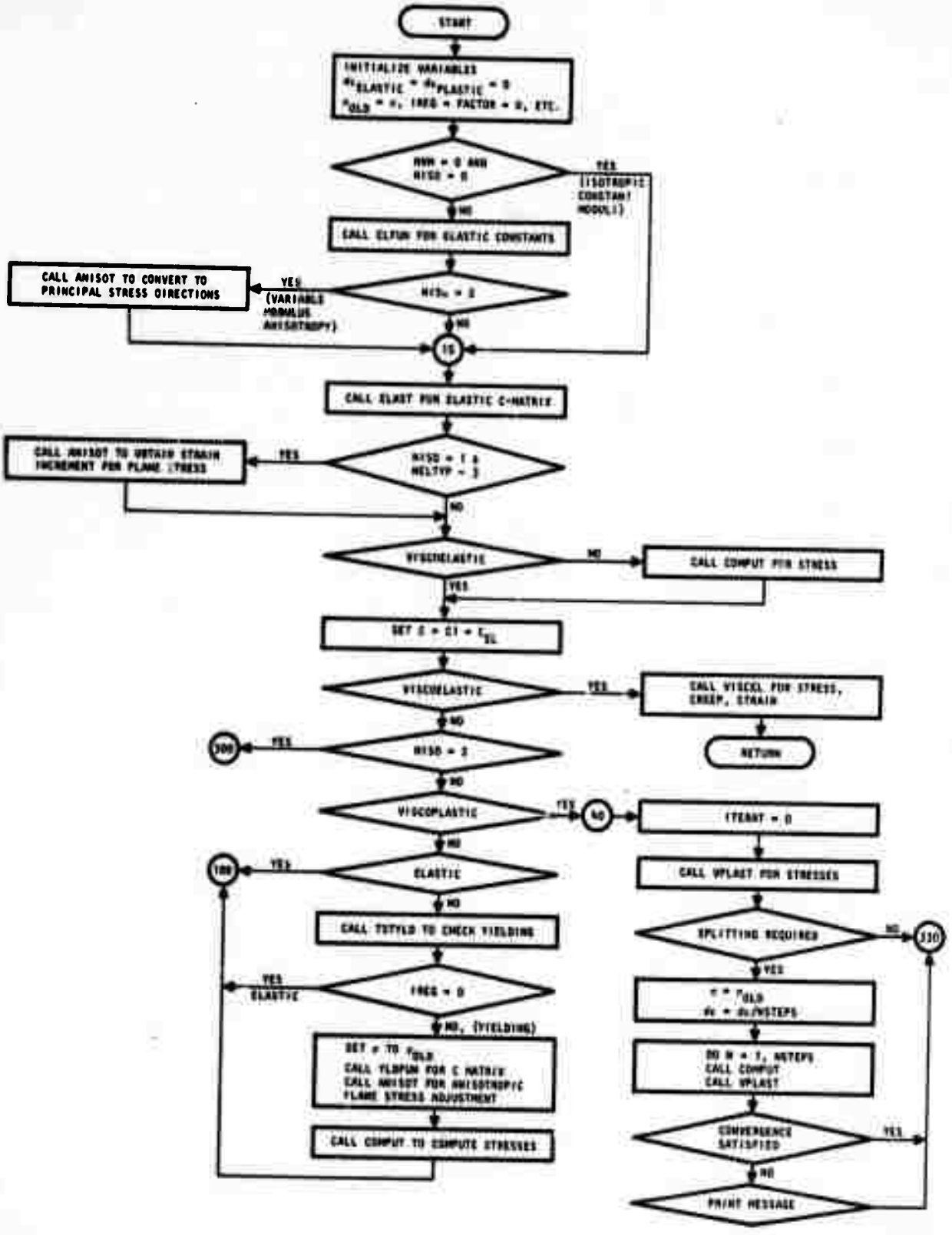

AA4692

FIGURE A-2. SUBROUTINE ELPL CONTROLS MATERIAL PROPERTY SUBROUTINES, TRANSFERS AXES FOR ANISOTROPIC MATERIALS, PERFORMS TESTS FOR STRAIN SPLITTING AND ITERATION.

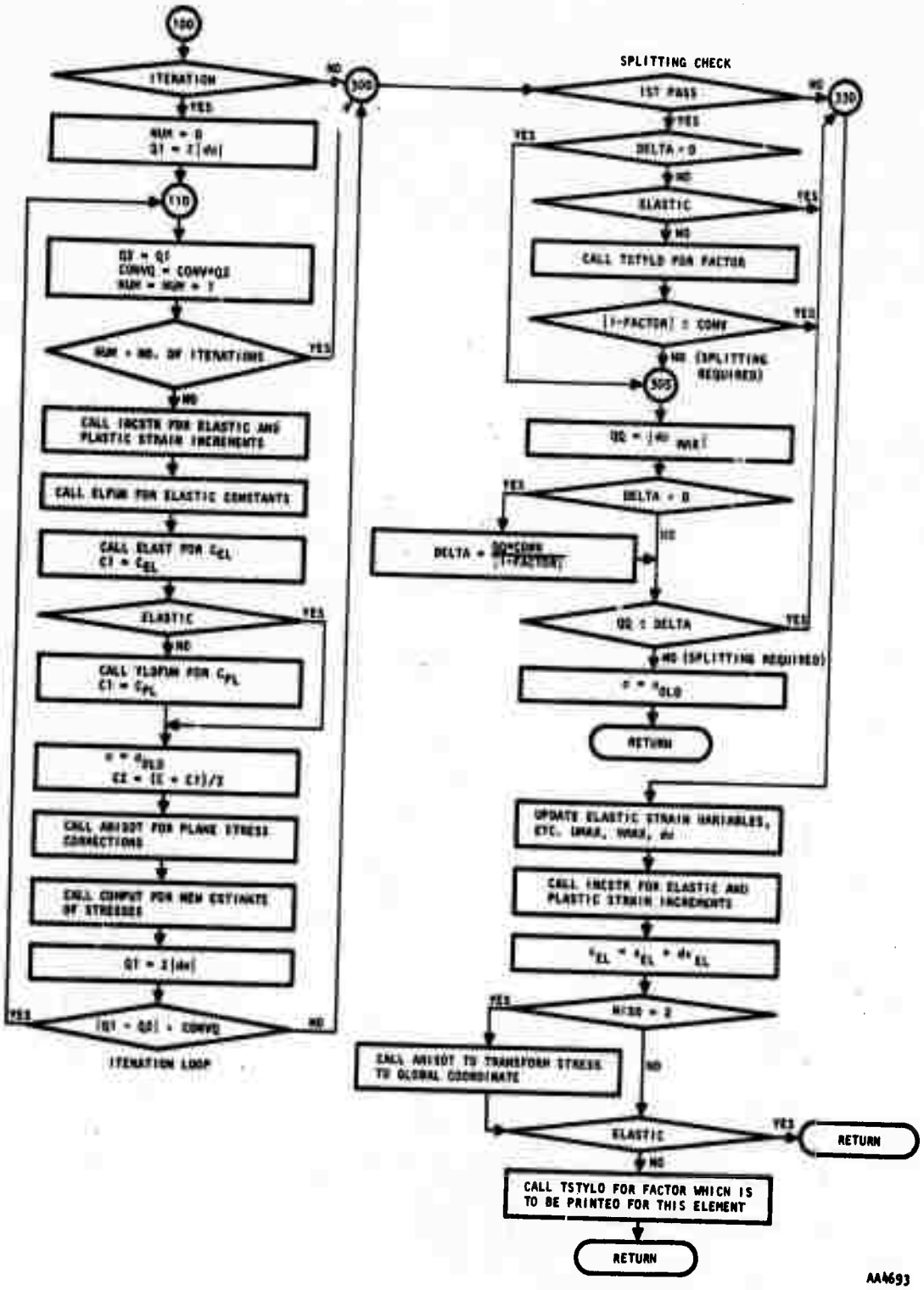

FIGURE A-2 (CONTINUED)

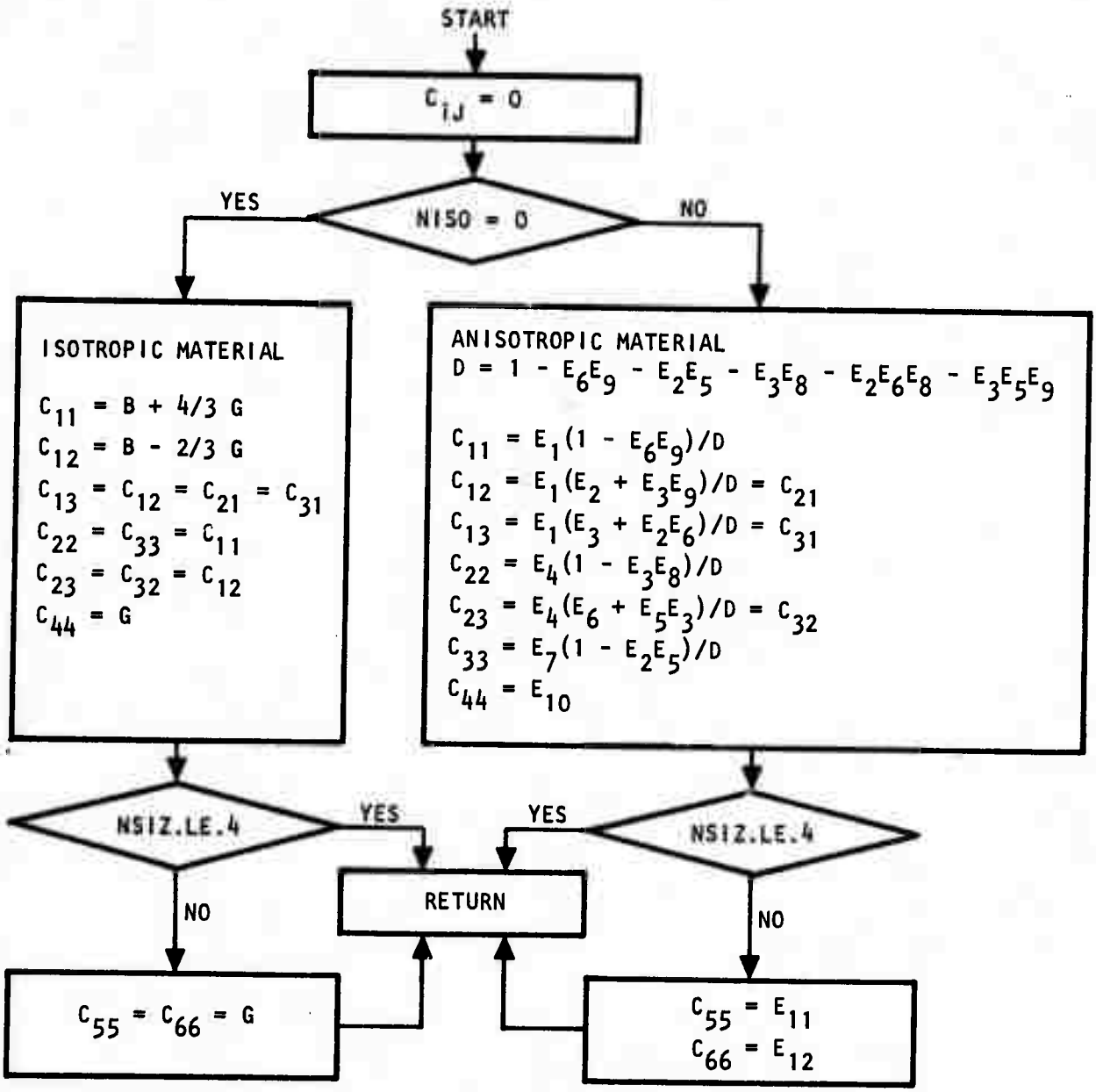

FIGURE A-3. SUBROUTINE ELAST--ELAST FORMULATES C-MATRIX USING COEFFICIENTS FOR EITHER ISOTROPIC OR ANISOTROPIC MATERIALS GENERATED BY ELFUN

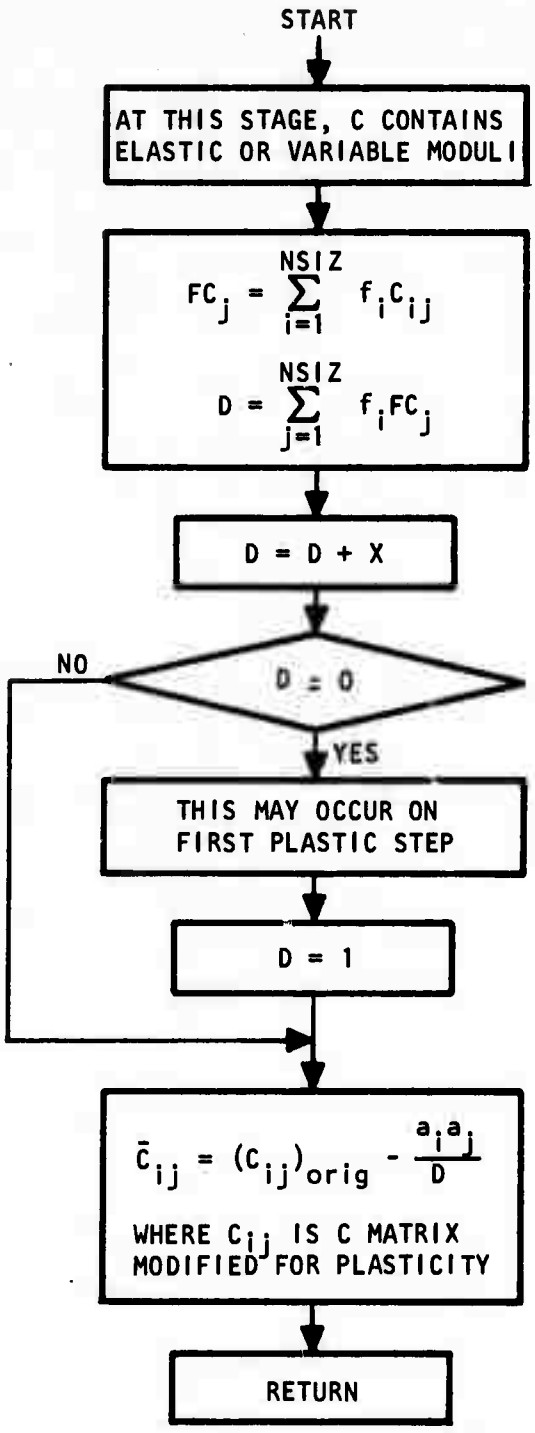

FIGURE A-4. SUBROUTINE PLAST--THIS SUBROUTINE MODIFIES C MATRIX GENERATED BY SUBROUTINE ELAST IN ORDER TO ACCOUNT FOR PLASTICITY. THE BASIC QUANTITIES FOR THIS MODIFICATION ARE DERIVATIVES OF THE YIELD FUNCTION WITH RESPECT TO THEIR ARGUMENTS AND ARE COMPUTED IN YLDFUN.

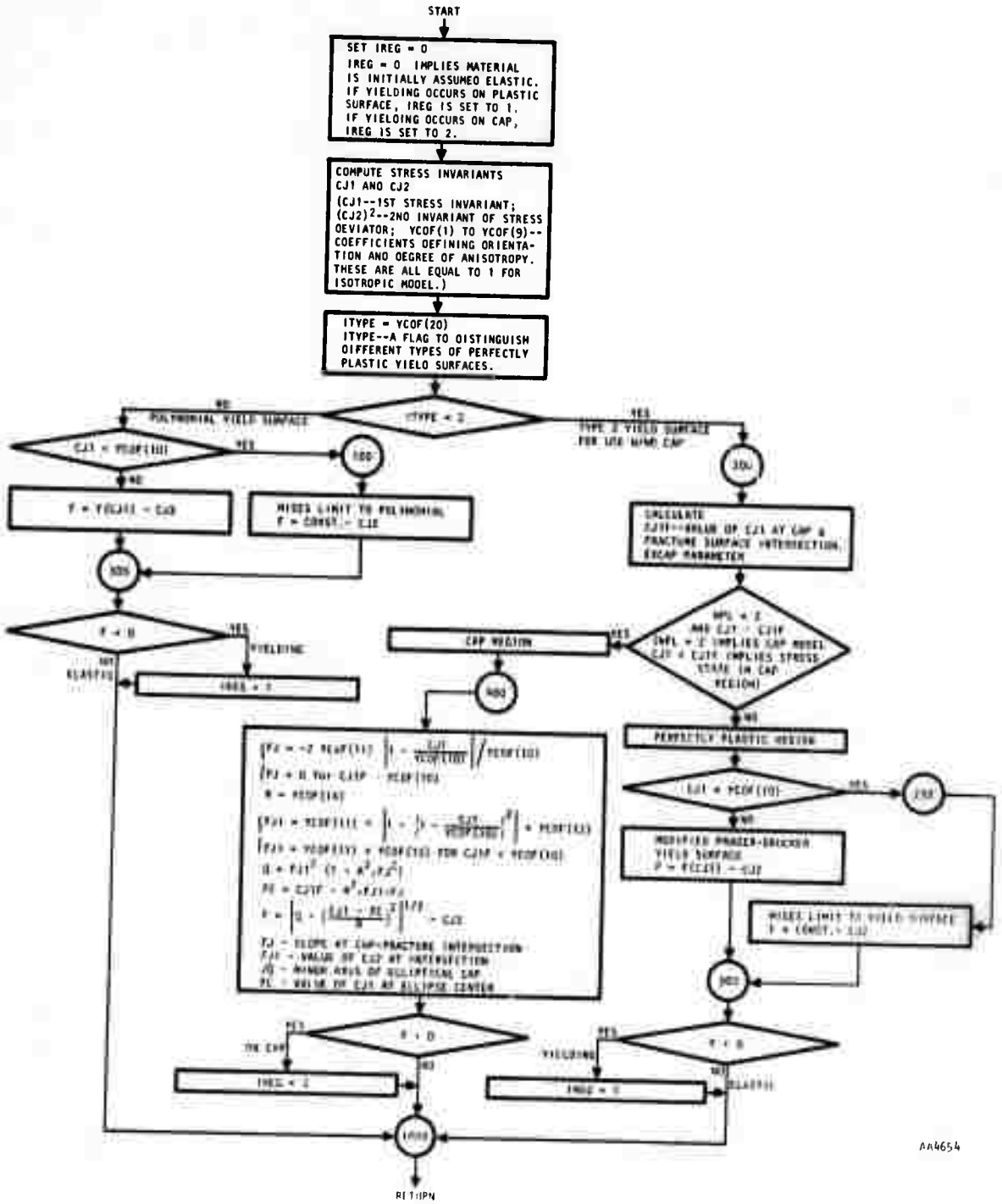

FIGURE A-5. SUBROUTINE TSTYLD--COMPARES CURRENT STATE OF STRESS WITH YIELD CRITERIA TO DETERMINE WHETHER YIELDING OCCURS

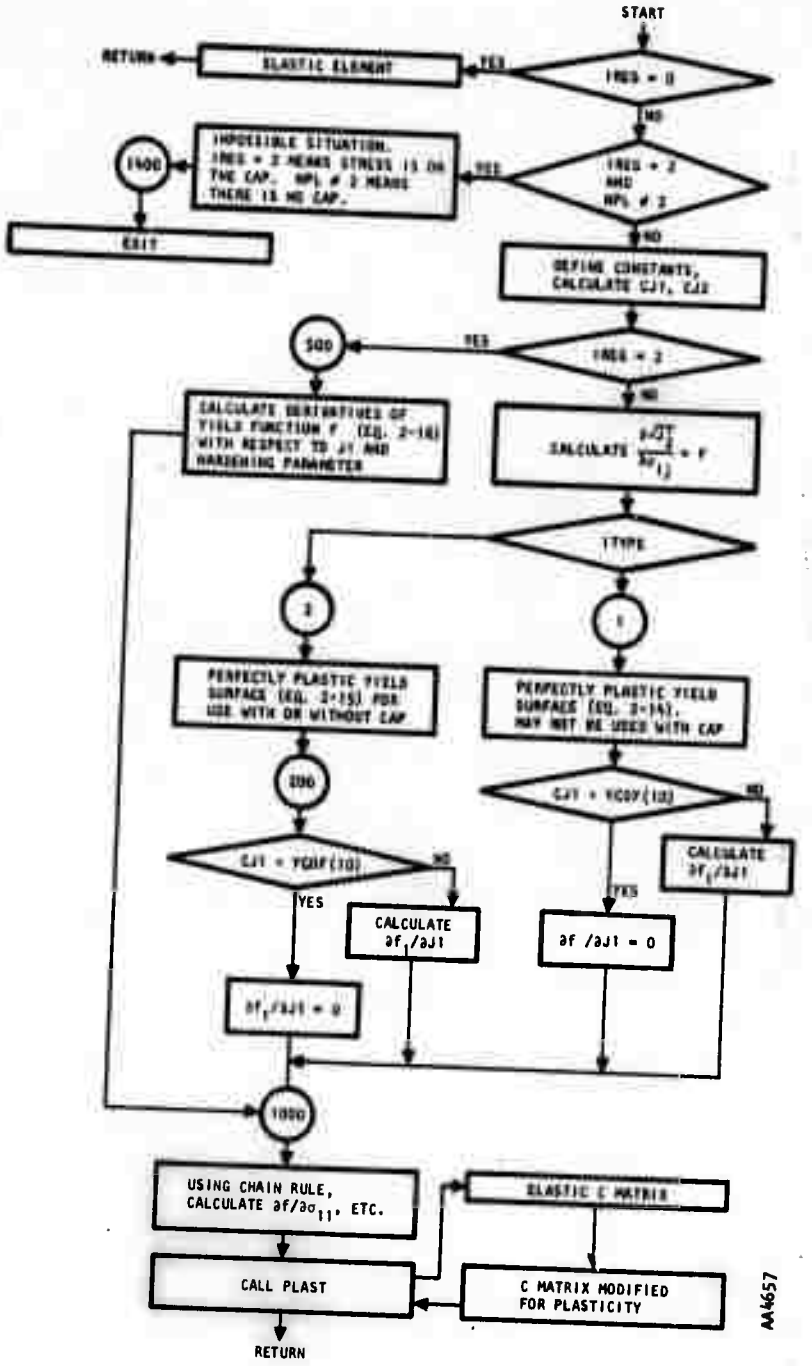

FIGURE A-6. SUBROUTINE YLDFUN--THIS SUBROUTINE CALCULATES THE DERIVATIVES OF THE YIELD FUNCTION WITH RESPECT TO THE STRESS COMPONENTS. THE YIELD FUNCTION WHOSE DERIVATIVES ARE COMPUTED IS DETERMINED BY THE INDICES IREG (SET IN (TSTYLD) AND ITYPE (SET BY INPUT))

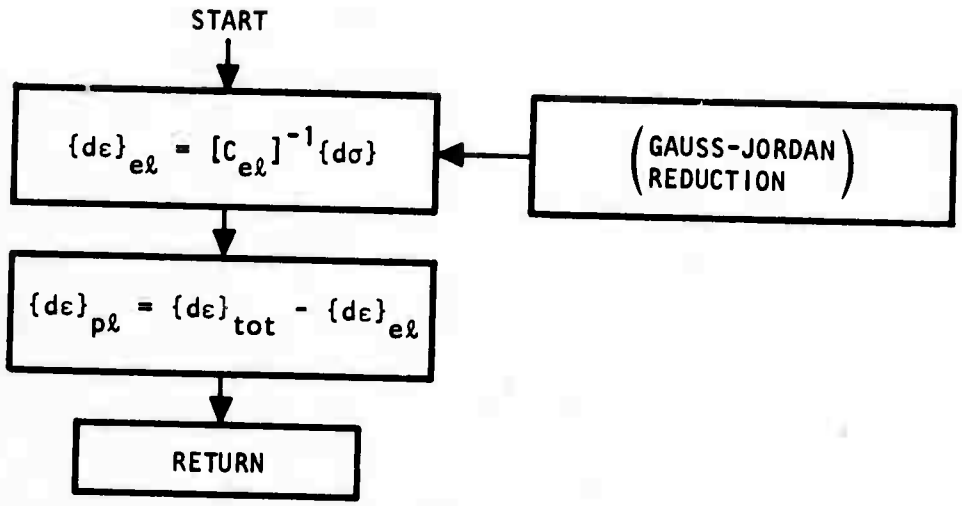

FIGURE A-7. SUBROUTINE INCSTR--INCSTR COMPUTES ELASTIC AND PLASTIC STRAIN INCREMENTS)

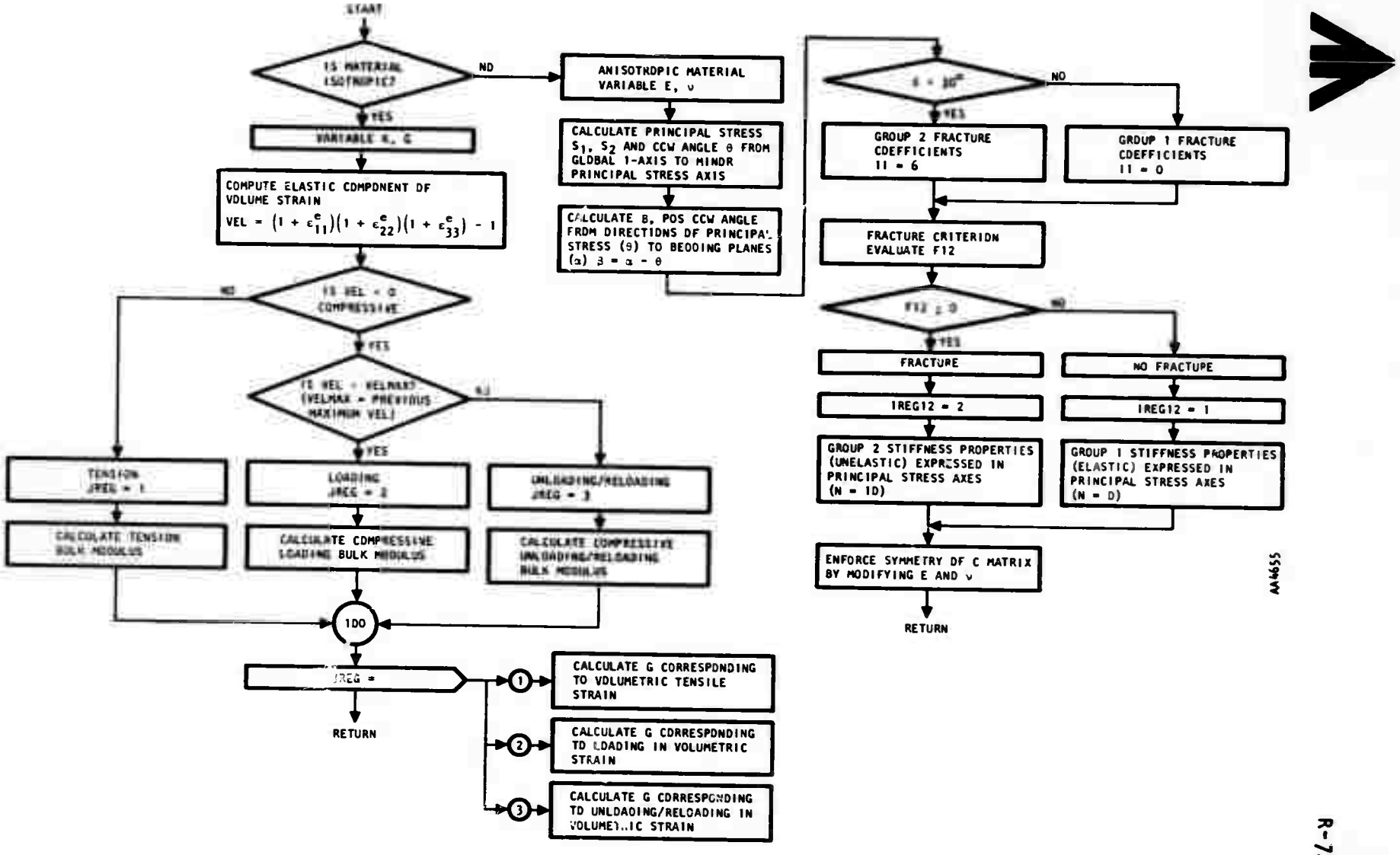

FIGURE A-8. SUBROUTINE ELFUN--THIS SUBROUTINE CALCULATES VALUES OF VARIABLE ELASTIC MODULI (K, G FOR ISOTROPIC MATERIAL, E, ν FOR ANISOTROPIC MATERIAL). INPUT FOR ISOTROPIC MATERIAL IS CURRENT AND PREVIOUS MAXIMUM VALUES OF ELASTIC VOLUME STRAIN. INPUT FOR ANISOTROPIC MATERIAL IS CURRENT VALUE OF STRESSES.

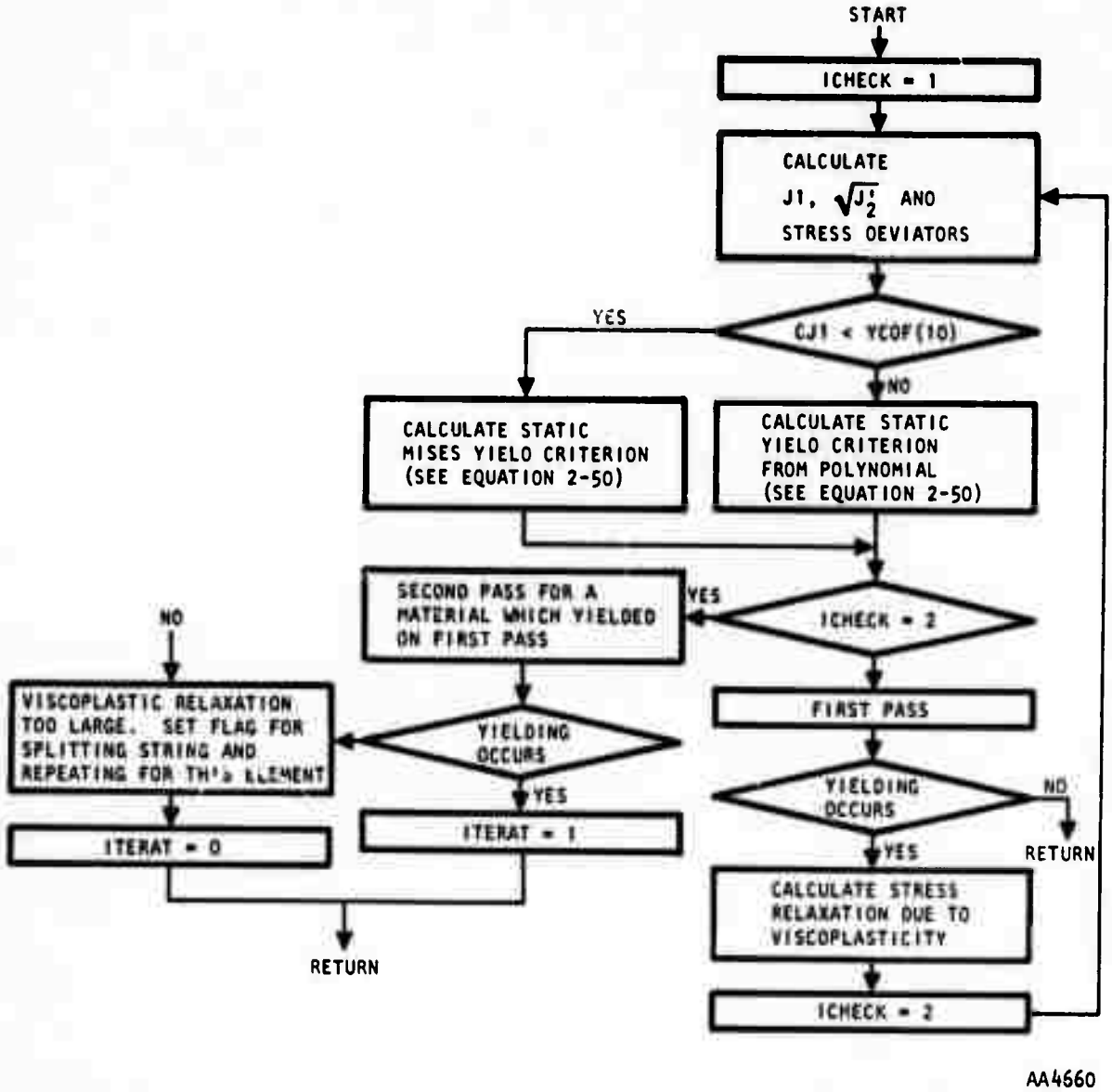

FIGURE A-9. SUBROUTINE VPLAST--THIS SUBROUTINE IS USED FOR A VISCOPLASTIC MATERIAL. IT CALCULATES THE STATIC YIELD CRITERION, DETERMINES WHETHER YIELDING OCCURS AND, IF YIELDING OCCURS, MODIFIES THE STRESSES TO ACCOUNT FOR VISCOPLASTIC STRESS RELAXATION.

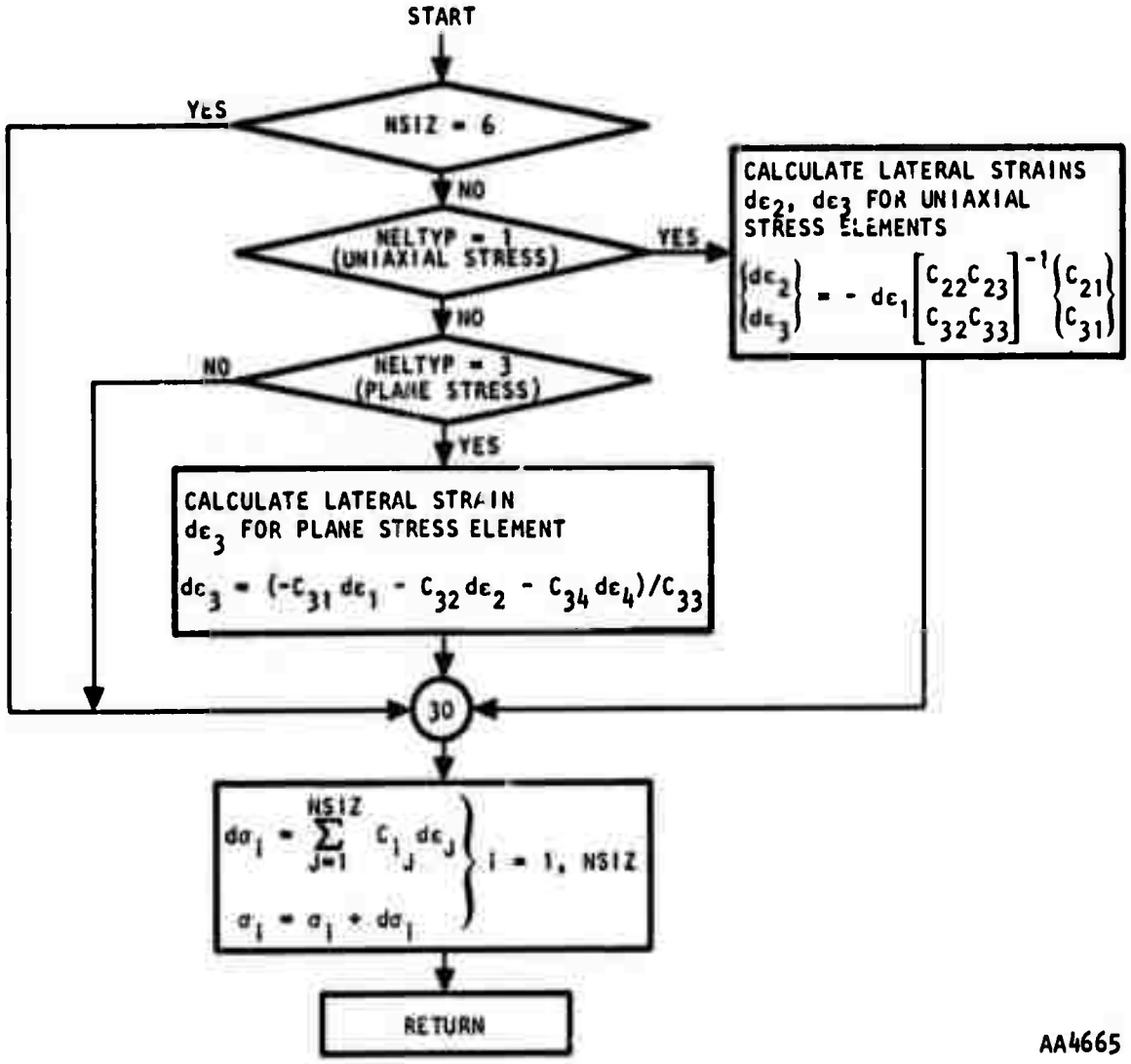

FIGURE A-10. SUBROUTINE COMPUT--COMPUT CALCULATES STRESS INCREMENTS AND ADDS THEM TO OLD STRESSES TO OBTAIN NEW STRESSES. STRAINS CORRESPONDING TO ZERO STRESSES (PLANE STRESS, UNIAXIAL STRESS) ARE COMPUTED.